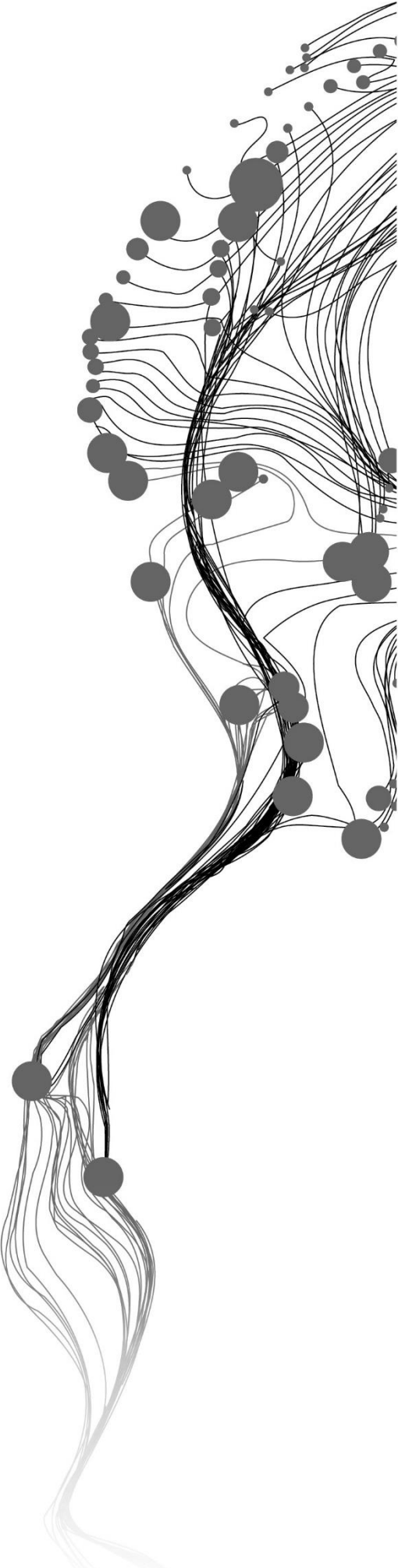


# **FOREST NET PRIMARY PRODUCTIVITY RESPONSE TO AN EXTREME CLIMATE EVENT**

MD SAIFUL ISLAM  
July, 2023

SUPERVISORS:  
dr. R. Darvishzadeh  
dr. E. Neinavaz





# FOREST NET PRIMARY PRODUCTIVITY RESPONSE TO AN EXTREME CLIMATE EVENT

MD SAIFUL ISLAM

Enschede, The Netherlands, July 2023

Thesis submitted to the Faculty of Geo-Information Science and Earth  
Observation of the University of Twente in partial fulfilment of the requirements  
for the degree of Master of Science in Geo-information Science and Earth  
Observation for Environmental Modelling and Management (GEM).  
Specialization: Track-3: Ecosystems and Natural Resources

**SUPERVISORS:**

dr. R. Darvishzadeh

dr. E. Neinavaz

**THESIS ASSESSMENT BOARD:**

Chair: prof.dr. A.K. Skidmore

Supervisors: dr. R. Darvishzadeh & dr. E. Neinavaz

External Examiner: dr. Andreas Hirner (German Aerospace Center (DLR))

Procedural Advisor: drs. R.G. Nijmeijer

#### DISCLAIMER

This document describes work undertaken as part of a programme of study at the Faculty of Geo-Information Science and Earth Observation of the University of Twente. All views and opinions expressed therein remain the sole responsibility of the author, and do not necessarily represent those of the Faculty.

# ABSTRACT

The Net Primary Productivity (NPP) is an essential indicator of monitoring vegetation health, carbon exchange, and the impact of extreme climate events, such as drought. Light Use Efficiency (LUE)-based models utilise remote sensing data for NPP estimation. However, estimation of NPP through these models has been mainly performed using low/moderate resolution remote sensing data. In this respect, this study utilised two LUE-based models, i.e., MOD17 and GLO-PEM and temporal high-resolution remote sensing (i.e. Sentinel-2) data to evaluate the performance of these models in estimating NPP and to detect the impacts of the 2018 drought on NPP in Bavaria Forest National Park (BFNP), Germany. The necessary data for NPP estimation, including Sentinel-2 imagery, climate data (i.e., daily mean and minimum temperature, vapour pressure deficit, soil moisture deficit), and land cover map, have been collected from Copernicus Open Access Hub, European Centre for Medium-Range Weather Forecasts, National Snow and Ice Data Center, and Copernicus Land Monitoring Service. The forest inventory data, MODIS- NPP, and Standardised Precipitation and Evapotranspiration Index (SPEI) values have been used for NPP verification and drought impact assessment. The two LUE models were used first to estimate the Gross Primary Productivity (GPP), and then NPP was estimated using a coefficient derived from GPP and NPP ratio. Different statistical analyses, including the Coefficient of Determination ( $R^2$ ), Person's Correlation Coefficient ( $r$ ), Linear Trend, and t-test, have been performed to verify the model outputs and their temporal change as well as to detect the drought and associated impacts. Analysis showed that the results obtained using the GLO-PEM model agree better with forest inventory NPP than the NPP estimated using the MOD17 model. When MODIS products were used for verification, both models' outputs were observed to behave almost similarly to MODIS products. Time series analysis of NPP showed a slight decrease in NPP in 2018 than the previous two years (i.e., 2016 and 2017), and then a significant reduction was found in 2019, 2020, and 2021. In 2022, a slight increase was noted in NPP values, indicating restoration and the recovery's start. However, an overall downward trend in NPP values was found as the slope values of the linear trend were negative in different sample points. The lagged correlation results revealed the delayed impacts of Vapor Pressure Deficit (VPD) and soil moisture deficit on NPP. Besides, a lagged correlation was also found between SPEI and NPP, indicating the legacy impacts of drought. The substantial reduction of NPP and negative NPP values may be attributed to the drought and associated disturbances, such as environmental stress, immature leaf senescence, defoliation, crown dieback, tree mortality, insect infestation, and logging. In a nutshell, the LUE-based models using Sentinel-2 data showed good prospects in NPP estimation and extreme climate impact detection.

The study encountered a few limitations, such as an image gap in the Sentinel-2 time series due to cloud cover and insufficient reference data to validate and verify the model outputs. Besides, the downscaling of climate data, atmospheric distortion in the Sentinel-2 images, and inherent limitations of NDVI, like soil background reflectance and saturation problems, may have caused errors in data. Future research may require increasing the satellite image frequency using the harmonized data of Sentinel-2 and Landsat data and improving the models' ability to estimate autotrophic respiration at daily timestep.

**Keywords:** Net primary productivity; Light use efficiency; Drought; Sentinel-2; MOD17; GLO-PEM; SPEI; Bavaria Forest National Park

## ACKNOWLEDGEMENTS

In this auspicious moment, I would like to express my gratitude to several individuals and organizations whose help and support made completing this thesis—this M.Sc. programme, to a large extent, possible.

First, I want to express my sincere gratitude to my supervisors, dr. Roshanak Darvishzadeh and dr. Elnaz Neinavaz, for their precious time, help, advice, and the chance to work under their guidance. I am very grateful you shared your vast knowledge and expertise, which has changed how this study turned out. Your helpful comments, edits, and timely advice have been a big part of enhancing the quality of this thesis.

I am thankful to the chair of the thesis assessment board, prof.dr. Andrew Skidmore, for his valuable comments, constructive criticism, and evaluation during the proposal defense, midterm assessment, and thesis defense. I am also grateful to dr. Andreas Hirner, the external examiner of this thesis, for spending his valuable time evaluating the thesis and commenting during the defense. I sincerely thank drs. Raymond Nijmeijer for his effort, support, and help not only during this thesis but during my entire journey of this master's programme also. I express gratitude to all my teachers at Lund University and the University of Twente.

I am grateful to the GEM Programme Board and the European Commission for granting me an Erasmus+ scholarship for studying in this programme. I especially thank prof.dr. Andy Nelson, the programme coordinator; prof.dr. Petter Pilesjö and prof.dr. Jonas Ardö, the Lund University coordinator of GEM during our time; Ulrik Martinson, Raymond Nijmeijer, Laura Windig, Esther Hondebrink, Tia den Hartog-Muharamiah, and Eva Kovacs for their effort and assistance throughout my studies at Lund University and the University of Twente.

I want to take this opportunity to express my gratitude to my friends and acquaintances in Lund and Enschede who made my time enjoyable and helped me go through the difficulties by expressing love, care, and comfort. To Jana, thank you for all the moments, inspiration, and care for making my time easy and hopeful. I will cherish them my entire life. To Afif, thank you for all the help and assistance you have offered me. Thanks to Finn, Ibrahim, Chris, Anna, Maaz, Ademi, Anatoli, and Hendra for all your time and laughter on different occasions in Lund and Enschede. To Zannat, thanks for helping me as my welcome student at ITC and for all the times at study, parties and trips that made my time enjoyable. To Towhid, Muna, Mahir, Soikot, and Ebadullah, thanks for all the good times at parties, sports, and trips, making my time comfortable in Enschede. To Jessica, thanks for your company at DLR and parties during my stay in Munich. To dr. Milladur Rahman at Lund, thank you for looking after me and inviting me to your family and Bangladeshi community, which helped me feel at home in this foreign land. To Rafikul and dr. Salatul Islam, it was so nice to share an apartment with you. Thanks for all the advice, travels, and encouragement.

I cannot express my gratitude to my family in words. Their unconditional love, support, encouragement, and guidance made me what I am today. Their high hope for me always inspires me to move forward. I wish my heavenly father could see me at this stage today. Thanks to all my friends and relatives in Bangladesh, who always inspired me to achieve something better.

Above all, I am immensely grateful to almighty God for giving me strength and always making a way out of my problems throughout my study in this programme.

# TABLE OF CONTENTS

---

|   |           |
|---|-----------|
| <b>1. Introduction</b> .....  | <b>1</b>  |
| 1.1. Background of the study .....  | 1         |
| 1.2. Aim and objectives, research questions, and hypothesis .....                   | 5         |
| 1.2.1. Aim.....   | 5         |
| 1.2.2. Specific objectives .....  | 5         |
| 1.2.3. Research questions.....  | 5         |
| 1.2.4. Hypothesis.....  | 6         |
| 1.3. Study area.....  | 6         |
| <b>2. Data and Methods</b> .....  | <b>7</b>  |
| 2.1. Data.....  | 7         |
| 2.1.1. Climate and soil moisture data.....  | 7         |
| 2.1.2. Sentinel-2 imageries .....   | 10        |
| 2.2. Methods .....  | 11        |
| 2.2.1. Climate and soil moisture data pre-processing.....                           | 11        |
| 2.2.2. Estimation of vapor pressure and soil moisture deficit.....                  | 12        |
| 2.2.3. Pre-processing of Sentinel-2 image and FAPAR estimation .....                | 13        |
| 2.2.4. Estimation of PAR .....  | 14        |
| 2.2.5. Land cover map and maximum light use efficiency parameter.....               | 14        |
| 2.2.6. MOD17 model.....   | 17        |
| 2.2.7. GLO-PEM model.....   | 19        |
| 2.2.8. Model implementation and post-processing of NPP data .....                   | 20        |
| 2.2.9. Verification.....  | 20        |
| 2.2.10. Spatio-temporal distribution of NPP.....                                    | 21        |
| 2.2.11. Change detection, the relation of NPP with climate variables and SPEI ..... | 22        |
| 2.2.12. Significance of correlation and probability distribution .....              | 23        |
| <b>3. Results</b> .....   | <b>24</b> |
| 3.1. NPP from MOD17 and GLO-PEM model.....  | 24        |
| 3.1.1. Spatial distribution of NPP .....  | 24        |
| 3.1.2. Land cover wise quantification of NPP .....                                  | 29        |
| 3.2. Comparison of the estimated NPP with NPP from forest inventory .....           | 30        |
| 3.3. Comparison of the estimated NPP with MODIS products .....                      | 30        |
| 3.4. Inter-comparison of MOD17 and GLO-PEM NPP.....                                 | 33        |
| 3.5. Temporal change in NPP.....  | 33        |
| 3.6. Relation of NPP with climate variables and SPEI values .....                   | 36        |
| <b>4. Discussion</b> .....  | <b>42</b> |
| 4.1. MOD17 and GLO-PEM with Sentinel-2 data.....                                    | 42        |
| 4.2. Model outputs and performance .....  | 43        |
| 4.3. Impacts of the 2018 drought on NPP .....                                       | 45        |
| <b>5. Conclusion</b> .....  | <b>47</b> |
| References.....   | 49        |
| Annex I.....  | 58        |
| Annex II.....   | 60        |
| Annex III .....   | 61        |
| Annex IV.....   | 62        |

## LIST OF FIGURES

---

|  |    |
|--|----|
| <b>Figure 1.</b> The boundary of Bavaria Forest National Park with a topographic and hill shade map in the background (right). The location of Bavaria Forest National Park in the south-eastern part of the Germany (left). .....   | 6  |
| <b>Figure 2.</b> Methodological flowchart of the study. ....   | 9  |
| <b>Figure 3.</b> Monthly SPEI values from 2016 to 2021 with 01-month (a) and 03-month (b) time scales. ....  | 12 |
| <b>Figure 4.</b> Land cover maps from Corine and BFNP management. The simplified versions show the three main stands (evergreen coniferous, deciduous, and mixed). The other vegetated (grass, transitional woodland shrub, pasture, and meadows) and non-vegetated areas are merged into the “other” class. ....  | 15 |
| <b>Figure 5.</b> This Box and Whisker plot demonstrating the variations of the maximum light use efficiency (LUE) for different types of plants. The unit of measurement is $\text{gCMJ}^{-1}$ . ....  | 16 |
| <b>Figure 6.</b> Spatial distribution and temporal change of NPP from MOD17 model from 2016 to 2019 in the late growing season. The upper maps show the NPP values with positive and negative values, whereas the lower maps show only positive ones. ....   | 25 |
| <b>Figure 7.</b> Spatial distribution and temporal change of NPP from MOD17 model from 2020 to 2022 in the late growing season. The upper row shows the NPP values with positive and negative values, whereas the lower row shows only positive ones. ....   | 26 |
| <b>Figure 8.</b> Spatial distribution and temporal change of NPP from GLO-PEM model from 2016 to 2019 in the late growing season. The upper row shows the NPP values with positive and negative values, whereas the lower row shows only positive ones. ....   | 27 |
| <b>Figure 9.</b> Spatial distribution and temporal change of NPP from GLO-PEM model from 2020 to 2022 in the late growing season. The upper row shows the NPP values with positive and negative values, whereas the lower row shows only positive ones. ....   | 28 |
| <b>Figure 10.</b> Comparison between MOD17 (x-axis) and MODIS-NPP (y-axis) on some selected dates. The figures on x-axis and y-axis of each sub-figure is in $\text{kg}/\text{m}^2$ unit. The red line represents the linear trend line between the variables. ....  | 31 |
| <b>Figure 11.</b> Comparison between GLO-PEM (x-axis) and MODIS-NPP (y-axis) on some selected dates. The figures on x-axis and y-axis of each sub-figures are in $\text{kg}/\text{m}^2$ unit. The red line represents the linear trend line between the variables. ....  | 32 |
| <b>Figure 12.</b> The comparison of coefficient of determination (R-squared values) between the estimated NPP from MOD17 and GLO-PEM models. ....  | 33 |
| <b>Figure 13.</b> Spatial distribution of the slope of the linear trend in NPP from 2016 to 2022. The slope values in legend have a scale factor of 0.0001. The symbols here represent the locations of the sample points from which NPP values have been extracted. ....  | 34 |
| <b>Figure 14.</b> Time series plots and linear trend lines of three representative pixels from different types of land cover. The x-axis of the plots represents NPP in $\text{kg}/\text{m}^2/\text{day}$ units, whereas the y-axis shows the dates. ....  | 35 |
| <b>Figure 15.</b> Mean NPP values from MOD17 model in pre-drought (2016-2018) and post-drought (2019-2022) periods. ....   | 36 |
| <b>Figure 16.</b> Mean NPP values from GLO-PEM model in pre-drought (2016-2018) and post-drought (2019-2022) periods. ....   | 36 |
| <b>Figure 17.</b> Correlation coefficients ( $r$ ) of MOD17 NPP with daily minimum temperature, soil moisture deficit, and lag-1 soil moisture deficit. The correlation of NPP with real-time soil moisture deficit and lag-1 soil moisture deficit is in a negative direction. The x and y axis shows sample point numbers and r-values, respectively. .... | 37 |

**Figure 18.** Correlation coefficients of MOD17 NPP with real-time VPD and lag-3 VPD. The x and y axis shows sample point numbers and r-values, respectively..... 38

**Figure 19.** Probability density function distribution of the correlation coefficient values ( $r$ ) of MOD17-NPP with daily minimum temperature (upper left), lag-1 soil moisture deficit (upper right), real-time VPD (lower left), and lag-3 VPD (lower right) ..... 38

**Figure 20.** Correlation coefficients of GLO-PEM NPP with daily mean temperature, real-time soil moisture deficit, and lag-1 soil moisture deficit. The x and y axis shows sample point numbers and r-values, respectively..... 39

**Figure 21.** Correlation coefficients of GLO-PEM and real-time VPD and lag-3 VPD. The x and y axis shows sample point numbers and r-values, respectively..... 39

**Figure 22.** Probability density function distribution of the correlation coefficient values ( $r$ ) of GLO-PEM NPP with daily mean temperature (upper left), lag-1 soil moisture deficit (upper right), real-time VPD (lower left), and lag-3 VPD (lower right) ..... 40

**Figure 23.** Correlation coefficients of MOD17 and GLO-PEM NPP with lagged SPEI values with 03-month time scale. The lag period for GLO-PEM and MOD17 is 8 and 6, respectively. The x and y axis shows sample point numbers and r-values, respectively..... 41

## LIST OF TABLES

---

|   |    |
|---|----|
| <b>Table 1.</b> The input variables of some widely used light use efficiency-based models.....  | 4  |
| <b>Table 2.</b> An overview of the relevant data collected from GEE, including the data variables and their basic properties.....   | 8  |
| <b>Table 3.</b> Specification of Sentinel-2 data collected for this study.....  | 10 |
| <b>Table 4</b> The maximum LUE values used in this study (Running & Zhao, 2019). The same parameter value has been used for grassland and pasture. ....   | 17 |
| <b>Table 5.</b> The basic information about the primary productivity datasets was collected for verification purposes.....  | 20 |
| <b>Table 6.</b> The table shows a land cover-wise quantitative representation of NPP in Aug/Sep from 2016 to 2022. The numbers are in kilogram units. The calculation considers only positive values to avoid error-related distortion..... | 29 |
| <b>Table 7.</b> The summation of the mean daily NPP in all the sample points of the forest inventory. The numbers are in kgC/m <sup>2</sup> /day units.....   | 30 |

# 1. INTRODUCTION

## 1.1. Background of the study

The primary production of vegetation refers to a complex set of processes in which plants produce biomass by converting solar energy, carbon dioxide, and water (Roy et al., 2001). It serves as the major driver of ecosystem function and a measure of ecosystem dynamics. Through the carbon and water cycles, it contributes to the regulation of the global climate (Roy et al., 2001). It also serves as a point of entry for carbon from the atmosphere into the terrestrial biosphere. Many ecosystem services, including food and shelter for wildlife; food and fibre for humans, carbon sequestration; and climate change mitigation, depend on primary productivity (Song et al., 2013). The agenda 2021 of the United Nations (UN) sets directives for efficient monitoring of forests involving earth observation and modelling to combat deforestation (United Nations, 1992). Besides, one of the Sustainable Development Goals (SDG) that calls for monitoring forest health and growth is the conservation and sustainable management of terrestrial ecosystems to lessen the effects of human activity and climate change (United Nations, 2018). In EU Forest Strategy for 2030, the European Commission also emphasized the strengthening of forest monitoring, referring to productivity as an important indicator of forest growth in the Pan-European Ministerial Conference on the Protection of Forests (European Commission, 2021).

The measure of productivity deals with the quantity of carbohydrates produced by photosynthesis in a specific time interval over a given area (Roy et al., 2001). Green plants store a portion of absorbed solar energy (400 to 700 nm domain) in organic substances by photosynthesis, known as Gross Primary Productivity (GPP). Then, plants use some of this energy in organic compounds for their autotrophic respiration ( $R_a$ ), known as plant carbon loss. The balance after this carbon loss through  $R_a$  is called Net Primary Productivity (NPP) (Sala and Austin, 2000). NPP is an effective indicator for monitoring the forest health and stand age (He et al., 2012). A positive value of NPP indicates more carbon uptake by plants than release, which reflects the ecosystem's health and growth. Contrarily, a negative NPP means that respiration or decomposition outperforms plants' carbon absorption. Hence, NPP is a vital indicator of resource use, ecosystem health, and biosphere carbon fluxes (Cao et al., 2004a). NPP can also be used as an indicator to investigate the impact of an extreme climatic event like drought on the ecosystem (Lai et al., 2018; Nanzad et al., 2021). Since realized or actual light use efficiency (LUE) is regulated by temperature, humidity, and soil moisture (Potter et al., 1993), the drought impacts photosynthesis, eventually negatively affecting the carbon balance (He et al., 2014). Drought limits the plant's ability to draw water to its leaves reducing photosynthesis (Choat et al., 2012), affecting the balance between gross productivity and autotrophic respiration to reduce the NPP (He et al., 2014). Numerous studies revealed that the drought reduced the NPP of the terrestrial ecosystem on a local to global scale (Ciais et al., 2005; Zeng et al., 2005; Zhao & Running, 2010). This impact on productivity can also disrupt ecosystem services like timber, food, and fibre production, which has socio-economic consequences. The European landscape experienced a drought in 2018 that caused a temperature rise and precipitation deficit across the continent (Ahmed et al., 2021). Therefore, estimating forest NPP to determine its changes due to the drought event is vital.

Numerous models have been developed to estimate the NPP in diverse ecosystems utilizing different combinations of input variables, processes, and parameters for various biomes and environmental conditions (Cramer et al., 1999). These models can be classified as prognostic and diagnostic (Sasai et al., 2007). The prognostic models estimate the ecosystem carbon flux for future times using the climate data

predicted from the climate models [i.e., Biome Biogeochemical Cycles (BIOME-BGC) (Running & Hunt, 1993); Integrated Biosphere Simulator (IBIS) (Kucharik et al., 2000); Lund-Potsdam-Jena General Ecosystem Simulator (LPJ-GUESS) (Sitch et al., 2003)]. For example, LPJ-GUESS, which is a Dynamic Global Vegetation Model (DGVM) estimates ecosystem dynamics (i.e., GPP, NPP) in different spatial extent and time steps using climatic, solar radiation, carbon dioxide, and soil physical properties as input variables (Sitch et al., 2003). The DGVMs are complex process-based models that combine biogeography, plant physiology and biogeochemistry, vegetation dynamics, and biophysical processes in terrestrial ecosystem modelling. Due to their numerous input parameters, which can only be retrieved at a very coarse spatial resolution, these models have the drawback of being unable to be employed in (near) real-time.

The diagnostic models produce a realistic simulation of carbon fluxes throughout recent times using satellite and climate measurements [i.e., Carnegie-Ames-Stanford Approach (CASA) (Potter et al., 1993); Production Efficiency Model (PEM) (Nemani et al., 2003)]. The remote sensing-based diagnostic models can further be divided into three approaches (Song et al., 2013): (i) Statistical models estimate NPP based on a regression model linking NPP with one or more explanatory variables, such as meteorological parameters, evapotranspiration, atmospheric carbon dioxide, and Spectral Vegetation Indices (SVI). In this approach, the NPP is considered a dependent variable, whereas the meteorological parameters or SVIs are considered independent variables. Some examples of such type of NPP estimations include Goward et al. (1985), Tucker & Sellers (1986), and Sims et al. (2006); (ii) Parametric models, also known as LUE or production efficiency models, apply the LUE concept that refers to the quantity of carbon produced by absorbing per unit amount of Photosynthetically Active Radiation (PAR) (Monteith, 1972; Lieth, 1975; Monteith, 1977; Asrar et al., 1984). These models estimate the Absorbed Photosynthetically Active Radiation (APAR) from the product of the Fraction of Absorbed Photosynthetically Active Radiation (FAPAR) and PAR. FAPAR is generally measured from SVIs like Normalized Difference Vegetation Index (NDVI) as it linearly correlates to NDVI—a measure of the amount of chlorophyll and how much energy it absorbs (Myneni et al., 1997). It can also be estimated from Leaf Area Index (LAI) retrieved from earth observation data. Some examples of parametric (LUE-based) models are the Global Production Efficiency Model (GLO-PEM) (Prince & Goward, 1995), CASA (Potter et al., 1993), and MOD17 (Running et al., 2000); and (iii) Process-based models simulate biological processes that have impacts on NPP, i.e., photosynthesis, respiration, and transpiration. The algorithms of these models are not based on the LUE concept. However, they may use one or more input variables extracted from remote sensing data. For example, Running et al. (1989) and Liu (1997) used remote sensing data to estimate LAI as an input variable of the Forest-BGC and Boreal Ecosystem Productivity Simulator (BEPS) process-based model, respectively. Also, Smith et al. (2002) estimated canopy nitrogen content using hyperspectral remote sensing data as an input variable of the Photosynthesis and Evapotranspiration (PnET) model.

Among these three categories of models where remote sensing data are used, the LUE models have become popular, due to the abundance of remote sensing data with worldwide coverage and high temporal frequency. The advantage of LUE-based models over statistical or empirical models is that they consider the influences of environmental stressing factors on photosynthesis while modelling primary productivity. They involve fewer input variables and parameters and consist of a more straightforward algorithm than process-based models. These models have been used extensively to estimate the NPP in various terrestrial ecosystems involving various input variables and study areas ranging from local to global scale. Many LUE-based models have been developed so far, maintaining the primary methodology to estimate NPP involving two steps, first calculating GPP by multiplying APAR with LUE and then subtracting  $R_a$  to derive NPP. The maximum or potential LUE is a conversion rate that can only be achieved in an optimum environmental condition. Therefore, these models use some environmental scalars or stressor fractions to downregulate the maximum LUE to adjust its value in a given environmental condition. Some widely used LUE-based models are CASA (Potter et al., 1993), MOD17 (MODIS) (Running et al., 2000), GLO-PEM (Prince &

Goward, 1995a), C-Fix (Veroustraete et al., 1994), Biosphere Model Integrating Eco-physiological and Mechanistic Approaches using Satellite Data (BEAMS) (Sasai et al., 2005), Eddy Covariance-Light Use Efficiency (EC-LUE) (Yuan et al., 2007a), etc. Among these models, only the CASA model takes a different path by simulating NPP directly without estimating GPP beforehand. These models mainly differ in selecting and calculating maximum LUE environmental limiting factors. This is the key part of the algorithm where different model proposes different methods. Another variable is plant  $R_a$  where models vary in ways. Thus, the models have some differences in input data and parameters. Some input variables in the LUE-based model require remote sensing measurements, including PAR, FAPAR, etc., that can be acquired from different remote sensing sensors. PAR is generally calculated from incident solar radiation, measured by meteorological satellite or interpolation of ground-based observation. On the other hand, FAPAR estimation requires SVIs calculated from multispectral satellite imageries. Many satellite-based sensors that acquire multispectral images have been used in NPP estimation models, including MODIS, Landsat, SPOT-VGT, AVHRR, Sentinel-2, PROBA-V, IKONOS, etc. The type of sensor plays an important role in ecosystem modelling as they vary in temporal, spectral, and spatial resolutions. The source of other data like temperature, humidity, and soil moisture includes meteorological stations and remote sensing-based estimation.

MODIS is the most commonly used Satellite sensor in NPP modelling, followed by the Landsat (i.e., Palma et al., 2021; Chirici et al., 2022; Wang et al., 2022; Q. Liu et al., 2022). Understandably, MODIS is popular for its higher temporal resolution and a longer data availability period; however, the spatial resolution is lower than Landsat and Sentinel-2 data. The Sentinel-2 sensor created an opportunity to explore using high spatial and temporal resolution data for estimating vegetation carbon flux. Although a few studies have been conducted to generate NPP using Sentinel-2 data [i.e., Zheng & Takeuchi (2022) in a mangrove forest; Mngadi et al. (2022) in an urban forest; Miettinen et al. (2021) in a boreal forest], there are no studies that estimated NPP using LUE models and Sentinel-2 data in the temperate mixed forest.

As explained earlier, the LUE models vary in the source of input variables, environmental scalars,  $R_a$  and their estimating methods. Table 1 presents the input variables of some widely used LUE-based models. As can be seen from Table 1, among these models, GLO-PEM and MOD17 require a smaller number of input variables and hence seem to be more feasible models for NPP estimation.

**Table 1.** The input variables of some widely used light use efficiency-based models.

| Model   | Ref.                      | SOL | PAR | FAPAR | SW | NDVI | Max. LUE | Temp. | Topt | VPD | SM | LE | H | Prec. | ET | PET | RH | EF |
|---------|---------------------------|-----|-----|-------|----|------|----------|-------|------|-----|----|----|---|-------|----|-----|----|----|
| EC-LUE  | Yuan et al., 2007         |     | ✓   | ✓     | ✓  | ✓    | ✓        | ✓     |      |     | ✓  | ✓  | ✓ |       |    |     |    | ✓  |
| CASA    | Potter et al., 1993       | ✓   |     | ✓     | ✓  | ✓    | ✓        | ✓     | ✓    |     | ✓  |    |   | ✓     | ✓  |     |    |    |
| MOD17   | Running et al., 2000      |     | ✓   | ✓     | ✓  | ✓    | ✓        | ✓     |      | ✓   |    |    |   |       |    |     |    | ✓  |
| GLO-PEM | Prince & Goward, 1995     |     | ✓   | ✓     | ✓  | ✓    | ✓        | ✓     |      | ✓   | ✓  |    |   |       |    |     |    | ✓  |
| C-Fix   | Veroustraete et al., 1994 | ✓   |     | ✓     | ✓  | ✓    | ✓        | ✓     |      |     | ✓  | ✓  | ✓ |       |    |     |    |    |

Note: SOL = total incoming solar radiation; PAR = Photosynthetically active radiation; FAPAR = Fraction of absorbed PAR; SW = Shortwave radiation; NDVI = Normalized difference vegetation index; Max. LUE = Maximum or potential light use efficiency; Temp. = Temperature, Topt = Optimum temperature; VPD = Vapor pressure deficit; SM = Soil moisture; LE = Latent heat flux; H = Sensible heat flux; Prec. = Precipitation; ET = Evapotranspiration; PET = Potential evapotranspiration; RH = Relative humidity; EF = Evaporative fraction.

The MOD17 algorithm was mainly developed to be applied using MODIS satellite data with coarse spatial resolution (Running et al., 1994; Running et al., 2000; Zhao et al., 2005). The performance of this algorithm has been evaluated by comparing it to eddy covariance flux tower data and forest inventory data in many studies (i.e., Reichstein et al., 2003; Turner et al., 2006; Shim et al., 2014; Sjöström et al., 2013; Zhu et al., 2016).. The performance of the MOD17 algorithm when used with high spatial resolution data such as Sentinel-2 data remains unexplored. In the case of the GLO-PEM model, the algorithm was developed to estimate all of the input variables except PAR using remote sensing data such as AVHRR, a coarse spatial resolution sensor which was used for the original model run. Furthermore, it took an indirect approach to estimate temperature, vapor pressure deficit (VPD), and soil moisture from the thermal band of AVHRR data instead of using meteorological observation, contributing to the uncertainty in the model output. Thus, this study intends to use these input variables (i.e., temperature, VPD, soil moisture) from meteorological data in this model. This approach will give new insight into the model's performance when the environmental scalars are estimated using meteorological measurements rather than estimates based on thermal images.. The algorithms of the selected two models are also different. For instance, MOD17 uses minimum temperature and VPD as a scalar, whereas GLO-PEM uses mean temperature, VPD, and soil moisture deficit. Moreover, the two models take different approaches to estimating Maintenance Respiration ( $R_m$ ), but similar approach to estimating Growth Respiration ( $R_g$ ).

This study investigates the NPP estimation by employing MOD17 and GLO-PEM models with Sentinel-2 data and investigate its changes during the drought event. The variation in selected models' algorithms, input variables, and high spatial resolution data will provide new scientific evidence in NPP estimation in the temperate ecosystem. The findings will also help explore the potential of Sentinel-2 data in LUE-based NPP models. The study takes place in Bavaria Forest National Park (BFNP), a mixed temperate forest inhabited mainly by coniferous (i.e., Spruce) and deciduous (i.e., European Beech) trees. The main advantage of this study area is its mixed forest type, which will help us understand the application of our modelling approach for various plant species. West-central Europe, where the study area is situated, suffered from a drought in 2018, one of the most severe meteorological droughts in the last four decades (Aalbers et al., 2023). The study period extends from 2016 until 2022 and allows obtaining the temporal variation of NPP before and after the 2018 Drought.

## **1.2. Aim and objectives, research questions, and hypothesis**

### **1.2.1. Aim**

The aim of the study is to investigate the changes in net primary productivity retrieved using Sentinel-2 data during an extreme climatic event in a mixed temperate forest.

### **1.2.2. Specific objectives**

- I. To evaluate the performance of MOD17 and GLO-PEM models in estimating NPP using Sentinel-2 data.
- II. To investigate the temporal changes in NPP values from 2016 to 2022 to detect the impact of the 2018 drought event.

### **1.2.3. Research questions**

- I. What is the relation between the estimated NPP from the MOD17 and GLO-PEM models?
- II. To what extent has the 2018 drought event affected the primary productivity of forest stands in BFNP?

### 1.2.4. Hypothesis

- I. The estimated NPP from both models has a relation with the NPP estimated from MODIS products and forest inventory data; however, the relationship is stronger with the GLO-PEM model than MOD17.
- II. There is a decrease in estimated NPP during the drought year in or after 2018.

### 1.3. Study area

The Bavaria Forest National Park (BFNP) is situated at the Eastern Bavaria Forest in Germany along the border of the neighbouring Czech Republic (Figure 1). The park was established in 1970. The total area of the BFNP is around 242 km<sup>2</sup> with an elevation in-between 650 and 1,453 m from the average sea level. The park is part of an ancient mountainous area called Bohemian Masse, formed of granite and gneiss, which are a type of crystalline rocks (van der Knaap et al., 2020). It has a cool and humid climate with varying temperatures and precipitation in high and low elevations. The yearly mean temperature varies in-between 3°C (at high altitude) and 6.5°C (at low altitude).

In the same way, precipitation also varies from 1,000 mm (at low elevation) to 2,500 mm (at high elevation). The forest ground remains ice-covered for around two months in a year (maximum temperature < 0°C), whereas frost days account for more than four months (minimum temperature < 0 °C). Most of the area of BFNP is covered by forest (about 97%), inhabited by coniferous, deciduous, and some other types of plants also. The dominant species in BFNP include Norway spruce (*picea abies*), European beech (*fagus sylvatica*), Silver fir (*abies alba*), Larch (*larix*), White birch (*Bopern papyrifera*), Sycamore maple (*acer pseudoplatanus*), and Common rowan (*sorbus aucuparia*). BFNP also contains dead wood, including fallen and standing dead trees resulting from Bark beetle infestation (Krzystek et al., 2020).

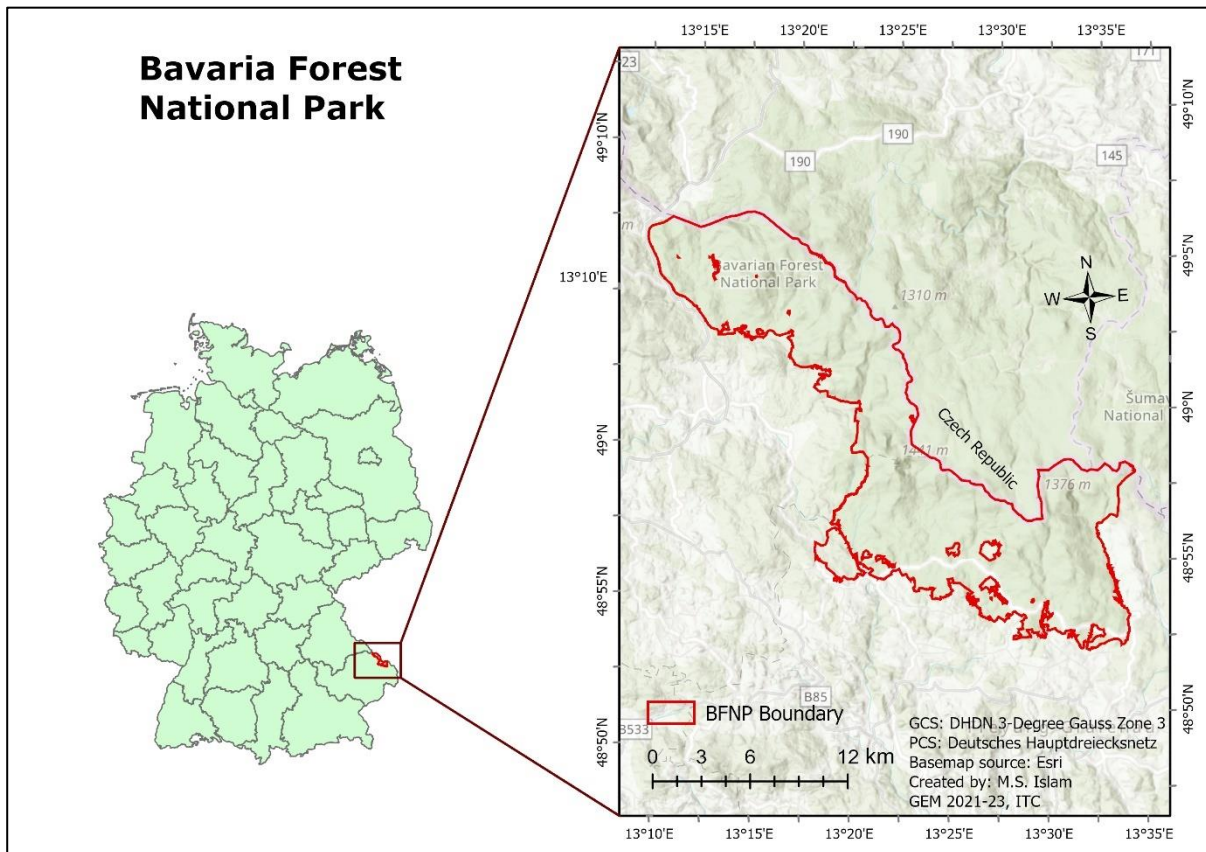


**Figure 1.** The boundary of Bavaria Forest National Park with a topographic and hill shade map in the background (right). The location of Bavaria Forest National Park in the south-eastern part of the Germany (left).

## 2. DATA AND METHODS

The study used satellite imageries, climate reanalysis data (fusion between ground observation and model estimation where satellite-based measurements are also involved), available primary productivity products and forest inventory data. In supplement to the detailed description of the data and methods, Figure 2 shows a general overview of the workflow of data, methods, and outputs.

### 2.1. Data

#### 2.1.1. Climate and soil moisture data

The estimation of NPP involves different climate variables that mainly work as downregulating factors of the maximum LUE values. The climate variables include minimum temperature, mean temperature, dew point temperature, relative humidity, saturation vapour pressure, vapour pressure deficit, soil moisture, field capacity of the soil, soil moisture deficit, and incident solar radiation. Most of these climate variables have been used to estimate the scalars of LUE for both models except the incident solar radiation. For instance, the MOD17 model requires minimum temperature and vapour pressure deficit scalars. The estimation of vapour pressure deficit requires relative humidity and saturation vapour pressure. The mean temperature and dew point temperature are required to estimate the relative humidity, whereas saturation vapour pressure requires mean temperature. On the other hand, the GLO-PEM model requires temperature and soil moisture deficit scalars in addition to VPD scalars. Estimating soil moisture deficit involves the soil's field capacity or maximum water retention capacity. Apart from these climate variables, incident solar radiation is required to estimate the PAR.

Most of the climate data has been collected from the ERA5 dataset of the European Centre for Medium-Range Weather Forecasts (ECMWF) disseminated by the Climate Data Store of Copernicus Climate Change Service (<https://www.ecmwf.int/en/forecasts/dataset/ecmwf-reanalysis-v5>). ERA5 indicates the fifth-generation version of the ECMWF Re-Analysis (ERA) dataset. The re-analysis dataset is prepared by combining the observed data from the weather station with the simulated data from the climate model into a complete and consistent dataset on a global scale. The data pre-processing, including data calling, downscaling, sub-setting, calculation, and exporting, was performed in Google Earth Engine (GEE) platform using JavaScript programming. Several datasets of ERA5 available on GEE vary in timestep, period of availability, and variables. Table 2 compiles the basic information of the climate variables collected from different data collections. The mean, minimum, and dew point temperatures are available in "ECMWF/ERA5/DAILY" data collection until 09<sup>th</sup> July 2020. Therefore, the mean and dew point temperatures after this date have been collected from "ECMWF/ERA5\_LAND/DAILY\_RAW" collection for the remaining period.

On the other hand, the minimum temperature after 09<sup>th</sup> July 2020 has been estimated from the hourly temperature data in the "ECMWF/ERA5\_LAND/HOURLY" data collection. A day's minimum hourly temperature was considered the daily minimum temperature. The incident solar radiation, also known as the short-wave radiation, has been collected from ECMWF/ERA5\_LAND/DAILY\_RAW data collection for the entire study period. The soil moisture data for a 01-meter depth has been collected from "NASA/SMAP/SPL4SMGP/007" data collection, which disseminates the soil moisture data generated from the Soil Moisture Active Passive (SMAP) satellite of National Aeronautics and Space Administration (NASA) that carries both active and passive remote sensing sensors (<https://nsidc.org/data/spl4smgp/versions/7>). This data has been provided by National Snow and Ice

Data Center (NSIDC), United States. The daily soil moisture data has been calculated by averaging the three-hourly data of a day.

In addition to the pixel-wise climate data from ERA5, field-measured climate data from a weather station in the study area have been collected. This dataset contains hourly time series data of different climate variables, including mean, minimum, maximum temperature, dew point temperature, air pressure, humidity, wind speed, and wind direction. However, this data were not measured spatially but in a point hence we did not use these data for pixel-wise spatial estimation of NPP.

The monthly Standardized Precipitation and Evapotranspiration Index (SPEI) values (Vicente-Serrano et al., 2010) from 2016 to 2021 have been collected from Spanish National Research Council (<http://hdl.handle.net/10261/288226>) to show the drought occurrence and detect the drought impacts on NPP. This dataset is available on GEE platform in CSIC/SPEI/2\_8 data collection. The collected dataset contains SPEI values with one-month and three-month time scales with 0.5-degree spatial resolution. The one-month time scale means the input variables (precipitation, evapotranspiration) of the index have been accumulated over the past one month, whereas the three-month scale is based on a three-month accumulation period.

**Table 2.** An overview of the relevant data collected from GEE, including the data variables and their basic properties.

| No. | Data Collection on GEE     | Variables                | Period         | Timestep                           | Spatial Resolution |
|-----|----------------------------|--------------------------|----------------|------------------------------------|--------------------|
| 1.  | ECMWF/ERA5/DAI LY          | Mean temperature         | 2016-July 2020 | Daily                              | 27830 m            |
|     |                            | Minimum temperature      | 2016-July 2020 | Daily                              | 27830 m            |
|     |                            | Dew point temperature    | 2016-July 2020 | Daily                              | 27830 m            |
| 2.  | ECMWF/ERA5_LAN D/DAILY_RAW | Mean temperature         | July 2020-2022 | Daily                              | 11132 m            |
|     |                            | Dew point temperature    | July 2020-2022 | Daily                              | 11132 m            |
|     |                            | Incident solar radiation | 2016-2022      | Daily                              | 11132 m            |
| 3.  | ECMWF/ERA5_LAN D/HOURLY    | Minimum temperature      | July 2020-2022 | Daily, calculated from hourly data | 11132 m            |
| 4.  | NASA/SMAP/SPL4S MGP/007    | Soil moisture            | 2016-2022      | Daily, calculated from 3-hrs data  | 11000 m            |
| 5.  | CSIC/SPEI/2_8              | SPEI                     | 2016-2021      | Monthly                            | 55660 m            |

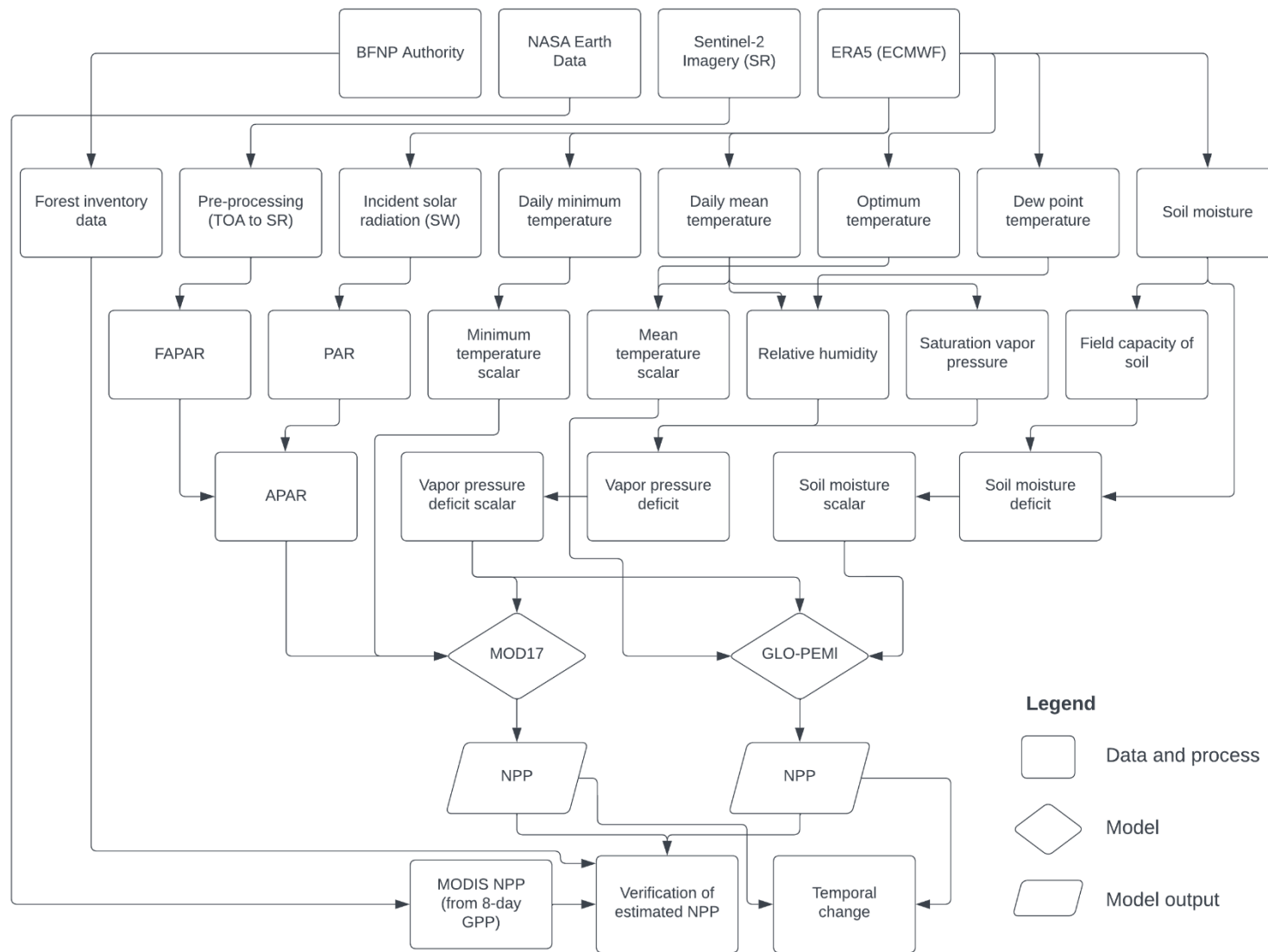


Figure 2. Methodological flowchart of the study. .

### 2.1.2. Sentinel-2 imageries

The satellite imageries from the Sentinel-2 sensor were collected from Copernicus Open Access Hub from 2016 to 2022. Since BFNP is a mountainous region, cloud cover is a big obstacle for optical remote sensing. Therefore, special attention was given to selecting images with no cloud or lowest cloud in the area of interest. Although Sentinel-2 has 10-day revisit time and reduced to 5 days for the constellation of Sentinel-2A and Sentinel-2B, only one usable image has been found in a month due to the high cloud cover percentage. The focus of the investigation was on the growing season. Therefore, most of the images collected were acquired between March and October. In total, 45 images have been collected from 2016 to 2022. The basic properties of Sentinel-2 imageries are given in this Table 3. The Sentinel-2 images have different spatial resolutions for various bands; however, the spatial resolution reported in Table 3 is for Band-4 and Band-8, which were used in this study. The Level-1C image contains top-of-atmospheric reflectance data in cartographic geometry, whereas the Level-2A image contains atmospherically corrected surface reflectance data in cartographic geometry.

**Table 3.** Specification of Sentinel-2 data collected for this study.

| No. | Year | Acquisition Date | Level    | Tile   | Spatial Resolution |
|-----|------|------------------|----------|--------|--------------------|
| 1.  | 2016 | 09-05-2016       | Level-1C | T33UUQ | 10 m               |
| 2.  |      | 08-07-2016       | Level-1C | T33UUQ | 10 m               |
| 3.  |      | 27-08-2016       | Level-1C | T33UUQ | 10 m               |
| 4.  |      | 16-10-2016       | Level-1C | T33UUQ | 10 m               |
| 5.  | 2017 | 25-03-2017       | Level-1C | T33UUQ | 10 m               |
| 6.  |      | 24-04-2017       | Level-2A | T33UUQ | 10 m               |
| 7.  |      | 13-06-2017       | Level-2A | T33UUQ | 10 m               |
| 8.  |      | 13-07-2017       | Level-2A | T33UUQ | 10 m               |
| 9.  |      | 17-08-2017       | Level-1C | T33UUQ | 10 m               |
| 10. |      | 26-09-2017       | Level-1C | T33UUQ | 10 m               |
| 11. |      | 16-10-2017       | Level-1C | T33UUQ | 10 m               |
| 12. | 2018 | 25-03-2018       | Level-2A | T33UUQ | 10 m               |
| 13. |      | 19-04-2018       | Level-2A | T33UUQ | 10 m               |
| 14. |      | 29-05-2018       | Level-2A | T33UUQ | 10 m               |
| 15. |      | 08-06-2018       | Level-2A | T33UUQ | 10 m               |
| 16. |      | 03-07-2018       | Level-2A | T33UUQ | 10 m               |
| 17. |      | 27-08-2018       | Level-2A | T33UUQ | 10 m               |
| 18. |      | 16-09-2018       | Level-2A | T33UUQ | 10 m               |
| 19. |      | 16-10-2018       | Level-2A | T33UUQ | 10 m               |
| 20. |      | 15-11-2018       | Level-2A | T33UUQ | 10 m               |
| 21. | 2019 | 30-03-2019       | Level-2A | T33UUQ | 10 m               |
| 22. |      | 24-04-2019       | Level-2A | T33UUQ | 10 m               |
| 23. |      | 19-05-2019       | Level-2A | T33UUQ | 10 m               |
| 24. |      | 28-06-2019       | Level-2A | T33UUQ | 10 m               |
| 25. |      | 23-07-2019       | Level-2A | T33UUQ | 10 m               |
| 26. |      | 27-08-2019       | Level-2A | T33UUQ | 10 m               |
| 27. |      | 31-10-2019       | Level-2A | T33UUQ | 10 m               |
| 28. |      | 30-12-2019       | Level-2A | T33UUQ | 10 m               |
| 29. | 2020 | 24-03-2020       | Level-2A | T33UUQ | 10 m               |
| 30. |      | 18-05-2020       | Level-2A | T33UUQ | 10 m               |
| 31. |      | 02-06-2020       | Level-2A | T33UUQ | 10 m               |
| 32. |      | 22-07-2020       | Level-2A | T33UUQ | 10 m               |

| No. | Year | Acquisition Date | Level    | Tile   | Spatial Resolution |
|-----|------|------------------|----------|--------|--------------------|
| 33. |      | 21-08-2020       | Level-2A | T33UUQ | 10 m               |
| 34. |      | 20-09-2020       | Level-2A | T33UUQ | 10 m               |
| 35. |      | 25-02-2021       | Level-2A | T32UQV | 10 m               |
| 36. | 2021 | 28-04-2021       | Level-2A | T33UUQ | 10 m               |
| 37. |      | 17-06-2021       | Level-1C | T33UUQ | 10 m               |
| 38. |      | 25-09-2021       | Level-2A | T32UQV | 10 m               |
| 39. |      | 09-03-2022       | Level-2A | T32UQV | 10 m               |
| 40. |      | 24-03-2022       | Level-2A | T32UQV | 10 m               |
| 41. |      | 27-06-2022       | Level-2A | T32UQV | 10 m               |
| 42. | 2022 | 17-07-2022       | Level-2A | T32UQV | 10 m               |
| 43. |      | 16-08-2022       | Level-2A | T32UQV | 10 m               |
| 44. |      | 10-10-2022       | Level-2A | T32UQV | 10 m               |
| 45. |      | 14-11-2022       | Level-2A | T32UQV | 10 m               |

## 2.2. Methods

### 2.2.1. Climate and soil moisture data pre-processing

The climate and soil moisture dataset underwent a series of pre-processing steps before they were ready to use as input variables for scalar estimation. The pre-processing works include unit conversion, downscaling, clipping, and harmonization to the same coordinate reference with an exact number of rows and columns. Using JavaScript code, the unit conversion, downscaling, and sub-setting steps were performed on the GEE environment. Several GEE scripts were prepared to call the data from relevant data collection (Table 2), pixel-wise downscale the data to match the pixel size of the Sentinel-2 image, subset them according to the geometry of BFNP's boundary, and finally export the data.

The bicubic resampling technique has been used to downscale the climate and soil moisture data. This technique preserves the essential information and minimizes the loss of details while reducing the pixel size. The mathematical algorithm of this technique involves interpolating the pixel values based on a 4x4 window of surrounding cells (Jähne, 1993). The Bicubic interpolation uses cubic polynomials to calculate the new pixel values between the original data points, considering a more extensive set of neighbouring pixels than other simpler interpolation techniques. This method is a commonly used technique in climate data down-sampling. Shah et al. (2023) reported that the bicubic resampling technique is a suitable interpolation method for climate data in a raster format.

The climate datasets were originally provided in the Kelvin unit, which was converted to the Celsius unit by subtracting 273.15. Since the operations involving multiple raster layers require an exact number of rows and columns, all the climate and soil moisture layers have been harmonised into the same geometry with an exact number of rows and columns. Before that, the raster layers were clipped by the boundary layer of BFNP. This harmonisation task was performed in ArcGIS Pro using a model in the model builder environment.

To visualise and analyse the SPEI values, a sample point from the middle part of BFNP was taken randomly (13.38242845688875, 48.98504189801222) to extract the monthly SPEI values from 2016 to 2021. Since the SPEI layer has a very coarse spatial resolution (about 55 km), one sample point is enough to show the SPEI values in the study area. Figure 3 shows a time series plot containing monthly SPEI values with a 01-month and 03-month time scale. In 2018, most SPEI values were around -1.5 and below -0.5 for the 03-

month and 01-month scales, respectively. After 2018, the increased number of values below -0.5 in both scales shows the drought situation's continuity. Furthermore, a short drought period can be seen in-between late 2016 and early 2017, although less severe than in 2018. In short, the 2018 drought is the most severe as most values (from April to November) are around -1.5 in the 03-month scale (more appropriate than the 01-month scale for drought monitoring), which indicates severe drought conditions (Rhee & Im, 2017). The SPEI values are interpreted as extremely wet ( $\geq 2$ ), very wet (1.5 to 1.99), moderately wet (1.0 to 1.49), near normal (0.99 to -0.99), moderate drought (-1.0 to -1.49), severe drought (-1.5 to -1.99), and extreme drought ( $\leq -2$ ) (Rhee & Im, 2017).

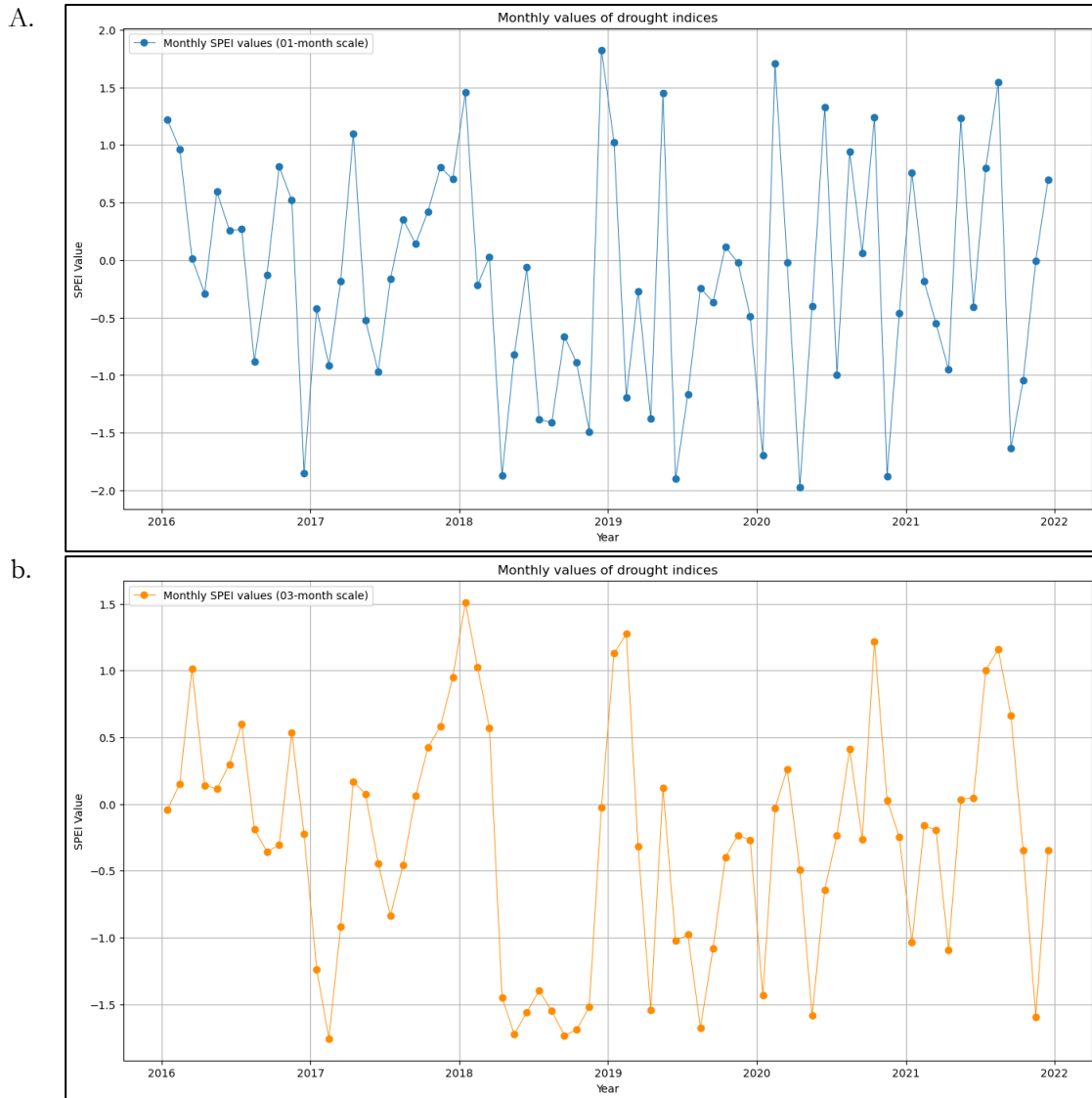


**Figure 3.** Monthly SPEI values from 2016 to 2021 with 01-month (a) and 03-month (b) time scales.

### 2.2.2. Estimation of vapor pressure and soil moisture deficit

The models require several scalars to down-regulate the maximum LUE values. The scalars include the VPD and soil moisture deficit scalars. Estimating these scalars requires estimating the VPD and soil moisture deficit in the first place. VPD can be defined as the difference between the saturation vapour pressure and actual vapour pressure. Saturation vapour pressure is the maximum water vapour in air at a particular temperature. It is the pressure water vapour molecules produce when air is saturated with moisture and in

equilibrium with a water surface like a liquid water body or wet soil. On the other hand, actual vapour pressure is the pressure water vapour molecules in the air at a specific temperature put on each other. It shows the total amount of water vapour in the air, regardless of how much water it can hold simultaneously. The VPD was estimated by the following equation (Eq. 1)

$$\text{VPD} = \text{ES} - (\text{ES} * \text{Rh}) \quad (1)$$

where VPD is Vapor pressure deficit, ES stands as Saturated vapor pressure, 'Es \* Rh' denotes as Actual vapor pressure, and Rh is Relative humidity. The ES in Eq.1 was estimated by the following equation (Eq. 2) using the mean temperature and some constant parameters as input variables.

$$\text{ES} = (6.112 * \exp((17.67 * T) / (T + 243.5))) * 100 \quad (2)$$

where T stands as Mean temperature. The VPD in Eq. 1 also requires Rh as an input variable. Rh is a measurement of the air's water vapour content in relation to the air's maximal water vapour capacity at a given temperature. The equation was used to calculate the Rh (Eq. 3) in the unitless equation as a fraction.

$$\text{Rh} = \exp((17.269 * T_d)/(273.3 + T_d) - (17.269 * T_a)/(237.3 + T_a)) \quad (3)$$

where T<sub>d</sub> and T<sub>a</sub> denote as Dew point temperature and Mean temperature, respectively.

Another water-related scalar is soil moisture deficit which is the difference between available soil moisture and the maximum water-holding capacity of soil at a given time. The maximum water-holding capacity of soil is also known as the field capacity. The value of the field capacity depends on several factors, like soil texture, organic matter content, soil structure, compaction, soil depth, slope, aspect, and drainage pattern (Cassel & Nielsen, 2018). In this study, the maximum available soil moisture from 2016 to 2022 has been considered as the maximum water-holding capacity of the soil, assuming that the soil was saturated at that specific occurrence.

### 2.2.3. Pre-processing of Sentinel-2 image and FAPAR estimation

The Sentinel-2 images collected for this study come from two sensors of the Sentinel-2 constellation, i.e., Sentinel-2A and Sentinel-2B. The Sentinel-2A was launched in June 2015, while the other sensor was launched in March 2017. The collected images contain both Level-1C and Level-2A products. The Level-1C products are radiometrically and geometrically corrected data, but they need further processing to remove the atmospheric distortions. Therefore, they underwent atmospheric and topographic corrections to convert them from top-of-atmospheric reflectance to surface reflectance. This processing was conducted using a software tool named Sen2Cor, also known as Sentinel-2 Level-2A Processor, developed by the European Space Agency (ESA) (<https://step.esa.int/main/snap-supported-plugins/sen2cor/sen2cor-v2-11/>). Sen2Cor uses advanced algorithms to quantify and eliminate air scattering and absorption from particles, water vapour, and ozone levels. Sen2Cor also performs terrain correction to mitigate the terrain (elevation, slope, aspect) originated distortion (Main-Knorn et al., 2017). This pre-processing was performed for the whole tile of the image.

The reflectance values of the Sentinel-2 images from red and near-infrared (NIR) bands were the input variables of FAPAR estimation. The FAPAR is the fraction of PAR that the green vegetations absorb for photosynthesis (Yang et al., 2014). In remote sensing-based ecosystem modelling, it is typically estimated from a vegetation index. In this study, the FAPAR was estimated using the NDVI based on an empirical relationship between these two variables. Myneni & Williams (1994) examined the relations between FAPAR

and NDVI under different conditions that may affect the reflectance from vegetation, i.e., soil reflectance, leaf orientation and optical properties, and atmospheric and bidirectional effects. They established a linear model between FAPAR and NDVI, which has been used in this study. The model is expressed in the following equation (Eq. 4). The band math tool of SNAP software was used to process the estimation of NDVI and FAPAR. Later, ArcGIS Pro was used to post-process the FAPAR layers, i.e., sub-setting and harmonization with other variables.

$$\text{FAPAR} = 1.164 * \text{NDVI} - 0.143 \quad (4)$$

The constant 1.164 is the slope or conversion coefficient of the relation, whereas the constant 0.143 represents the intercept or offset.

#### 2.2.4. Estimation of PAR

The primary productivity estimation also involves PAR as a significant variable. The electromagnetic spectrum's blue, green, and red wavelengths are included in this spectrum, which spans 400 to 700 nm. The metabolic reactions that are required for photosynthesis must be fuelled by PAR. Plant growth, development, and energy generation are fuelled by the complicated chemical processes that are started when the chlorophyll pigments inside plant cells absorb PAR. This study estimated PAR from the total incident solar radiation, also known as Shortwave Radiation (SWR), collected from the ERA5 reanalysis dataset provided by ECMWF. A GEE script was prepared and executed to call the data from ECMWF/ERA5\_LAND/DAILY\_RAW collection, downscale the data to 10 m spatial resolution, change unit from J/m<sup>2</sup>/day to MJ/m<sup>2</sup>/day, and export the data as GeoTIFF format. Some basic properties of this data collection, including the incident solar radiation variable, are given in Table 2. The SWR raster layers also underwent post-processing, like sub-setting by BFNP boundary and harmonisation to the same coordinate systems and row and column numbers of other data layers. Finally, the PAR was estimated by multiplying the SWR with a coefficient (0.45) (Running & Zhao, 2019). In addition to this pixel-wise PAR data estimated from the incident short wave radiation, a time series data of PAR with 20-minute intervals have been collected from a field-based measurement system. However, the topography of the study area is not flat. There is a variation in the elevation, which influences the quantity of the incident solar radiation. Therefore, instead of using the same PAR value for the entire study area measured in a point, the pixel-wise estimation of PAR from ERA5 data has been used in this study.

#### 2.2.5. Land cover map and maximum light use efficiency parameter

The land cover map is an essential input variable in ecosystem modelling as the models have plant type-specific parameters. Two land cover maps have been collected from Copernicus Land Monitoring Service, known as Corine Land Cover, and BFNP authority (Figure 4). The latest version of the Corine land cover map collected for this study was prepared in 2018 with 100 m spatial resolution (<https://land.copernicus.eu/pan-european/corine-land-cover>). This map was downscaled to 10 m spatial resolution using the bilinear resampling method. The land cover classes in the Corine land cover map are consistent with the plant types and their specific parameter values in the models (Table 4). Therefore, this map was used in the models. On the other hand, the land cover map from BFNP authority was used to mask the study area to keep only the vegetated areas for further analysis of the model outputs. Figure 4 shows the simplified version of both maps. The “other” class in Corine map contains mainly non-vegetated areas, whereas the “other” class in BFNP map contains meadows, dead wood, scrub pine, and other non-vegetated areas.

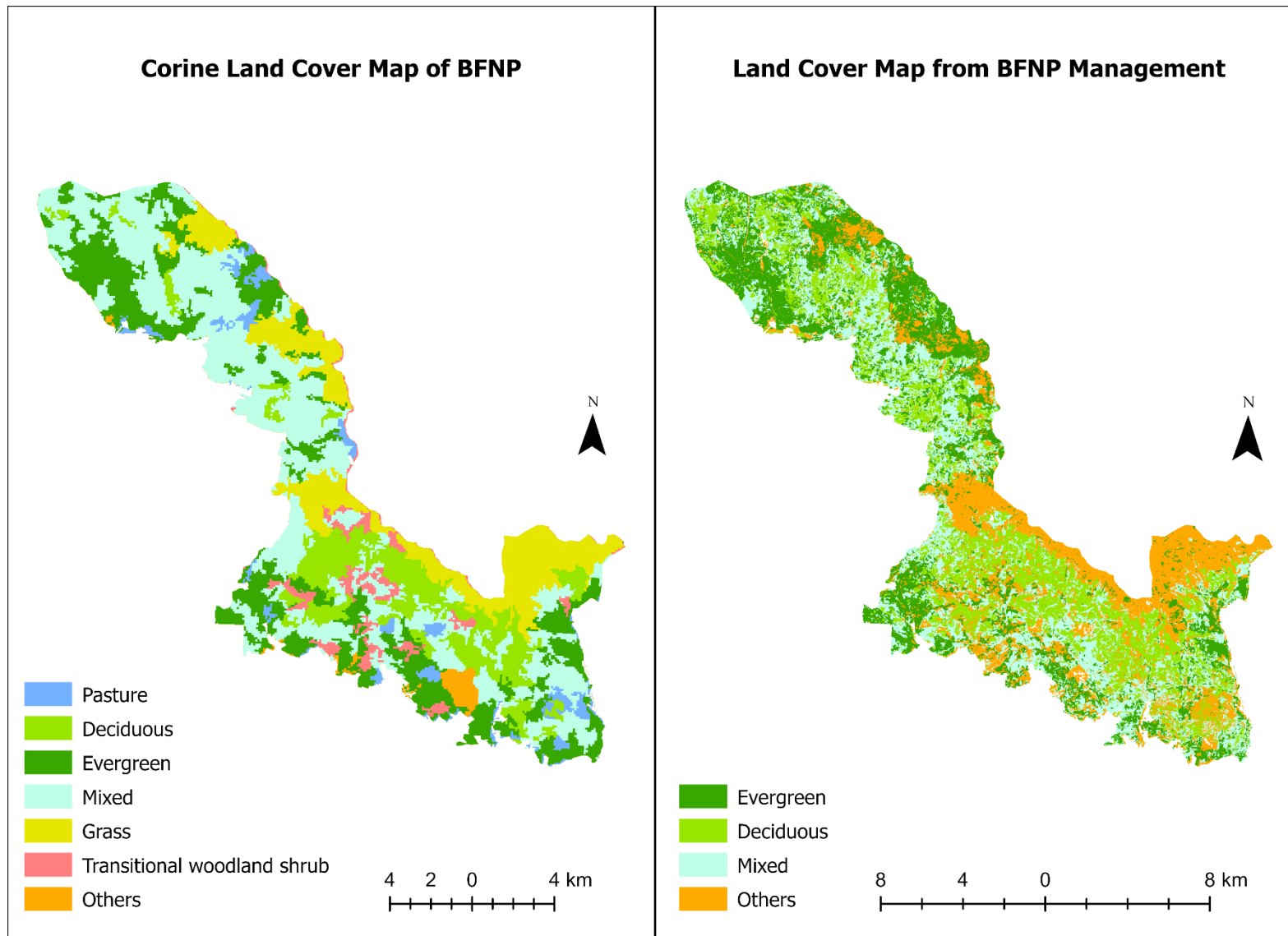


**Figure 4.** Land cover maps from Corine and BFNP management. The simplified versions show the three main stands (evergreen coniferous, deciduous, and mixed). The other vegetated (grass, transitional woodland shrub, pasture, and meadows) and non-vegetated areas are merged into the “other” class.

Maximum LUE describes an organism's capacity to effectively transform absorbed light into chemical energy through photosynthesis. It is a significant factor in determining the primary productivity and accumulation of plant biomass. The idea is frequently expressed as a ratio between the rate of carbon uptake, also known as the net photosynthetic rate and the amount of absorbed photosynthetically active radiation (PAR). In light usage efficiency models, estimating NPP is crucial. The determination of how effectively plants convert absorbed light energy into chemical energy is a key component of light usage efficiency models, which are used to estimate NPP. In LUE-based models, the variable of maximum LUE is used as a constant; however, the variable's value differs according to the types of plants. Besides, different values are suggested by different models. Moreover, many studies optimized this value for any specific ecosystem or plant type, which also differs from the original suggested value by the model developers. A thorough literature review was conducted to find the maximum LUE values in this study.

The literature suggests that the optimal range of the values of the maximum LUE varies with geographical location, plant types, and weather conditions. Furthermore, the estimation and calibration methods also influence the values of this parameter. An overview of the maximum LUE values for different types of ecosystems is available in Annex 1. The importance of this parameter varies from 0.5 to 1.8 gC/MJ. The parameter value ranges from 0.8 to 2.14 gC/MJ in the evergreen needle leaf plants. On the other hand, the range of the parameter values is slightly lower for the mixed forest (i.e., 1.9 to 2.14 gC/MJ). A visual representation of the variation of maximum LUE values according to the plant types can be seen in Figure 5, compiling data from the table in Annex I. The figure 5 shows the minimum, maximum, median, lower and upper quartile, and outlier for different plant types. Although many studies used various parameter values for different plants, some studies used a single value for different plant types irrespective of geography and ecosystem types (i.e., Yuan et al., 2007b). However, this study used different maximum LUE values for different plant types since the conversion efficiency from energy to carbon depends on the plant's physiology. Table 4 shows the values of the maximum LUE found in the literature for different kinds of plants used in this study.

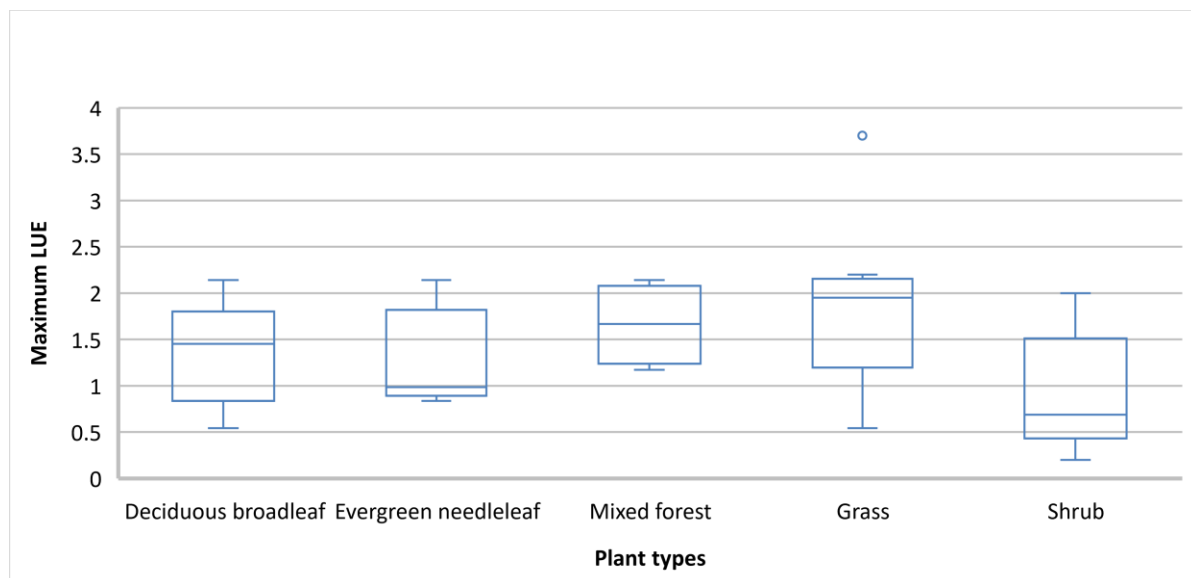


**Figure 5.** This Box and Whisker plot demonstrating the variations of the maximum light use efficiency (LUE) for different types of plants. The unit of measurement is gC/MJ.

**Table 4** The maximum LUE values used in this study (Running & Zhao, 2019). The same parameter value has been used for grassland and pasture.

| Plant/land cover type       | Max. LUE | Unit                     |
|-----------------------------|----------|--------------------------|
| Broad-leaved Deciduous      | 0.001165 |                          |
| Needle-leaved Coniferous    | 0.000962 |                          |
| Mixed Forest                | 0.001051 |                          |
| Grass                       | 0.000860 | kgC/m <sup>2</sup> /d/MJ |
| Transitional woodland shrub | 0.001281 |                          |
| Pasture                     | 0.000860 |                          |

### 2.2.6. MOD17 model

The MOD17 algorithm is considered as an LUE-based model, which fusions remote sensing-based data with environmental factors and mechanistic knowledge of plant physiological processes to estimate GPP and NPP at regional and global levels. The model has a rigorous algorithm to estimate the primary productivity that involves several parameters. The parameters have been calibrated for different plant stands to obtain the optimum values. The following equation was used to estimate GPP, which is a product of LUE and absorbed solar energy.

$$\text{GPP} = \text{APAR} * \epsilon \quad (5)$$

APAR is a product of PAR, which is useable for photosynthesis and fraction of that radiation absorbed by vegetations (i.e., FAPAR). It was calculated using the following formula.

$$\text{APAR} = \text{PAR} * \text{FAPAR} \quad (6)$$

FAPAR quantifies the fraction or amount of the incident solar radiation in the photosynthetically active wavelength range (400-700 nm) absorbed by the vegetation canopy. This model uses an empirical relation between FAPAR and a spectral vegetation index like NDVI to estimate the FAPAR. The structure of this relation can be seen in the following equation. In this study, as mentioned before, an empirical model of FAPAR estimation based on the relation between FAPAR and NDVI established by Myneni & Williams (1994) has been used. A short description of this formula was provided in Section 2.2.3.

$$\text{FAPAR} = a + b * \text{NDVI} \quad (7)$$

where a is the intercept of the relation and b is the coefficient or slope of the relation.

PAR accounts for the incident solar radiation from 400 to 700 nm wavelength. Solar radiation within this range of wavelength is also known as visible light. Plants can absorb this light to utilize in photosynthesis processes. That's why it's called photosynthetically active radiation. In this model, a fraction of total incident solar radiation, also known as shortwave radiation (175 – 10,000 nm), have been considered as PAR (Eq. 8).

$$\text{PAR} = (\text{SWRad} * 0.45) \quad (8)$$

where SWRad stands as an incident shortwave radiation or total incident solar radiation.

The LUE value is estimated by downregulating the plant-specific maximum LUE values. In this model, minimum temperature (TMIN) and VPD are used as environmental scalars (Eq. 9). The values of the scalars vary from 0 to 1. The maximum photosynthesis occurs when the scalar value is 1, whereas no photosynthesis occurs when the value is 0.

$$\epsilon = \epsilon_{\max} * TMIN\_scalar * VPD\_scalar \quad (9)$$

where  $\epsilon_{\max}$  is biome-specific maximum light use efficiency, TMIN\_scalar denotes as stress factor of minimum temperature (value ranges from 0 to 1), and VPD\_scalar stands as a stress factor of VPD (value ranges from 0 to 1).

TMIN\_scalar and VPD\_scalar can be estimated using the following Eq. 10 and Eq. 11, respectively (Lin et al., 2017). These equations were developed based on fuzzy logic principle. The values of the parameters of these equations for different plant types are given in Annex II.

$$TMIN\_scalar = \begin{cases} 0; & \text{When: } TMIN \leq TMIN_{min} \\ \frac{TMIN - TMIN_{min}}{TMIN_{max} - TMIN_{min}}; & \text{When: } TMIN_{min} < TMIN < TMIN_{max} \\ 1; & \text{When: } TMIN \geq TMIN_{max} \end{cases} \quad (10)$$

where TMIN denotes as daily minimum temperature, and TMIN<sub>min</sub> and TMIN<sub>max</sub> are the daily minimum temperature at which LUE is zero (biome-specific constant), and the daily minimum temperature at which optimum LUE equals to maximum LUE (biome-specific constant), respectively.

$$VPD\_scalar = \begin{cases} 0; & \text{When: } VPD \geq VPD_{max} \\ \frac{VPD_{max} - VPD}{VPD_{max} - VPD_{min}}; & \text{When: } VPD_{min} < VPD < VPD_{max} \\ 1; & \text{When: } VPD \leq VPD_{min} \end{cases} \quad (11)$$

where VPD is the vapor pressure deficit during the day time in Pa unit. VPD<sub>min</sub> and VPD<sub>max</sub> are the daylight average VPD at which the LUE is zero (biome-specific constant), and the daylight average VPD at which optimum LUE is equal to LUE<sub>max</sub> (biome-specific constant), respectively.

The estimation of NPP requires the estimation of autotrophic respiration (Ra), which is subtracted from the GPP. The Ra involves estimating maintenance (Rm) and growth respiration (Rg). In other words, Ra is the summation of Rm and Rg. The MOD17 model has an algorithm to estimate the Rm and Rg. For a living plant, Rm is estimated for the leaf, fine roots, and woody biomass (Running & Zhao, 2019). The algorithm includes equations for estimating the biomass volume of leaves, roots, and live wood. Then the Rm is estimated based on the relationship between biomass and temperature sensitivity to respiration (Q<sub>10</sub>). However, the Rm from leaf and roots are estimated at daily timestep, whereas the Rm from live wood is estimated at annual timestep. Later, the aggregated annual Rm from the daily Rm of leaf and roots are summed up to the annual Rm of live wood to get the annual Rm of the entire plant. On the other hand, Rg is estimated as a percentage (25%) of the discrepancy between GPP and Rm (Bruhn et al., 2022). Therefore, the NPP output from MOD17 is at the annual timestep.

Since this study intended to estimate NPP at daily timestep, a coefficient was used to estimate NPP from the GPP. Waring et al. (1998) found a linear relationship between the GPP and NPP based on the field-based measurement of primary productivity of both evergreen and deciduous plants. He reported an NPP/GPP ratio 0.47 with a 0.04 standard deviation ( $r^2 = 0.98$ ). However, this ratio may not be universal for all geographic and ecosystem types. Nevertheless, the study area of the current research is relatively small and entirely falls within the temperate ecosystem. Hence, there is no significant environmental variation in the study area. Therefore, we followed above mentioned ratio to estimate NPP from GPP.

$$\text{NPP} = \text{GPP} - \text{Ra} = \text{GPP} - \{\text{GPP} (1 - 0.47)\} \quad (12)$$

### 2.2.7. GLO-PEM model

The GLO-PEM model follows the fundamental structure of the LUE-based models. However, it uses three environmental scalars, unlike two scalars in the MOD17 model. The scalars of the GLO-PEM model are mean temperature, VPD, and MD. Besides, this model uses a mean temperature scalar instead of a minimum temperature scalar. The model structure is given in Eq. 13. The full description of the model algorithm is available in Prince & Goward (1995), Goetz et al. (1999), and Cao et al. (2004).

$$\text{GPP} = \sum_t \text{PAR} \times f\text{PAR} \times \varepsilon_m \times f(T_a) \times f(\text{VPD}) \times f(\text{SM}) \quad (13)$$

where  $\varepsilon_m$  is the maximum light use efficiency, and  $f(T_a)$  is the mean temperature scalar,  $f(\text{VPD})$  is the vapor pressure deficit scalar, and  $f(\text{SM})$  is the soil moisture scalar.

The following equation (Eq. 14) was used to calculate  $f(T_a)$  for GLO-PEM model (Cao et al., 2004b).

$$\text{Temp}_{\text{scaler}} = \frac{(T - T_{\min})(T - T_{\max})}{(T - T_{\min})(T - T_{\max}) - (T - T_{\text{opt}})^2} \quad (14)$$

where T is the daily mean temperature,  $T_{\min}$  is the constant minimum temperature ( $-1^\circ\text{C}$ ),  $T_{\max}$  stands as the constant maximum temperature ( $50^\circ\text{C}$ ), and  $T_{\text{opt}}$  is the optimum temperature. This parameter is defined as the long-term mean temperature of the growing season. This study estimated this parameter by averaging the hourly temperature of the growing season (from April to September) from 1990 to 2022.

The  $f(\text{VPD})$  for the GLO-PEM model was estimated using the following equation (Prince & Goward, 1995b).

$$\text{VPD}_{\text{scaler}} = (1.2e^{-0.35D}) - 0.2 \quad (15)$$

where D stands as the vapor pressure deficit.

The following equation was used to estimate the  $f(\text{SM})$  scalar of the GLO-PEM model (Cao et al., 2004b).

$$\text{SoilMoisture}_{\text{scaler}} = 1 - \exp(0.081(\delta\theta - 83.03)) \quad (16)$$

where  $\delta\theta$  stands as the soil moisture deficit.

The GLO-PEM model has an equation to estimate the autotrophic respiration or  $R_a$ . This equation estimates  $R_a$  based on the relationship between temperature and biomass. Moreover, the biomass is estimated from a non-linear relation with the minimum reflectivity in the visible channel. Since the model was developed based on the AVHRR reflectance data, the equation was established from the reflectance values of the visible channel of the AVHRR sensor. However, the spectral range of visible bands in Sentinel-2 differs from the AVHRR sensor. Therefore, it is not feasible to use this equation in this study. Hence, the same technique of NPP estimation from GPP as the MOD17 model was also used for the GLO-PEM model.

### 2.2.8. Model implementation and post-processing of NPP data

Both models have been implemented in a MATLAB environment. Two separate MATLAB scripts were prepared for MOD17 and GLO-PEM models, and two additional scripts were for data preparation, model execution, and exporting to GeoTIFF format. MOD17 and GLO-PEM scripts include many conditional loops that incorporate all the land cover and plant-specific parameters in the scalars and NPP estimation. All the input variables, including the PAR, FAPAR, climate, and soil moisture variables, were converted to a matrix from the raster format. Then they were transformed into an array. Then these arrays were used to estimate NPP executing the MOD17 and GLO-PEM scripts. The array output of the NPP was transformed into a matrix format. Finally, the matrices were exported into GeoTIFF format with WGS 1984 coordinate system.

Post-processing the NPP data involves the removal of NO VALUES and reprojecting the raster layers to fix the pixel size at 10 m. During the data exporting to GeoTIFF format from MATLAB, the pixel outside the BFNP boundary were assigned an extra-large value by default: the no value. These values were removed from the raster layers using the extract by attributes tool in ArcGIS Pro. Then, the layers were reprojected to WGS 1984 UTM Zone 33N coordinate system to match the rows and column numbers and the pixel size of the input variables.

### 2.2.9. Verification

In the absence of the eddy covariance flux tower-based time series measurement of the productivity and  $R_a$  data, secondary GPP, NPP, and forest inventory data have been collected from various sources to verify the model output of this study. One of the common primary productivity datasets is the MODIS GPP and NPP products generated from the MOD17 model using the MODIS remote sensing data. This dataset has been producing the primary productivity data since 2001. Since MODIS NPP data comes with an annual timestep, MODIS GPP data have been collected as this data are provided with an 8-day composite. Later, GPP values were converted to NPP values for verification purposes. In addition, some field-measured biomass and NPP data have been collected from the BFNP authority for the year 2016 (i.e., January, May, July, August). Table 5 provides an overview of the secondary datasets collected from various sources to verify the model outputs of this study.

**Table 5.** The basic information about the primary productivity datasets was collected for verification purposes.

| No. | Dataset          | Timestep | Period    | Format          | Spatial Resolution | Source          |
|-----|------------------|----------|-----------|-----------------|--------------------|-----------------|
| 1.  | MODIS GPP        | 8-days   | 2016-2021 | Raster          | 500 m              | NASA Earth Data |
| 2.  | Forest Inventory | Monthly  | 2016      | Point shapefile | -                  | BFNP Authority  |

The input variables are entirely different in MODIS products. The MODIS products use MODIS reflectance data for FAPAR estimation. Moreover, it uses coarse-resolution MODIS land cover maps (500

m spatial resolution) and climate and soil moisture data from different sources than the source used for this study.

The MODIS-GPP data comes with an 8-day interval, whereas the MODIS-NPP data is at an annual timestep. Since the NPP generated from this study are at daily timestep, instead of using MODIS-NPP data, we have estimated NPP from MODIS-GPP with 8-day composites using an NPP/GPP ratio (Eq. 17) (Waring et al., 1998). In addition to GPP data, the MODIS-GPP datasets also contains net photosynthesis as separate band. It is also possible to estimate NPP from this data instead of using GPP directly (Eq. 18). The net photosynthesis can be defined as the difference between GPP and  $R_m$ .

$$\text{MODIS NPP} = \text{MODIS GPP} * 0.47 \quad (17)$$

$$\text{MODIS NPP} = 0.8 * (\text{MODIS GPP} - R_m) = 0.8 * P_{snNet} \quad (18)$$

Where  $P_{snNet}$  stands as the net photosynthesis. MODIS NPP have been estimated using both the formulas and kept whichever provided the highest values of the Coefficient of Determination (expressed as  $R^2$ ). One difficulty in using MODIS products for verification is the mismatch in the acquisition dates of MODIS data (8-day composite) and Sentinel-2 data. To resolve this issue, this study considers the nearest dates of MODIS products from the Sentinel-2 acquisition dates. A list of the dates for both MODIS products and Sentinel-2 data is given in Annex III. The difference between the MODIS and Sentinel-2 dates varies from 0 to 3 days. Another difficulty is the mismatch in the spatial resolution. The MODIS products have a very coarse spatial resolution, i.e., 500 m, whereas the NPP data of this study has a 10 m resolution. Therefore, the MODIS products have been downscaled using the bilinear resampling technique to match the spatial resolution of NPP data estimated in this study.

For verification purposes, 107 random points have been generated to collect the NPP values from both the estimated NPP and MODIS NPP layers. The sample points were generated only on certain types of land covers where vegetation exists, excluding the urban, roads, and water body land cover types. To do this the study area was masked to keep only the vegetated areas. The vegetation land cover types of BFNP include coniferous stand, deciduous stand, mixed stand, meadows, and transition stands between forest and meadows and line vegetation. After generating 107 sample points using simple random sampling techniques, NPP values from both estimated NPP and MODIS-NPP were extracted using the “extract multi values to points” tool in ArcGIS Pro. Moreover, estimated NPP data was also extracted for locations of the forest inventory sampling plots. Finally, these data have been used to calculate the  $R^2$  by squaring Pearson’s correlation coefficient ( $r$ ) and plotting the scatter diagram. The  $R^2$  values indicate how much of one variable can be explained by the other variable. Then, the  $R^2$  between MOD17 NPP and GLO-PEM NPP has also been calculated for inter-model comparison.

#### 2.2.10. Spatio-temporal distribution of NPP

Since the models generate one raster layer for every timestep and it is not possible to show all the NPP maps for every date to present the spatio-temporal distribution of NPP, August has been selected as a representative month in BFNP from the late growing season to show the spatial distribution as the plant foliage matures at this time. However, September is selected for 2021 in the absence of any suitable image in August or July. For a better interpretation and comparison, the NPP values are classified into five classes for all the NPP layers from both models. The classes are  $3.5 \times 10^{-3}$  to  $9.0 \times 10^{-3}$ ,  $2.5 \times 10^{-3}$  to  $3.5 \times 10^{-3}$ ,  $1.0 \times 10^{-3}$  to  $2.5 \times 10^{-3}$ ,  $0.5 \times 10^{-3}$  to  $1.0 \times 10^{-3}$ , and  $\leq 0.5 \times 10^{-3}$  kgC/m<sup>2</sup>/timestep. For better visibility and interpretation of the changes in NPP across the place and time, NPP layers with only positive values have also been created along with the original NPP layers.

### 2.2.11. Change detection, the relation of NPP with climate variables and SPEI

Temporal change in the estimated NPP has been calculated pixel and patch-wise (land cover type-wise). For pixel-wise change detection, some sample pixels were selected from every land cover type following the simple random sampling, and time series pixel values (i.e., NPP values) have been extracted from 2016 to 2022. The number of sample points for different land cover types are 25, 17, 45, and 12 for evergreen, deciduous, mixed, and others (i.e., grass, pasture, shrub), respectively. On the other hand, for patch-wise change detection, spatial averaging of the pixel values was applied to generate the time of NPP values. The change in the NPP values was analysed by estimating a linear trend and the year-wise change.

To investigate the overall direction of the NPP over the study period, a linear trend has been estimated in all the time series extracted at the sample point locations. Time series NPP values were extracted from 2016 to 2022 for each sample point. Hence, each point has 45 NPP values. Then, a linear trend was estimated for every sample point. The sample point-wise slope values of the linear trend have been considered to determine the direction of the trend and fluctuation rate. Since showing a time series plot of all the sample points with trend lines is not possible, a map showing the point-wise slope values has been prepared. The slope values were divided into four classes, showing spatial variation. To detect if there is any significant change or break point after the 2018 drought (Aalbers et al., 2023), a one-tailed t-test has been performed between the pre-drought (2016-2018) and the post-drought (2019-2022) NPP time series (Eq. 19). The null hypothesis of the t-test was that the mean NPP of the pre-drought period was not greater than the post-drought period. On the other hand, the alternative hypothesis was that the mean NPP of the post-drought period was less than the pre-drought period. The t-test output is the p-values; the significance level was 0.01 for 99% confidence intervals (Eq. 20). That means the null hypothesis will be rejected if the p-values are less than 0.01.

$$t = (X_1 - X_2) / \sqrt{[(s_1^2 / n_1) + (s_2^2 / n_2)]} \quad (19)$$

where  $X_1$  and  $X_2$  are the mean NPP during the pre- and post-drought periods, respectively;  $s_1$  and  $s_2$  are the standard deviations of the pre- and post-drought NPP time series, respectively;  $n_1$  and  $n_2$  are the sample sizes of the both time series.

After calculating the t-value, the test calculates the p-value to test the hypothesis (Eq. 20).

$$p\text{-value} = 1 - F(t, df) \quad (20)$$

where  $F$  is the Cumulative Distribution Function (CDF) of the t-distribution;  $t$  is the calculated t-value from the t-test;  $df$  is the degree of freedom associated with the t-test.

Pearson's correlation coefficient ( $r$ ) has been calculated between the NPP estimated from both models and climate variables.. Since  $r$ -values show both the magnitude and direction of the relations, and both positive and negative relations exist between NPP and climate data,  $r$ -values have been calculated instead of  $R^2$ . The NPP estimated by the MOD17 model was correlated to the daily minimum temperature, soil moisture deficit, and vapour pressure deficit. On the other hand, the NPP estimated from the GLO-PEM model was correlated to daily mean temperature, vapour pressure deficit, and soil moisture deficit. Since water stress originating from VPD and soil water deficit can have delayed impacts on NPP, real-time and lagged correlations were calculated for these two variables. Since the Sentinel-2 data series contains mostly one image in a month, each lag period means at least a one-timestep-month lag. However, there are

gap months in the data series. Hence, the exact time for each lag period would be at least one or more months. The climate variables have been chosen based on the scalars used for each model.

Although the lagged correlation between VPD and soil moisture deficit indicates the drought influence on NPP, the correlation between estimated NPP and SPEI values has been performed to detect the drought impacts on NPP. Real-time and lagged correlation with several lag periods between SPEI (both 01-month and 03-month scale) and estimated NPP have been calculated to find the maximum impact scenario. Finally, the lagged correlation with the maximum overall r-values has been reported in the result section.

#### **2.2.12. Significance of correlation and probability distribution**

The p-values of the correlations of the inter-comparison of estimated NPP from both models and the estimated NPP with climate variables and SPEI have been calculated using the following formula (Eq. 21) in excel. Then, the significance of the correlations have been reported based on a significance level. The correlation is significant if the p-value is less than the significance level. The selected significance level is mentioned in the result section.

$$p\text{-value} = \text{TDIST}((\text{ABS}(r) * (\text{SQRT}(N-2)) / \text{SQRT}(1 - r^2)), \text{DF}, 2) \quad (21)$$

where TDIST is the t-test distribution, ABS is absolute value function, r is correlation coefficient, N is sample size, DF is degree of freedom, and 2 indicates the two-tailed test.

Then, the Probability Distribution Function (PDF) of the correlation values of the estimated NPP and climate variables have been estimated for a better understanding of the distribution of the r-values using the Kernel Density Estimation (KDE) method. The PDF helps understand the maximum statistical probability or likelihood of the influence of the independent variables (i.e., climate data) on the dependent variables (i.e., NPP).

## 3. RESULTS

### 3.1. NPP from MOD17 and GLO-PEM model

#### 3.1.1. Spatial distribution of NPP

The spatial distribution of NPP from MOD17 and GLO-PEM models and their temporal changes from 2016 to 2022 is shown in Figure 6, Figure 7, Figure 8, and Figure 9. The NPP maps of positive values are shown separately in addition to the combined illustration of positive and negative values.

The findings show that NPP is heterogeneously distributed over the study area considering the distribution of the plant types. Both models show a decrease in the volume of NPP in the first few years, then an increase in the latter part of the study period from 2016 to 2022. In the case of the MOD17 model, the first two years of 2016 and 2017 show the maximum volume of NPP across the study area. In these two years, almost all pixels show positive values of NPP, as there is no significant visual difference between the illustration of combined (positive and negative) and positive-only layers (Figure 6).

The MOD17 model shows a reduction in NPP in 2018 onwards as the prevalence of the first class is almost diminished. The magnitude of the NPP reduction is found to be maximum in-between 2018 and 2019, and no significant recovery is noticed until 2022. Most of the pixels in 2019, 2020, and 2021 belong to the fourth and fifth class of NPP ( $\leq 1.0 \times 10^{-3} \text{ kgC/m}^2$ ). Although a slight recovery occurred in 2021, especially in the southern and south-eastern parts of BFNP, the major recovery occurred in 2022. The prevalence of class four and five has mostly been converted to the third and second classes this year (Figure 7). Many areas with negative NPP values are found in 2019, 2020, and 2021, dispersed throughout the study area. The spatial distribution of the pixels with negative NPP suggests that the extent of negative NPP increased in 2020 than in 2019 and then decreased in 2021 (Figure 7). This scenario implies a slight recovery in 2021, especially in the southern part of BFNP, as some sparsely distributed areas are changed to the second class of NPP. Although the GLO-PEM model shows maximum NPP value in 2016 and 2017, the quantity of NPP is lower as most of the study area is dominated by the NPP second class compared to the dominance of the first class in the other model (Figure 8).

The GLO-PEM model also shows similar behaviour regarding the change and recovery from 2018 to 2022 (Figure 8 and Figure 9). However, there are some differences in the quantity and extent of the change. Although the MOD17 model shows an overall reduction of NPP in 2018, there is a slight increase in the GLO-PEM model, especially in the southern part of the study area (Figure 8). From 2019 onwards, the GLO-PEM model also generated low NPP until 2022, which experienced a recovery. From 2019 to 2022, the overall quantity of NPP is lower in the GLO-PEM model than in the MOD17 model. The GLO-PEM model also identifies the appearance of the negative values in 2019 and their increase and decrease in 2020 and 2021, respectively (Figure 8, and Figure 9). In short, both models identified the maximum NPP reduction in 2020. The northern part of the study area underwent the maximum extent of fluctuations compared to the southern part.

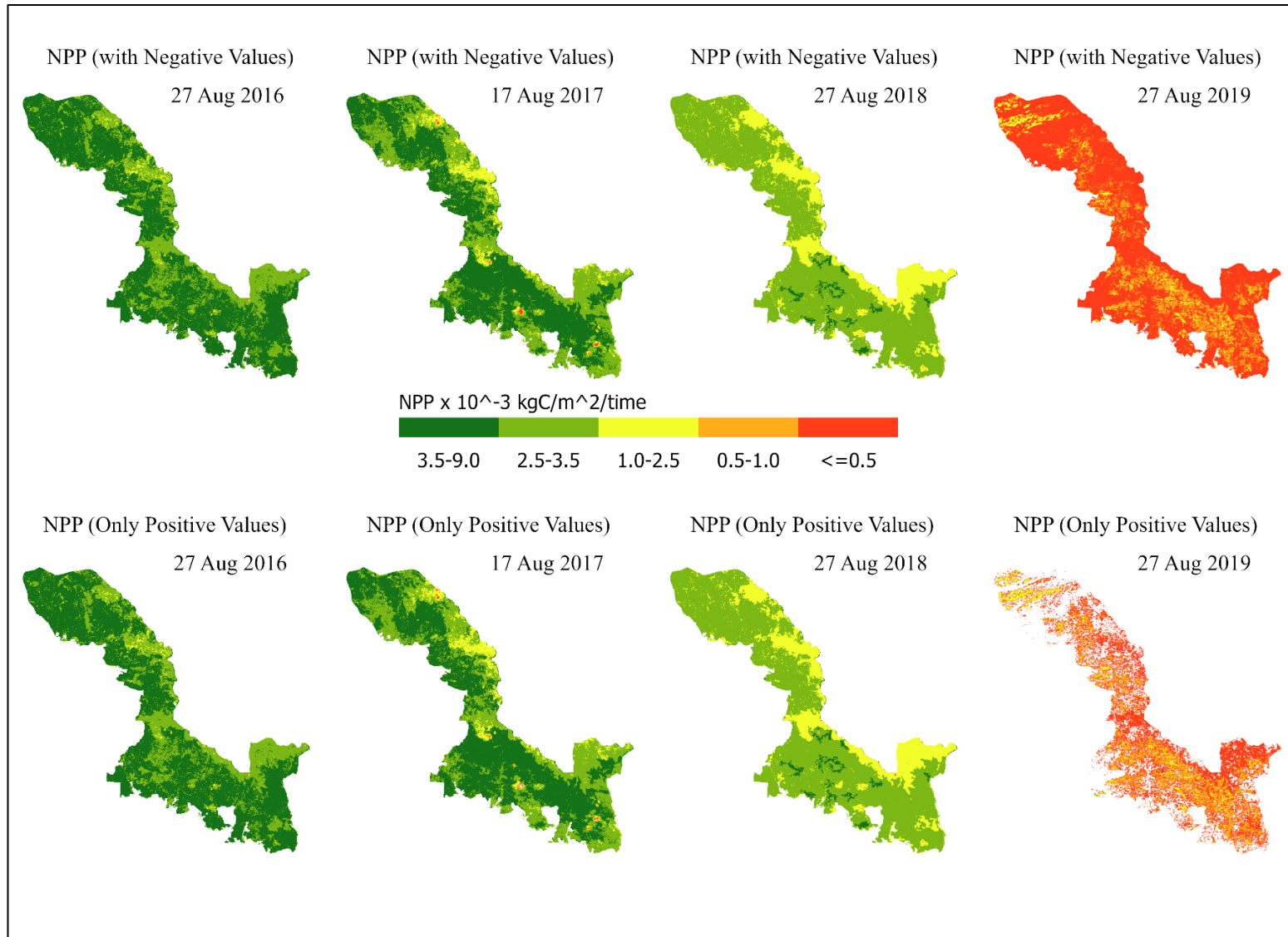


**Figure 6.** Spatial distribution and temporal change of NPP from MOD17 model from 2016 to 2019 in the late growing season. The upper maps show the NPP values with positive and negative values, whereas the lower maps show only positive ones.

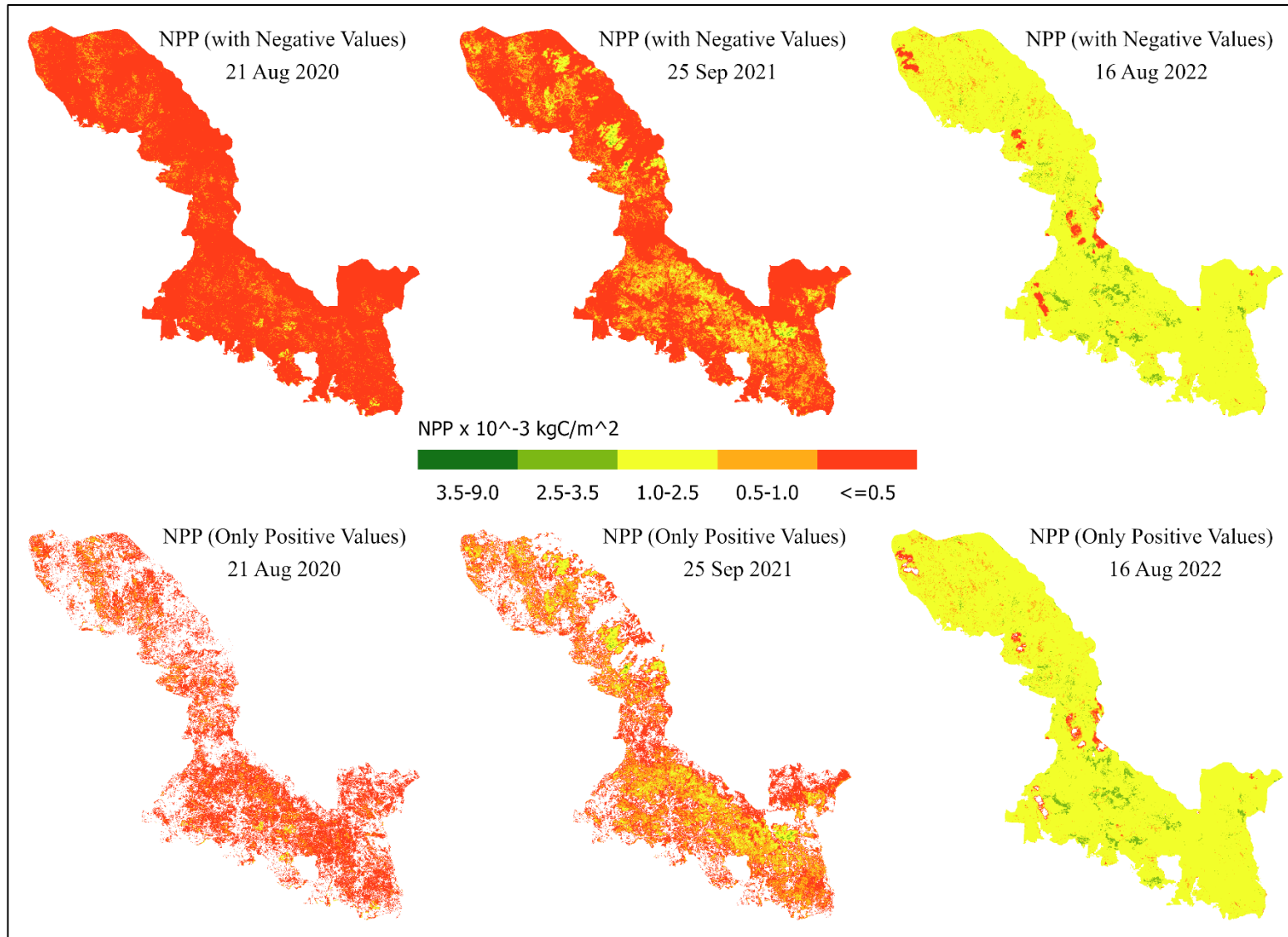


**Figure 7.** Spatial distribution and temporal change of NPP from MOD17 model from 2020 to 2022 in the late growing season. The upper row shows the NPP values with positive and negative values, whereas the lower row shows only positive ones.

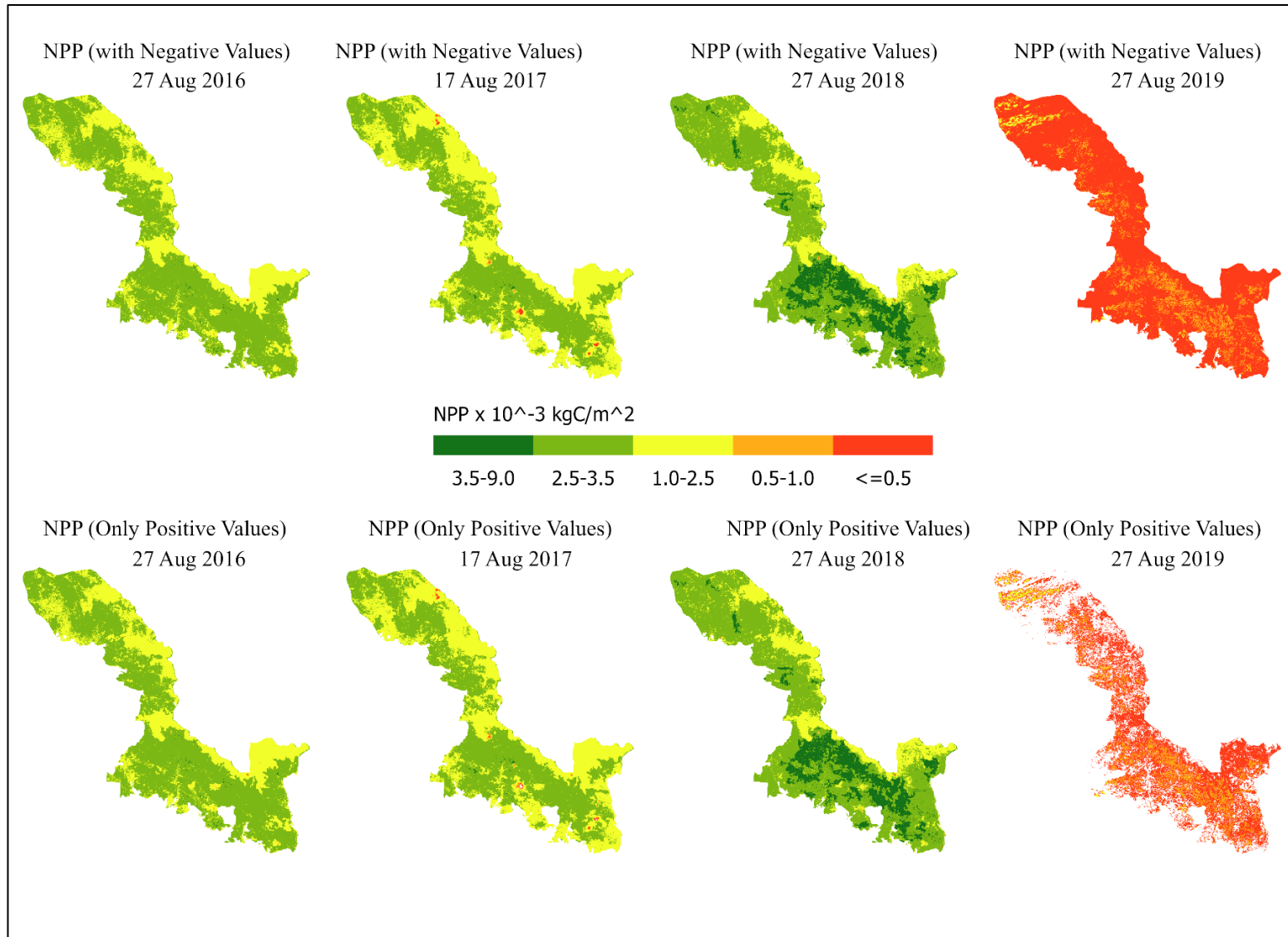


**Figure 8.** Spatial distribution and temporal change of NPP from GLO-PEM model from 2016 to 2019 in the late growing season. The upper row shows the NPP values with positive and negative values, whereas the lower row shows only positive ones.

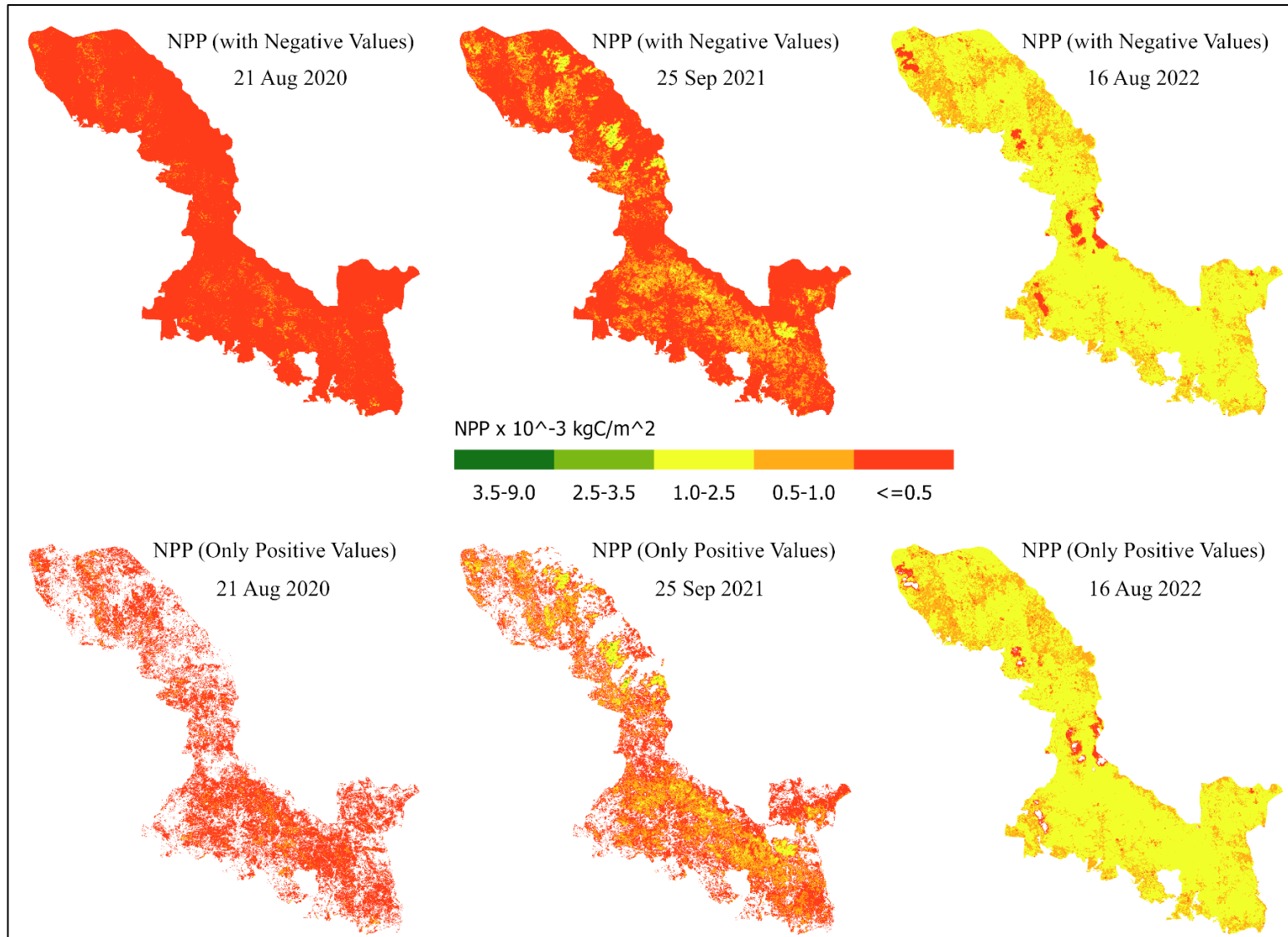


**Figure 9.** Spatial distribution and temporal change of NPP from GLO-PEM model from 2020 to 2022 in the late growing season. The upper row shows the NPP values with positive and negative values, whereas the lower row shows only positive ones.

### 3.1.2. Land cover wise quantification of NPP

A quantitative representation of the temporal changes according to land cover classes (e.g., Deciduous, Evergreen, Mixed, others) described above can be found in Table 6. The MOD17 model estimated that the total amount of NPP in BFNP gradually decreased from about 82890 kg in 2016 to about 3178 kg in 2020, then it started increasing to about 40870 kg in 2022. Almost a similar pattern is found for NPP values using GLO-PEM model, except there found an increase in NPP values in 2018. Moreover, the amount of estimated NPP is generally lower in the GLO-PEM model than in the MOD17 model. The land cover-wise NPP quantification also shows a similar decrease (from 2016 to 2020) and increase (from 2021 to 2022) in the MOD17 model. Overall, the highest productivity is found in mixed forest-type stands, followed by evergreen, others (i.e., grasses, shrubs, meadows), and deciduous stands applying both GLO-PEM and MOD17 models.

Furthermore, the land cover-wise estimation of GLO-PEM shows a slight increase in 2018 and a decrease afterwards, like the overall estimation covering the entire BFNP. In short, both models recorded the lowest productivity in 2020 for all land cover types. Moreover, the recovery started in 2021 and continued in 2022, although the productivity did not reach the initial level of 2016.

**Table 6.** The table shows a land cover-wise quantitative representation of NPP in Aug/Sep from 2016 to 2022. The numbers are in kilogram units. The calculation considers only positive values to avoid error-related distortion.

| LC Type   | Models  | 2016     | 2017     | 2018     | 2019    | 2020    | 2021    | 2022     |
|-----------|---------|----------|----------|----------|---------|---------|---------|----------|
| BFNP      | MOD17   | 82890.64 | 80727.05 | 65439.92 | 6453.97 | 3178.69 | 7836.69 | 40870.09 |
|           | GLO-PEM | 60208.42 | 58422.31 | 69370.45 | 4675.61 | 2416.07 | 6921.38 | 30050.28 |
| Deciduous | MOD17   | 12090.16 | 13799.08 | 10632.72 | 1788.05 | 798.47  | 2319.24 | 6997.98  |
|           | GLO-PEM | 10265.77 | 10248.50 | 12176.41 | 1298.88 | 720.26  | 1971.68 | 5757.29  |
| Evergreen | MOD17   | 19916.78 | 17856.22 | 15770.22 | 827.22  | 388.10  | 842.25  | 8341.37  |
|           | GLO-PEM | 13438.39 | 12681.27 | 15351.89 | 597.76  | 260.53  | 723.35  | 5780.41  |
| Mixed     | MOD17   | 33313.33 | 33397.85 | 26974.08 | 2815.11 | 1508.42 | 3416.04 | 16717.65 |
|           | GLO-PEM | 24749.51 | 24203.01 | 28443.30 | 2037.19 | 1117.38 | 3027.95 | 12412.74 |
| Others    | MOD17   | 17570.37 | 15673.90 | 12062.90 | 1023.59 | 483.70  | 1259.16 | 8813.09  |
|           | GLO-PEM | 11754.75 | 11289.53 | 13398.85 | 741.78  | 317.90  | 1198.40 | 6099.84  |

Note: The others type includes grass, pasture, transitional woodland shrub, meadows.

### 3.2. Comparison of the estimated NPP with NPP from forest inventory

The comparison of the summation of mean daily NPP in different sample points of the forest inventory with the NPP extracted from the MOD17 and GLO-PEM layers for the same points shows that MOD17 NPP is found closer to the field-measured NPP than GLO-PEM NPP in May 2016 (Table 7). On the other hand, GLO-PEM NPP is closer to the forest inventory NPP in July and August compared to the MOD17 NPP. MOD17 has also overestimated the NPP more than the forest inventory NPP in July and August by 35 and 33%, respectively. Overall, the differences between the forest inventory NPP and GLO-PEM NPP are lower than the difference between MOD17 NPP and the forest inventory NPP. The  $R^2$  values between the summation of estimated NPP and field-measured NPP (Table 7) are found to be 0.32 and 0.84 for MOD17 and GLO-PEM models, respectively. Moreover, when compared point-wise instead of aggregating the values, the highest values of  $R^2$  are found in May for both MOD17 (0.25) and GLO-PEM (0.26) models.

**Table 7.** The summation of the mean daily NPP in all the sample points of the forest inventory. The numbers are in  $\text{kgC}/\text{m}^2/\text{day}$  units.

| Data source      | May 2016 | July 2016 | August 2016 |
|------------------|----------|-----------|-------------|
| Forest inventory | 0.29     | 0.31      | 0.27        |
| MOD17            | 0.30     | 0.42      | 0.36        |
| GLO-PEM          | 0.26     | 0.34      | 0.26        |

### 3.3. Comparison of the estimated NPP with MODIS products

The estimated NPP from MOD17 and GLO-PEM models have been compared with the MODIS products. (Running & Zhao, 2019). The comparison between the estimated NPP from the MOD17 model and the MODIS-NPP suggests mostly positive relations; however, the strength of the relations, which expressed as  $R^2$  values, varies from 0.16 to 0.72 (Figure 10). The scatter plots in Figure 10 suggest that the outputs of two models, MOD17 and MODIS-NPP, follow an upward identical pattern. However, the distribution of the observations in the scatter plots is different for all the sampling dates. The distribution shows both sparse and compact nature.

The GLO-PEM model also gives similar results when compared to the MODIS-NPP. However, the values of  $R^2$  differ from the MOD17 model (Figure 11). The correlation between the GLO-PEM model products versus MODIS-NPP varies from 0.16 to 0.70. In most cases, the  $R^2$  values between GLO-PEM and MODIS NPP are less than the  $R^2$  values between MOD17 and MODIS NPP. Like MOD17, the GLO-PEM NPP also shows sparse and compact nature of distribution against the MODIS NPP.

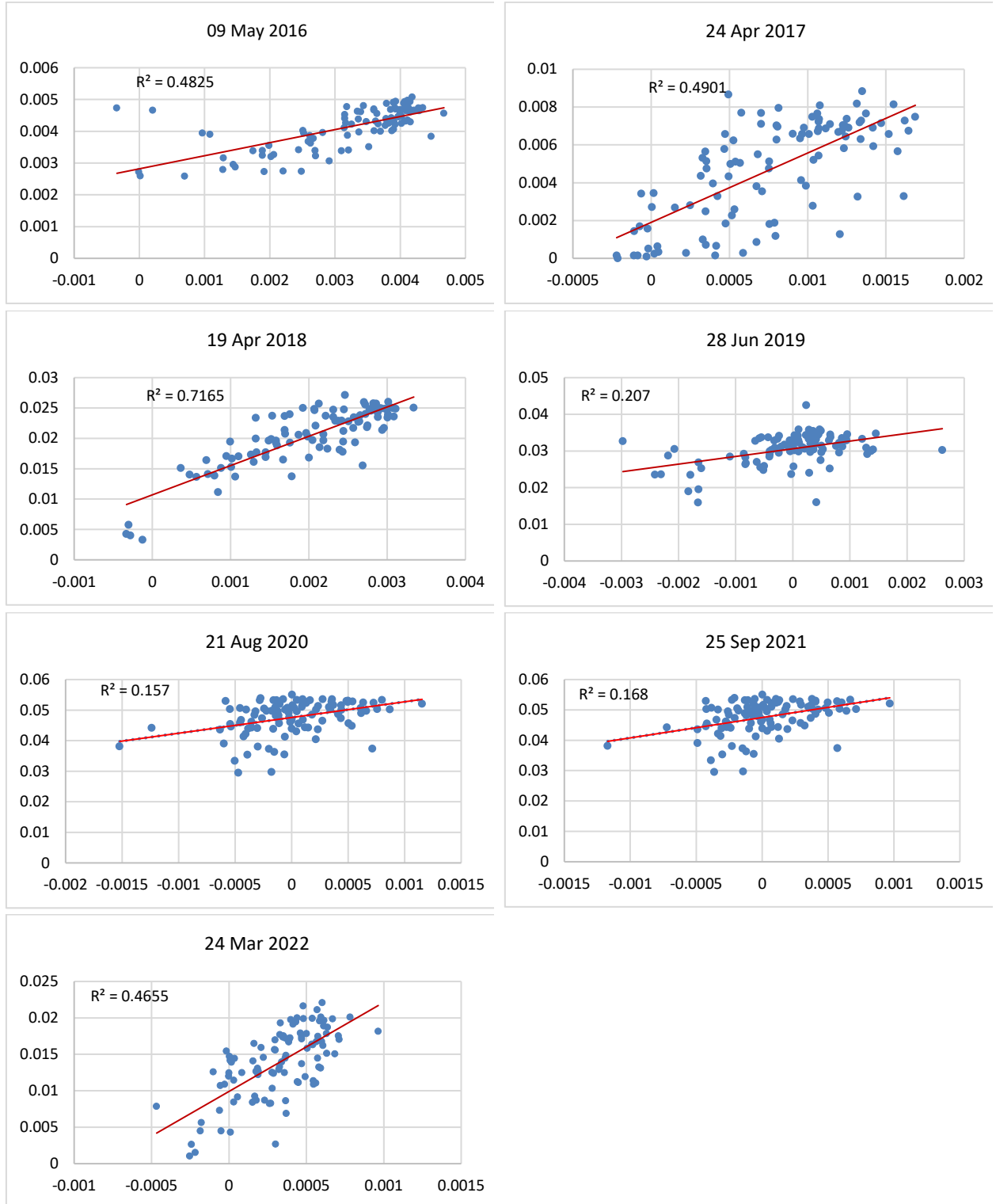


**Figure 10.** Comparison between MOD17 (x-axis) and MODIS-NPP (y-axis) on some selected dates. The figures on x-axis and y-axis of each sub-figure is in  $\text{kg}/\text{m}^2$  unit. The red line represents the linear trend line between the variables.

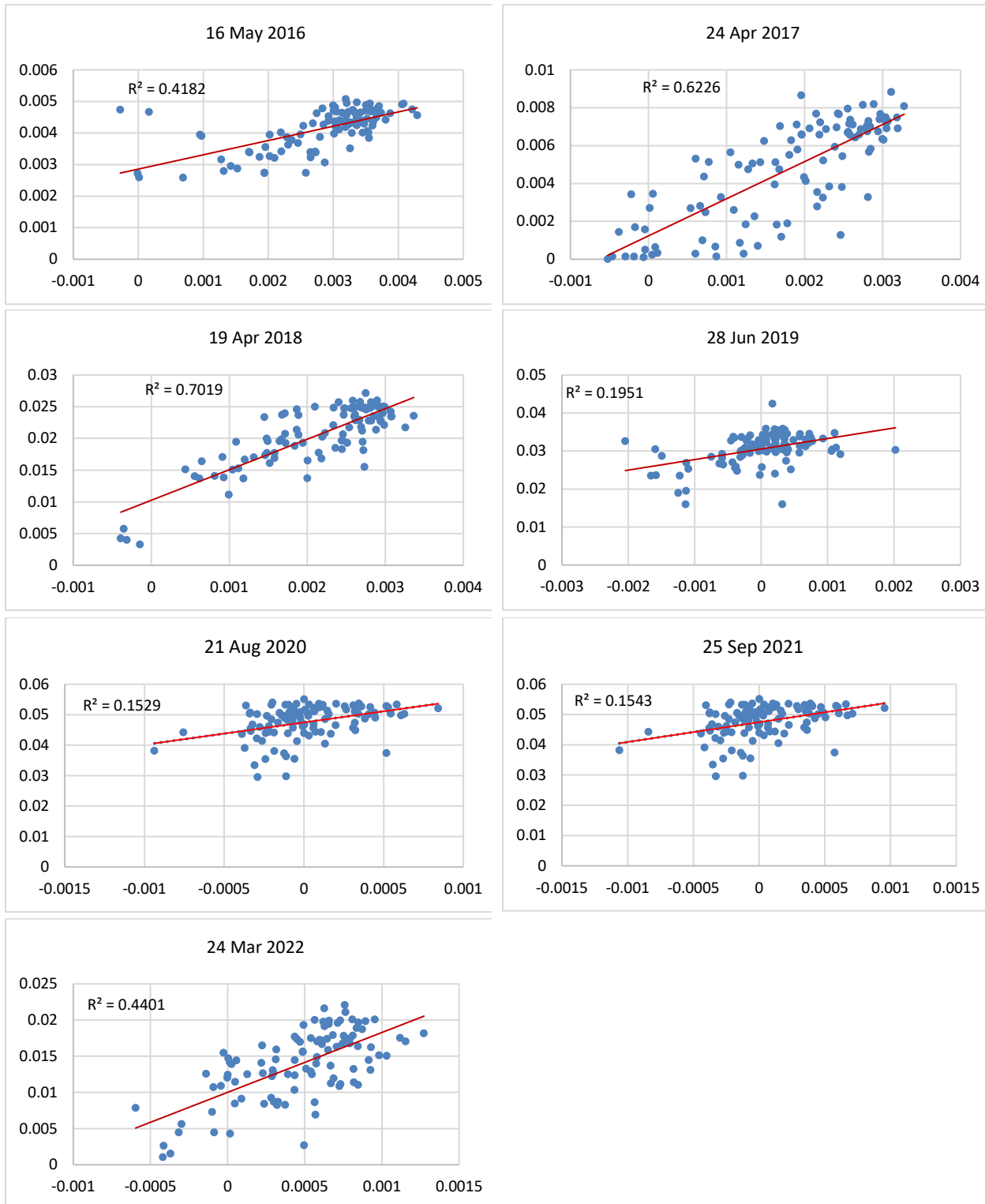


**Figure 11.** Comparison between GLO-PEM (x-axis) and MODIS-NPP (y-axis) on some selected dates. The figures on x-axis and y-axis of each sub-figures are in  $\text{kg}/\text{m}^2$  unit. The red line represents the linear trend line between the variables.

### 3.4. Inter-comparison of MOD17 and GLO-PEM NPP

An inter-comparison between the MOD17 and GLO-PEM models has been performed to investigate how the models perform against each other. The results show that most of the  $R^2$  values of this comparison are above 0.8, which suggests a strong positive relation between two models (Figure 12). Nevertheless, a few lower  $R^2$  are also found below 0.4. However, the p-values suggest that all correlations are significant in 0.01 level of significance (Annex IV).

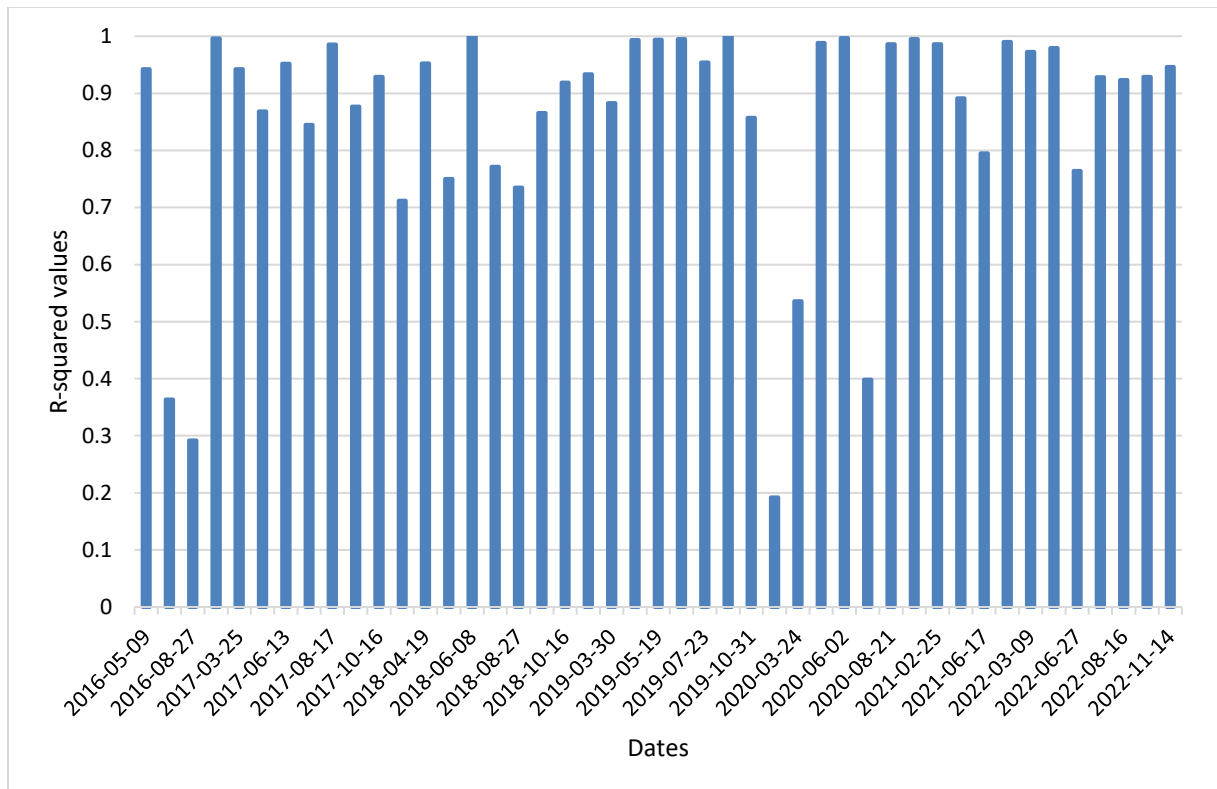


**Figure 12.** The comparison of coefficient of determination (R-squared values) between the estimated NPP from MOD17 and GLO-PEM models. The x-axis contains all the 45 dates of the Sentinel-2 data series of the study.

### 3.5. Temporal change in NPP

The temporal changes in NPP estimated from both models have been analysed and presented separately. A linear trend was calculated using the NPP values extracted from different sample points throughout the study area. Figure 13 shows the distribution of the slope values of the trend estimated from both models. The findings show a downward trend of NPP in all the sample locations for both models. However, there is a slight difference in the range and spatial distribution pattern of the slope values. In the case of the MOD17 model, the slope value ranges from  $5.0 \times 10^{-7}$  to  $1.8 \times 10^{-6}$  kg/m<sup>2</sup>. On the other hand, the slope values of the GLO-PEM model vary from  $5.0 \times 10^{-7}$  to  $1.6 \times 10^{-6}$  kg/m<sup>2</sup>. The spatial distribution of slope values suggests that any specific range of the fluctuation rates is not concentrated but distributed over space. Nevertheless, a spatial correlation pattern can be seen as the sample points within the same value range are located near each other in many parts of the study area.

A more clear picture of how the NPP changes over time can be seen in Figure 14, which has three plots for three representative pixels from evergreen, deciduous, and mixed, land cover types. The plots in

Figure 14 shows that the model identifies the seasonal cycles of the NPP very well. The NPP values after 2018 are very lower in all plots. However, there is a recovery trend in 2022, as the plots show higher peaks than in the previous three years.

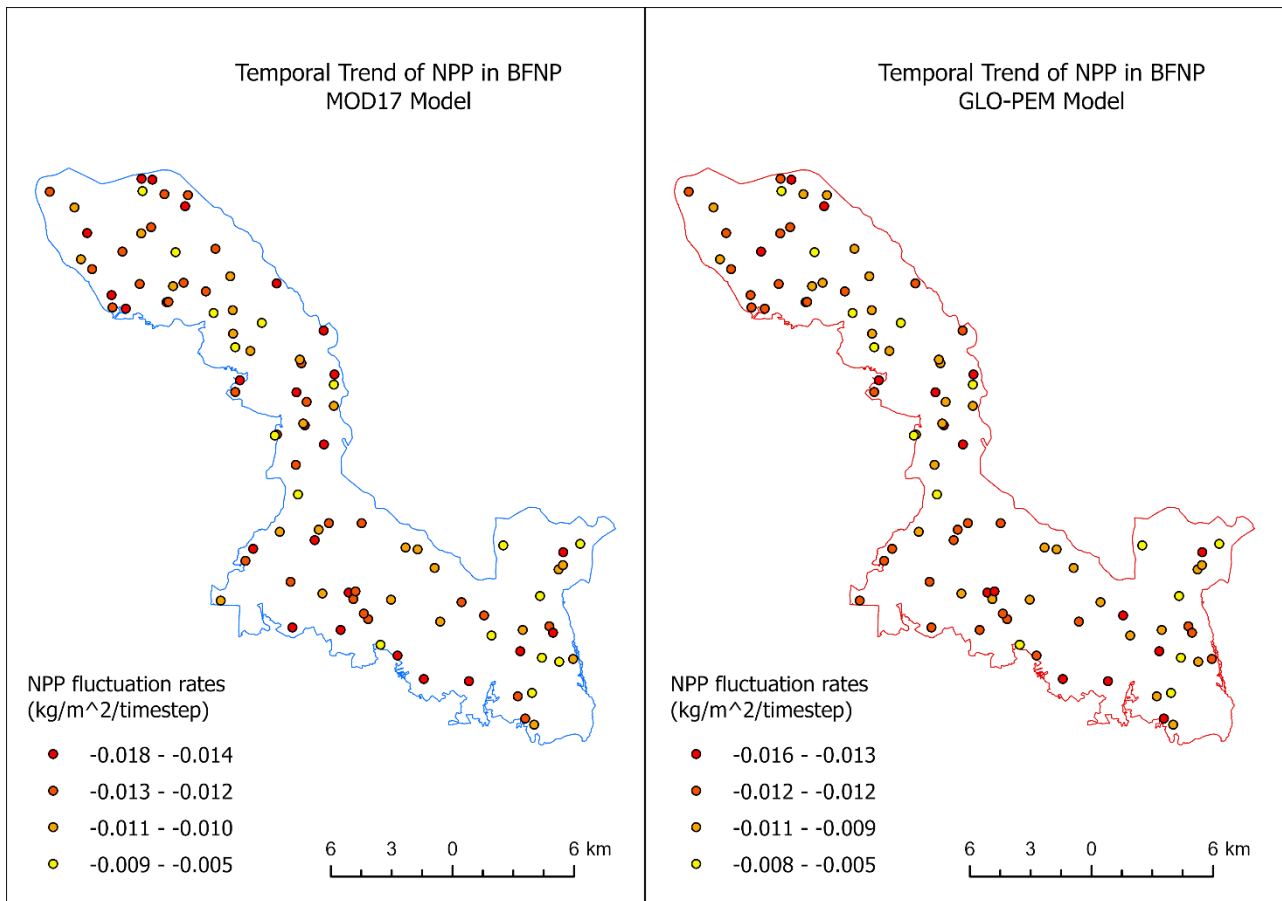


**Figure 13.** Spatial distribution of the slope of the linear trend in NPP from 2016 to 2022. The slope values in legend have a scale factor of 0.0001. The symbols here represent the locations of the sample points from which NPP values have been extracted.

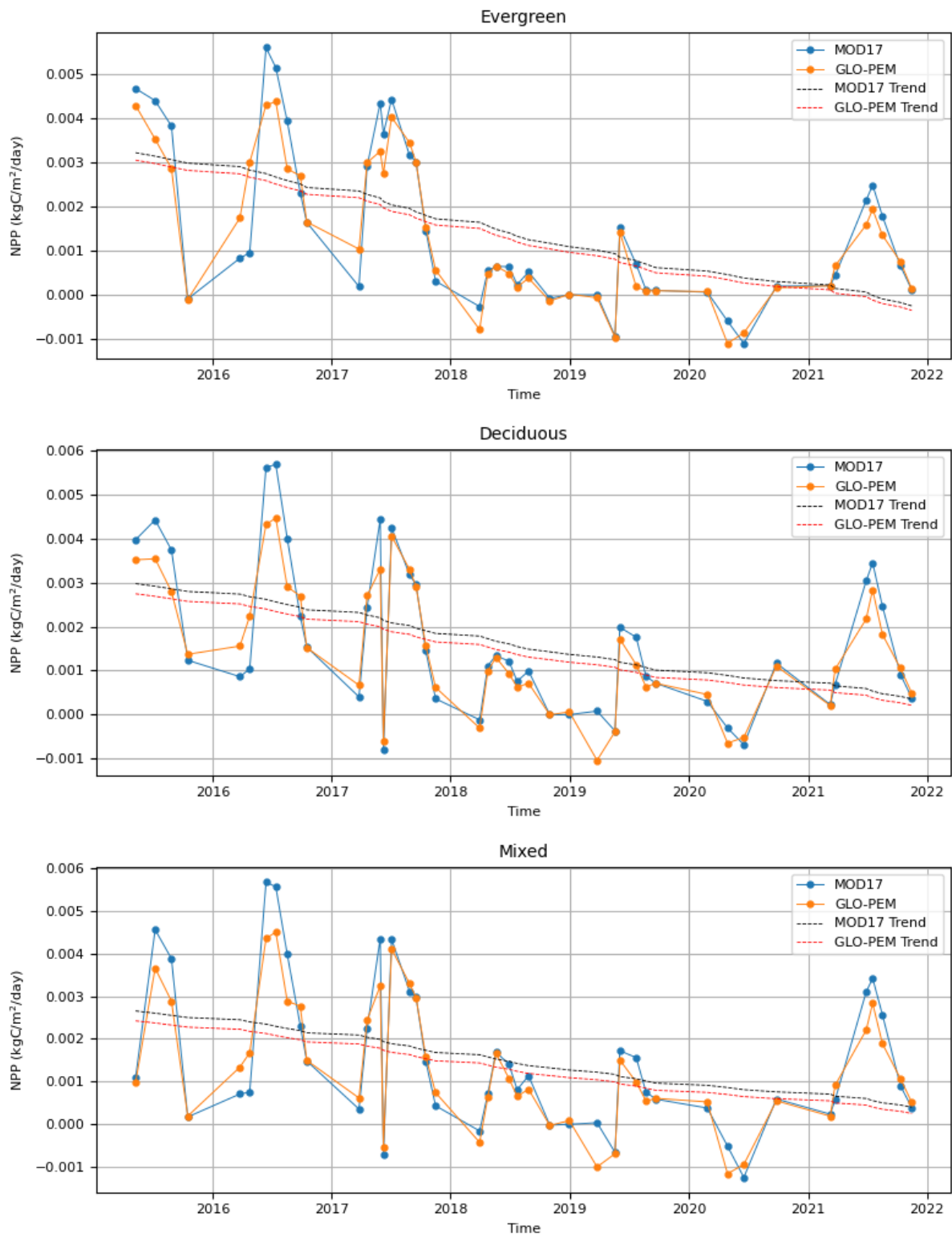


**Figure 14.** Time series plots and linear trend lines of three representative pixels from different types of land cover. The x-axis of the plots represents NPP in kg/m<sup>2</sup>/day units, whereas the y-axis shows the time.

The linear downward trend found in different sample points is further supplemented by the significant differences found in NPP between pre-drought (2016-2018) and post-drought(2019-2022) periods from the t-test. The mean NPP values largely decreased in the post-drought period compared to the pre-drought period in every sample point, as shown in Figure 15 (MOD17) and Figure 16 (GLO-PEM). The significance

of this change in mean NPP in the latter period is further confirmed by the p-values of the t-test. Almost all of the p-values are found to be less than 0.01 (Annex IV). This result suggests that the reduction in mean NPP in the post-drought period is statistically significant at a 0.01 significance level.

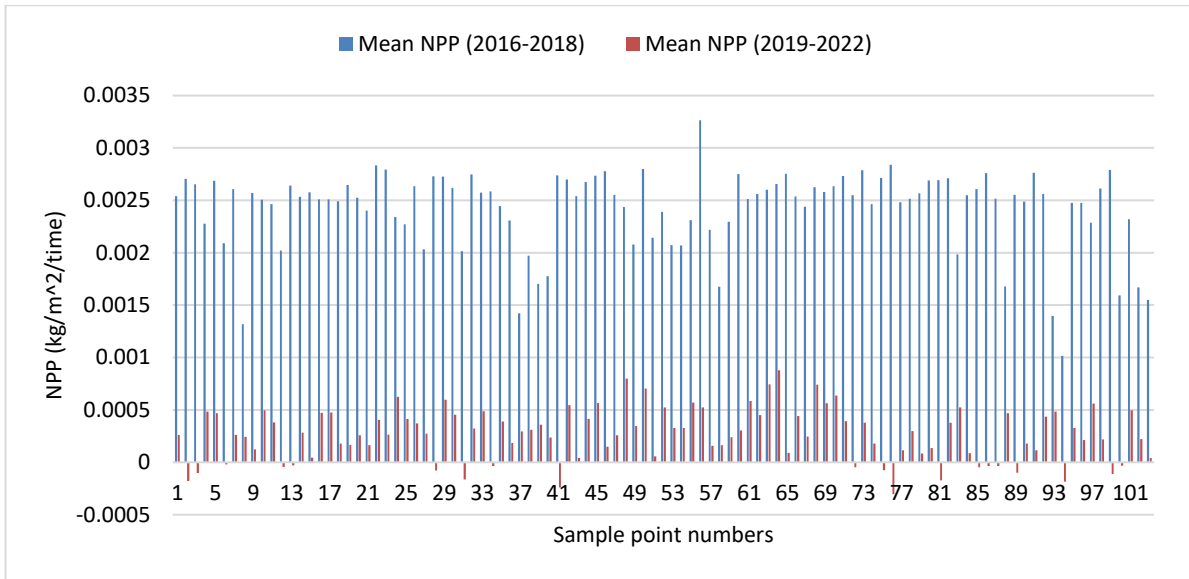


**Figure 15.** Mean NPP values from MOD17 model in pre-drought (2016-2018) and post-drought (2019-2022) periods.

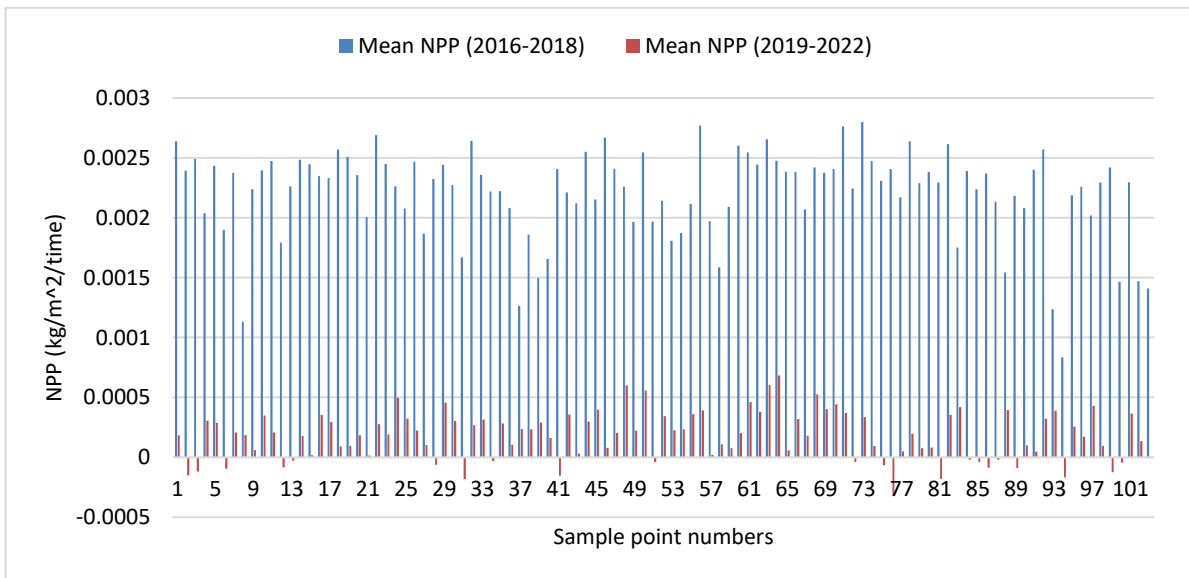


**Figure 16.** Mean NPP values from GLO-PEM model in pre-drought (2016-2018) and post-drought (2019-2022) periods.

### 3.6. Relation of NPP with climate variables and SPEI values

After finding significant changes in NPP value after 2018, the study attempted to investigate the relations between the NPP and the climate variables, such as daily minimum temperature, daily mean temperature, VPD, and soil moisture deficit. The MOD17-NPP have been correlated to daily minimum temperature, soil moisture deficit, and VPD of the study area. Figure 17 shows that the NPP values estimated by the MOD17 model are moderately-strong correlated to the climate variables such as minimum temperatures and soil moisture deficit. However, the r-values are higher with lagged soil moisture deficit with one lag period. The

correlation coefficient values are mostly around 0.4 for different sample points. In the case of VPD, the real-time correlation provides a positive correlation, whereas the lag-3 correlation provides higher negative r-values (Figure 18). The probability density distribution in Figure 19 shows that the  $R^2$  values of around 0.43, -0.47, 0.41, and -0.44 have the maximum probability of occurring when establishing the relation of MOD17 NPP with daily minimum temperature, lag-1 soil moisture deficit, real-time VPD, and lag-3 VPD, respectively. The p-values of the r-values between MOD17 NPP and climate variables suggest that about 84, 79, 99, 85, and 94% sample points for minimum temperature, real-time soil moisture deficit, lag-1 soil moisture deficit, real-time VPD, and lag-3 VPD, respectively, show significant correlations at a 0.05 significance level (Annex IV).

On the other hand, the GLO-PEM-NPP have also been correlated with daily mean temperatures, real-time and lag-1 soil moisture deficit, real-time VPD, and lag-3 VPD. The findings suggest that GLO-PEM-NPP is also moderately-strong correlated with the climate variables, as most correlation coefficient values are between 0.4 and 0.45 in both directions (Figure 20). Like MOD17, lag-1 soil moisture deficit shows the higher r-values than real-time values. Similarly, lag-3 VPD shows negative relations (with higher values), whereas real-time VPD shows positive relations with the estimated NPP (Figure 21). The probability density distribution in Figure 22 shows that the maximum likelihood of  $R^2$  between GLO-PEM NPP and climate variables lies around 0.4, 0.5, 0.3, and 0.4 for mean temperature, lag-1 soil moisture deficit, real-time VPD, and lag-3 VPD, respectively. The p-values of the r-values between GLO-PEM NPP and climate variables suggest that about 65, 78, 100, 35, and 74% sample points for mean temperature, real-time soil moisture deficit, lag-1 soil moisture deficit, real-time VPD, and lag-3 VPD, respectively, show significant correlations at a 0.05 significance (Annex IV).

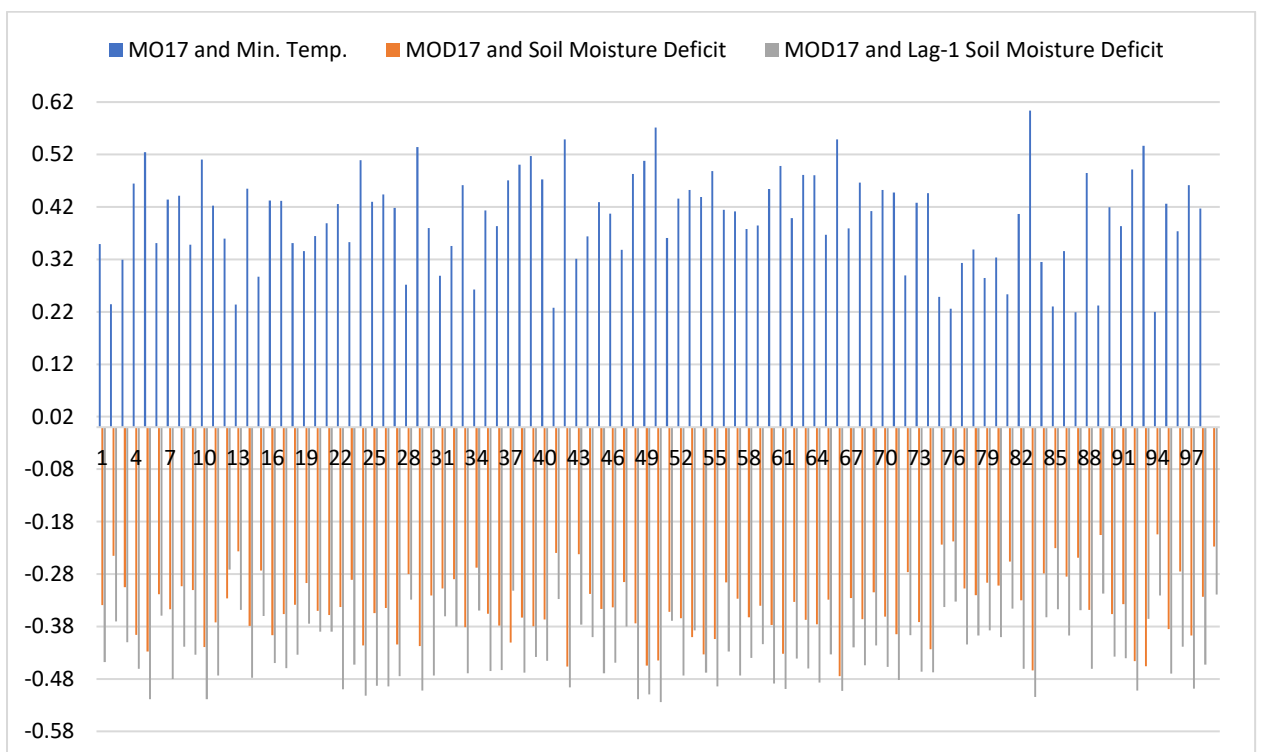


**Figure 17.** Correlation coefficients ( $r$ ) of MOD17 NPP with daily minimum temperature, soil moisture deficit, and lag-1 soil moisture deficit. The correlation of NPP with real-time soil moisture deficit and lag-1 soil moisture deficit is in a negative direction. The x and y axis shows sample point numbers and r-values, respectively.

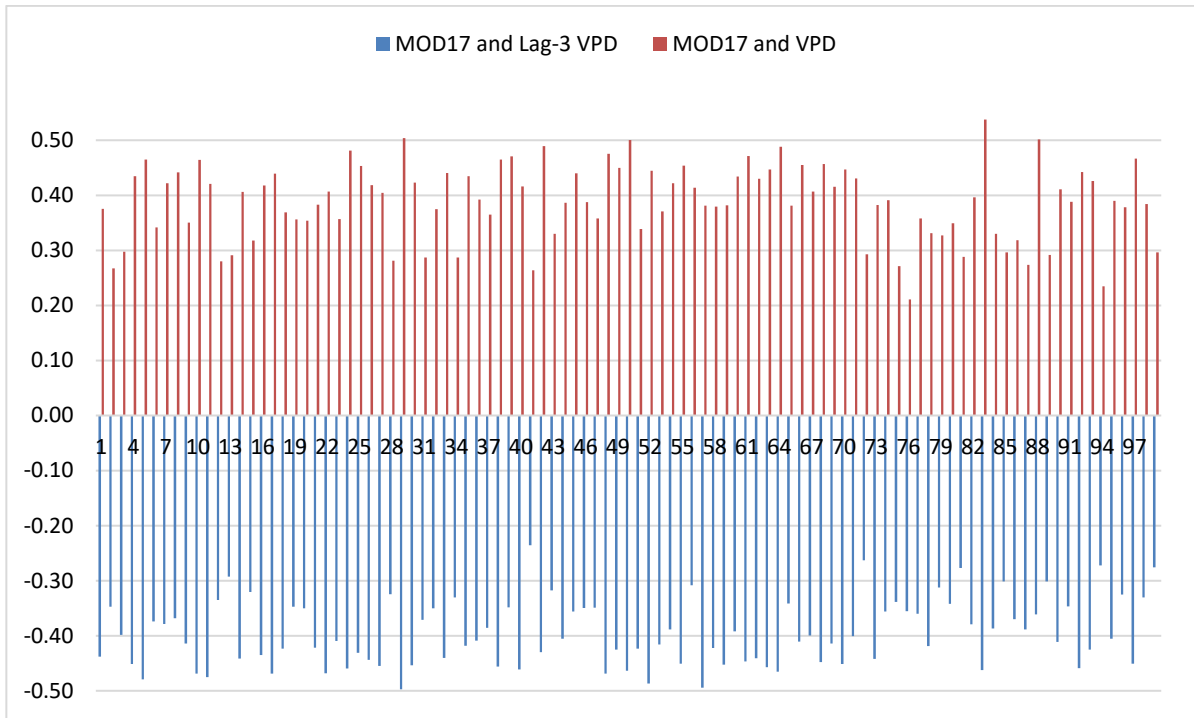


**Figure 18.** Correlation coefficients of MOD17 NPP with real-time VPD and lag-3 VPD. The x and y axis shows sample point numbers and r-values, respectively.

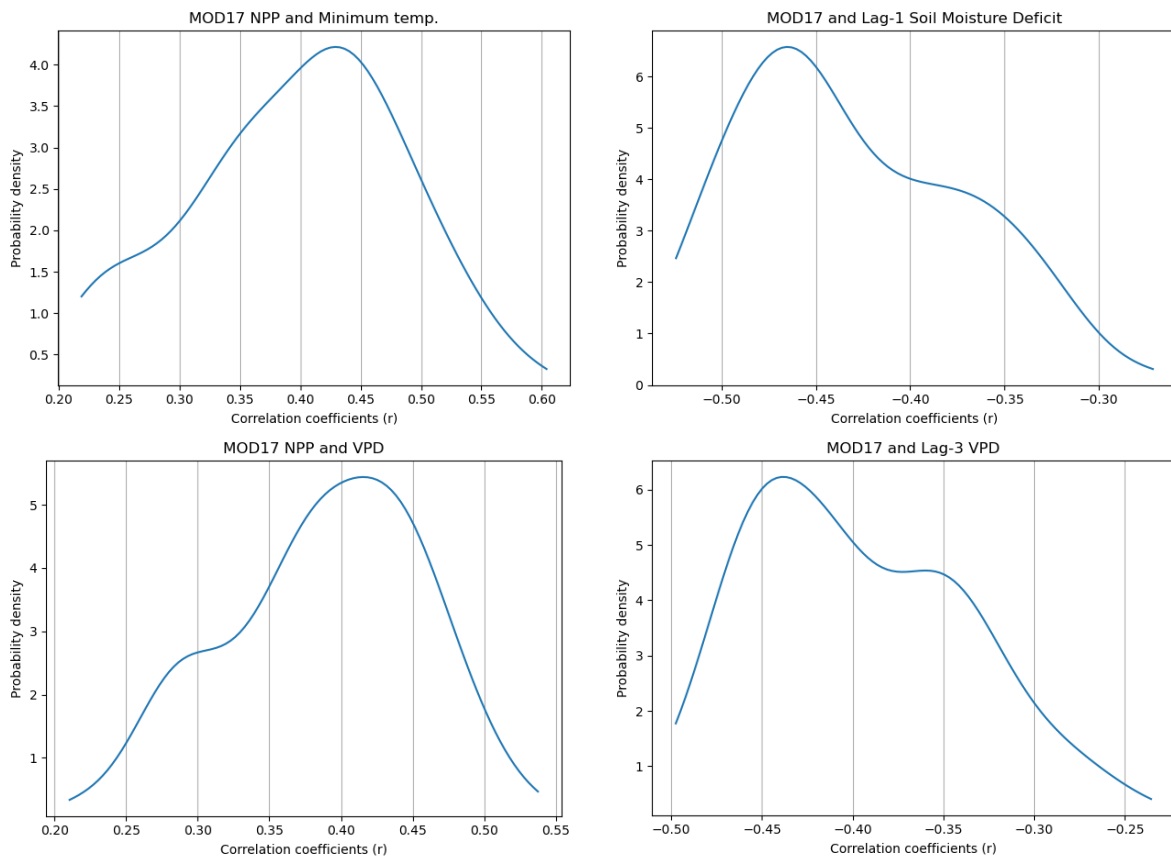


**Figure 19.** Probability density function distribution of the correlation coefficient values ( $r$ ) of MOD17-NPP with daily minimum temperature (upper left), lag-1 soil moisture deficit (upper right), real-time VPD (lower left), and lag-3 VPD (lower right).

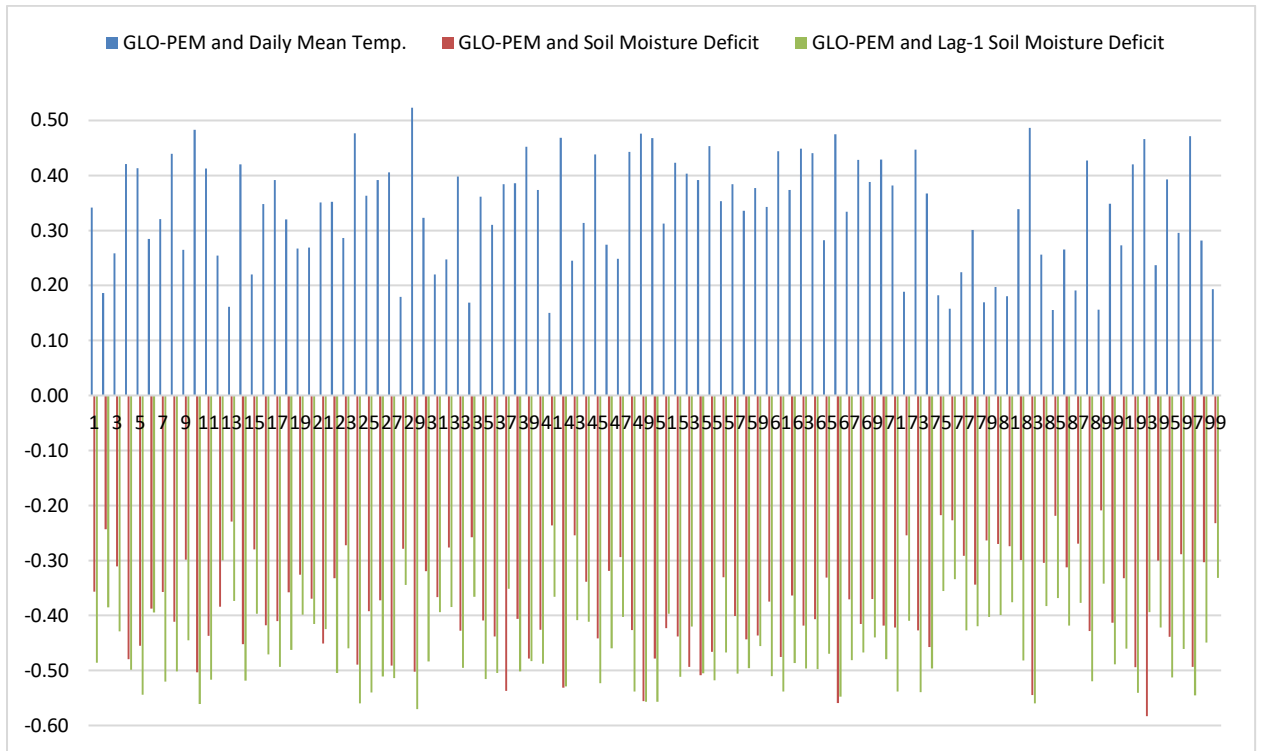


**Figure 20.** Correlation coefficients of GLO-PEM NPP with daily mean temperature, real-time soil moisture deficit, and lag-1 soil moisture deficit. The x and y axis shows sample point numbers and r-values, respectively.

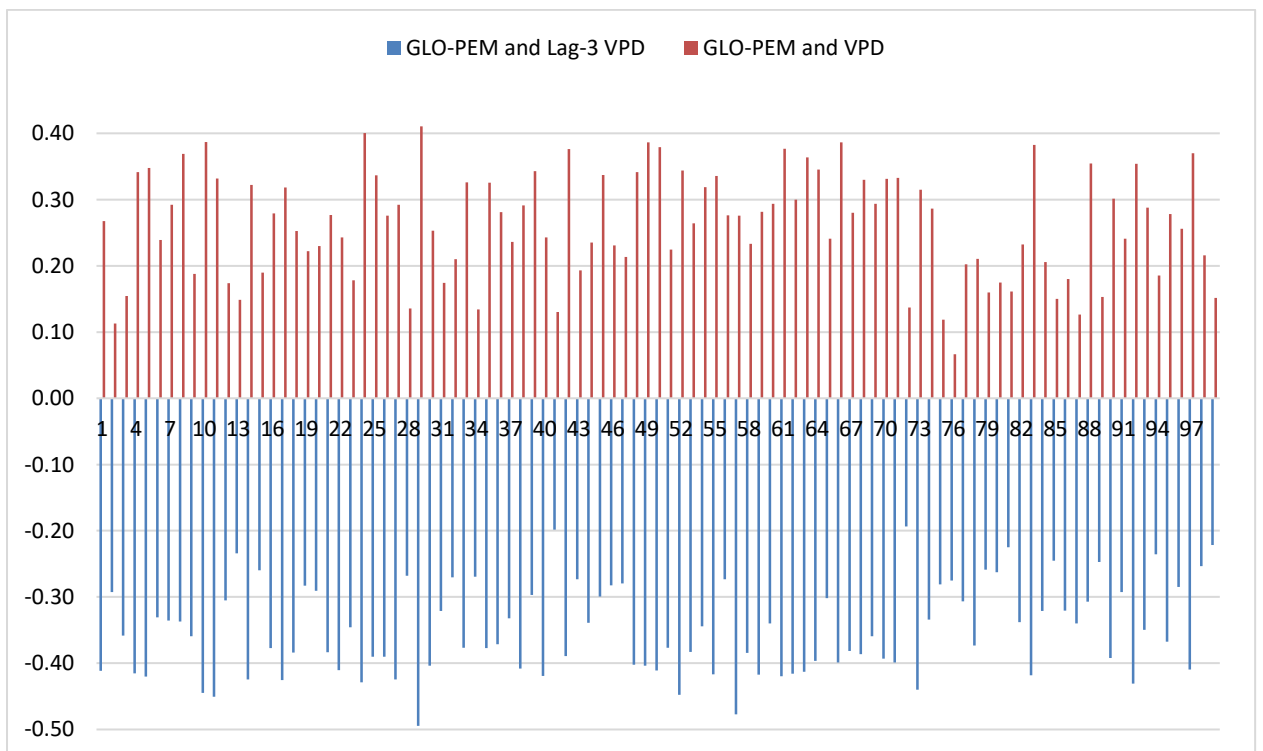


**Figure 21.** Correlation coefficients of GLO-PEM and real-time VPD and lag-3 VPD. The x and y axis shows sample point numbers and r-values, respectively.

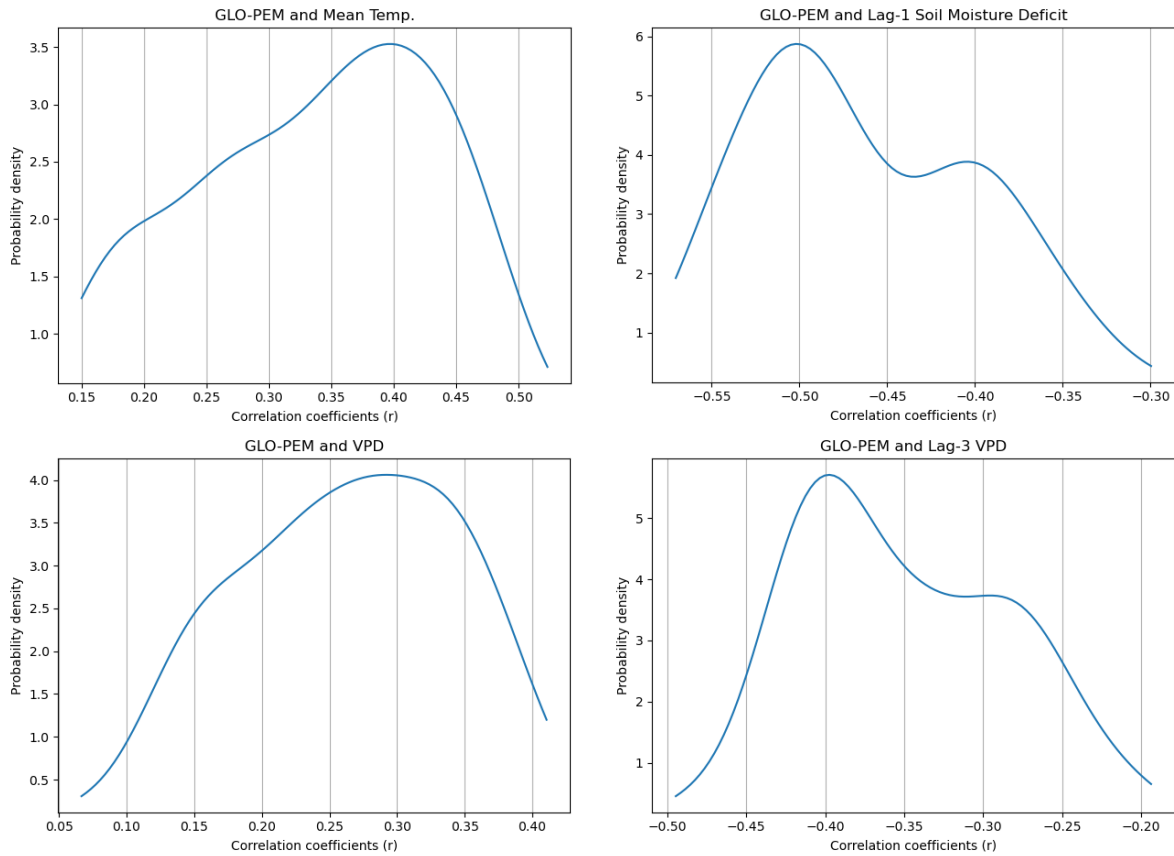


**Figure 22.** Probability density function distribution of the correlation coefficient values ( $r$ ) of GLO-PEM NPP with daily mean temperature (upper left), lag-1 soil moisture deficit (upper right), real-time VPD (lower left), and lag-3 VPD (lower right).

The correlation between monthly SPEI values and estimated NPP from both models revealed a lagged relation. After several trials, the maximum  $r$ -values of the estimated NPP with lagged SPEI values are found for a lag period of 6 and 8 for MOD17 and GLO-PEM, respectively (Figure 23). Both the 01-month and 03-month scales for monthly SPEI values were tried, and the 03-month scale SPEI values provided the overall maximum  $r$ -values. The  $p$ -values of the  $r$ -values between estimated NPP and lagged SPEI suggest that almost all the correlations are significant at a 0.05 significance level (Annex IV). Each lag period represents a monthly timestep. Therefore, a fluctuation in SPEI values has the maximum influence on NPP after at least 6 or 8 months, according to MOD17 and GLO-PEM models, respectively. However, due to the gap month in the Sentinel-2 time series data of this study, the exact lag period of lag-6 and lag-8 would be translated to one or more years. For example, considering the image acquisition dates in Table 3, the lag 8 for GLO-PEM represents the impacts of SPEI in May 2016 on the NPP in August 2017, similarly August 2017 correlates to August 2018, August 2018 correlates to July 2019, July 2019 correlates to August 2020, August 2020 correlates to July 2022 (due to data gap in 2021).

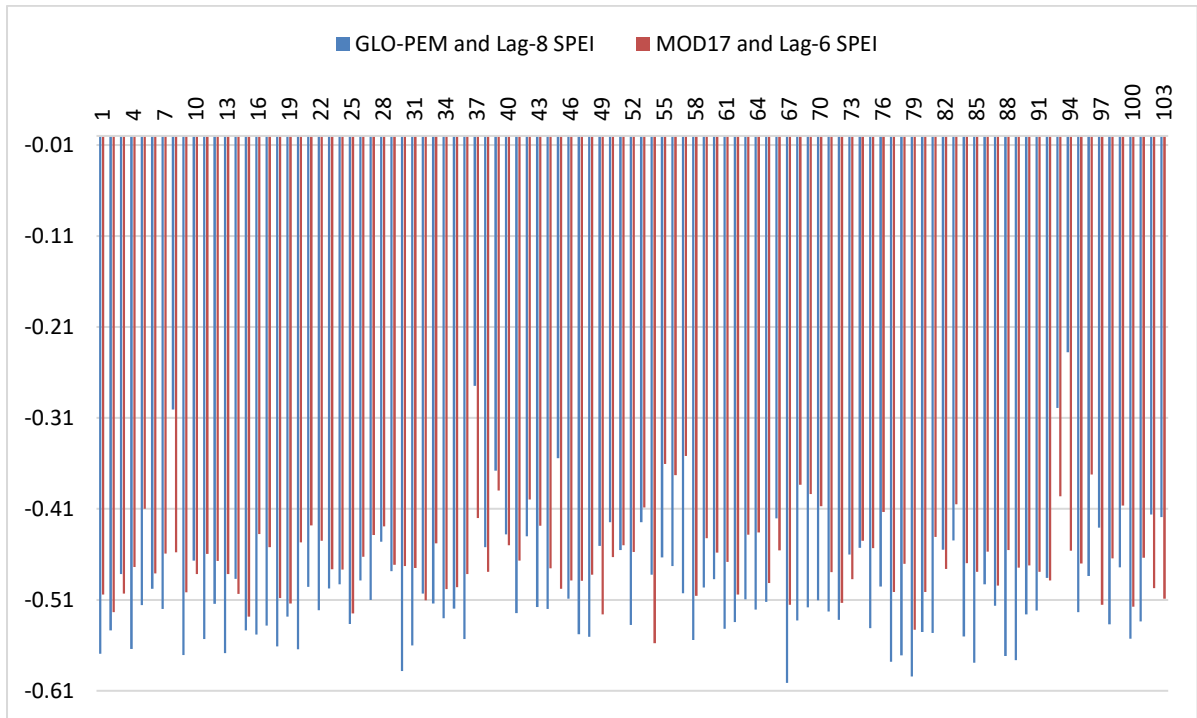


**Figure 23.** Correlation coefficients of MOD17 and GLO-PEM NPP with lagged SPEI values with 03-month time scale. The lag period for GLO-PEM and MOD17 is 8 and 6, respectively. The x and y axis shows sample point numbers and r-values, respectively.

## 4. DISCUSSION

The study employed two LUE-based models, i.e., MOD17 and GLO-PEM, with Sentinel-2 data to estimate NPP in a temperate forest for assessing the impact of the 2018 drought on NPP. The study found that the GLO-PEM model fits better with the NPP estimated using forest inventory data, whereas their relation with MODIS products shows considerable variation. The NPP shows a negative trend in different sample points during 2016 and 2022. The NPP during the post-2018 is significantly less than in the pre-2018 period. The NPP mostly showed a significant correlation between the climate variables and SPEI values. The critical finding is that the estimated NPP showed lagged correlation with VPD, soil moisture deficit, and SPEI values that revealed the delayed or legacy response of NPP to drought and associated impacts.

The following sections discuss MOD17 and GLO-PEM with Sentinel-2 data, model outputs and performance, and the impacts of the 2018 drought on NPP. The first section discusses the challenges of using the selected models with Sentinel-2 data at first. Then, the following two sections discuss the findings of the study. The second section discusses the models' performance related to the first objective. The third section (impacts of the 2018 drought on NPP) the temporal change of NPP and its relation to climate variables, which is associated with the second objective.

### 4.1. MOD17 and GLO-PEM with Sentinel-2 data

An important aspects of this study is to retrieve NPP from the high spatial resolution satellite imageries (i.e., Sentinel-2) for a better understanding of the application of these types of remote sensing data in ecosystem modelling. Another important aspect is using the LUE-based models (i.e., MOD17 and GLO-PEM) that require one of the critical input variables (i.e., FAPAR) to be directly estimated from the satellite image reflectance. Therefore, first of all, these two aspects of the study require some reflection as they brought the opportunity to explore new dimensions on the one hand, but there were also challenges on the other hand.

The spatial resolution of the satellite image is critical as the coarse resolution data average reflectance from many non-vegetation features along with the vegetation. In contrast, the high resolution tends to contain information from more homogenous land covers. Nouri et al. (2020) found that satellite data with high spatial resolution can detect the variation and changes in spectral information of vegetation more precisely than the coarse resolution data. The high-resolution data can also discriminate different vegetation types more accurately (Burchard-Levine et al., 2021), essential for NPP modelling as photosynthesis depends on vegetation types. The high spatial resolution satellite image has been found more effective in NPP estimation, especially due to its capacity to discriminate vegetation from other features and vegetation types (Pan et al., 2009; Wu & Bauer, 2012; Yan et al., 2018). However, using high spatial resolution data comes with challenges related to frequency. For instance, high-frequency or lower time interval data is available for coarse spatial resolution data (i.e., AVHRR, MODIS with daily or near-daily frequency). On the other hand, the high spatial resolution data comes with relatively lower frequency (i.e., Landsat and Sentinel-2 with eight days and five days, respectively). Therefore, the cloud-cover-related data gap in high spatial resolution optical remote sensing prevents obtaining a very frequent time series. This study also encountered this challenge as the cloud cover-related obstacle in BFNP caused image gap and error in the Sentinel-2 time series, preventing obtaining a clearer seasonal variation of NPP and precise temporal change. It is not feasible to interpolate the relatively large image gap since the interpolated images may fail to obtain accurate information on the vegetation change during the data gap. Harmonization of Landsat and Sentinel-2 data could increase the time series frequency as their spatial resolution is close.

As for another aspect, the major challenge of MOD17 and GLO-PEM models is the estimation of FAPAR from the vegetation indices, as the variation in indices and spectral resolution cause both underestimation and overestimation of FAPAR. There is a limitation in available knowledge about the relationship between vegetation spectral indices and FAPAR (Zhang et al., 2015), because the complex and heterogenous structure of vegetation cover and spectral uncertainties of the sensors affect the relations (Gobron et al., 2008). Furthermore, the inherent source of errors in vegetation indices such as soil brightness, soil moisture, and saturation of NDVI in dense vegetation also generates errors in FAPAR estimation (Clevers, 2014). Moreover, the selection of maximum LUE parameter values also affects outputs of MOD17 and GLO-PEM models. These values can be vegetation-specific or universal. The literature suggests a wide range of values (Annex I). Therefore, this is another challenge of using these models, influencing the models' performance.

Keeping these challenges in mind, if we look into the time series of this study, the time series is significantly fragmented due to the image gap. Therefore, it was not feasible to analyse the spatial and temporal distribution of NPP using the annual total or annual mean productivity. Hence, a representative month, i.e., August, was selected since this month lies between the mid and end of the growing season when the foliage reaches a mature stage. Another reason was in 2021, there were so many negative NPP values during mid-season or summer months, possibly due to a combination of errors related to atmospheric distortion, lower productivity, and tree mortality or logging that may not provide a meaningful temporal change scenario. However, despite selecting August as a representative month, we had to choose September for 2021 due to the image gap between August and July. When checking input variables of the summer months of 2021, it appeared that the NDVI had a prevalence of negative values that caused negative FAPAR, thus a negative NPP.

## **4.2. Model outputs and performance**

Our results revealed that using MOD17, NPP was overestimated in all three months in 2016 (i.e., May, July, and August) compared to forest inventory NPP. However, the latter two months are considerable here (35 and 33% overestimation in July and August, respectively) as the difference between estimated MOD17-NPP and measured NPP in May is marginal. The overestimation tendency of the MOD17 model was also observed in previous studies conducted by Turner et al. (2006). Although the previous studies (i.e., Ardö, 2015; Turner et al., 2006b) evaluated the MODIS-NPP products estimated by the same model using MODIS reflectance, the present findings indicate that the model persists in its overestimation nature when applied with Sentinel-2 reflectance. The previous study identified that one of the reasons for this overestimation is due to the high FAPAR value (Turner et al., 2006b). Ardö (2015) also showed that the MOD17 model yields higher NPP due to its sensitivity to plant's absorbed incoming solar radiation. Therefore, evaluating FAPAR estimated from the Sentinel-2 reflectance can be a future endeavor to adjust further and improve the prediction accuracy of NPP products using the MOD17 model. Although the  $R^2$  value for the MOD17 model using Sentinel-2 data is not very high in this study, a contrasting finding exists in literature where the MOD17 model with Sentinel-2 data agreed very strongly (average  $R^2 = 0.92$  for various species) with the flux tower-measured data (i.e., Mngadi et al., 2022). Hence, a more extended period of reference data like forest inventory or flux tower data could have possibly increased the  $R^2$  of MOD17-NPP in this study.

On the other hand, the GLO-PEM model estimated NPP well as it generated NPP closer to the forest inventory NPP than the MOD17 approach. The better agreement of the GLO-PEM model is also evident from the coefficient of determinants values, where about 84% of GLO-PEM NPP can be explained by the field-measured NPP, compared to 32% in the case of the MOD17 model. Liu et al. (2022) reported that the water-related stress scalars impact the performance of the LUE-based models more than the

temperature-related stress scalars. Therefore, using soil moisture deficit scalar in the GLO-PEM model may have contributed to the better fit in estimated NPP products.

As for the second approach for evaluating the NPP products in this study is comparing the MOD17- NPP and GLO-PEM- NPP to other NPP products (i.e., MODIS NPP products), promising results are found when compared to MODIS productivity products. The  $R^2$  values of 0.16 to 0.72 between the MOD17 and MODIS-NPP imply a considerable variation in their relationship.. A recent study attempted to estimate GPP using the MOD17 model with Sentinel-2 data, where they found 57% agreement between the model output and eddy covariance flux tower data (Junttila et al., 2023). Another study found 45 and 52% average agreement between the MOD17 model with MODIS data against the field-measured data on sunny and cloudy days, respectively (L. Liu et al., 2022). Although our approach of using Sentinel-2 data applying the MOD17 model and then comparing it to MODIS products differs from the previous studies, we can find a general idea that the MOD17 model performs moderately well against the evaluation data. The GLO-PEM model also shows similar findings where the MODIS-NPP can explain about 15 to 70% of estimated NPP based on the  $R^2$  values. However, a previous study found the average agreement between GLO-PEM and eddy covariance flux tower data 51 and 43% for sunny and cloudy days, respectively (L. Liu et al., 2022).

The large range of the  $R^2$  values between MOD17 and GLO-PEM NPP and MODIS NPP may be attributed to a few reasons. Firstly, the mismatch between the acquisition date of Sentinel-2 and the dates of the 8-day composite of MODIS data may have contributed to this large variation in the  $R^2$  values. Secondly, the MODIS products used climate data from GMAO-NASA with a different spatial resolution. On the other hand, this study used climate data from ECMWF (ERA5 reanalysis) after downscaling to 10 m spatial resolution. It might have caused some distortion in scalar calculations too. Besides, the MODIS products use MODIS land cover maps with a coarse spatial resolution (i.e., 500 m), whereas this study used resampled Corine land cover map with a fine spatial resolution (i.e., 10 m). Most importantly, this study used Sentinel-2 reflectance to estimate FAPAR instead of MODIS reflectance like the MODIS products. Moreover, different equations applied for the estimation of the FAPAR in both cases, which might have caused differences in the quantity of NPP. Furthermore, the MODIS products were downscaled from 500 m to 10 m spatial resolution to match the spatial resolution of the estimated NPP, which may have also caused distortion.

Overall, despite the shortcoming of the shorter period of field-measured NPP data, it can be concluded that the GLO-PEM model performed better than the MOD17 model. Moreover, although verification with MODIS-NPP products is not an ideal evaluation approach, the findings suggest that both models performed almost similarly when compared with MODIS-NPP products.

In addition, the spatial distribution of NPP from 2016 to 2018 corresponds well with the vegetation types. The difference in productivity can be distinguished between the tree and other (Figure 4) types of vegetation (i.e., grass, shrub, pasture, etc.), which implies that the model can quantify vegetation-specific NPP as the algorithm incorporates the land cover types and vegetation type-specific parameter values (i.e., maximum LUE, scalars). The higher NPP in trees than in grass-type vegetation is consistent with the findings of other studies that also found the same outcome (Xiao et al., 2019). From the spatiotemporal distribution and the land cover-wise quantification of NPP, two significant occurrences can be picked up for the discussion. Firstly, the estimated NPP is slightly lower in the GLO-PEM model compared to the MOD17 model. Out of three environmental scalars of GLO-PEM model, two are different than the scalars of MOD17. For instance, GLO-PEM uses a daily mean temperature scalar instead of the daily minimum temperature scalar (in MOD17) and a soil moisture deficit scalar. The use of one extra scalar, such as soil

moisture deficit and different temperature scalar, may downregulate the maximum LUE and lead to slightly higher than the scalars of the MOD17. Therefore, in most cases, the GLO-PEM model generated a lower NPP than MOD17. Secondly, deciduous trees show higher productivity during the stressed period than evergreen trees. Although the area size of the evergreen land cover is larger than the deciduous land cover in the study area, the results demonstrated that the NPP value is higher for the deciduous trees than for evergreen trees in 2019, 2020, and 2021. The review of the literature suggests that deciduous trees have a higher tolerance ability than evergreen trees in stressed environments due to higher water use efficiency (de Souza et al., 2020; di Francescantonio et al., 2020; Tomlinson et al., 2013).

### 4.3. Impacts of the 2018 drought on NPP

The second research question deals with the impacts of the 2018 drought, which was one of the most significant meteorological droughts in Europe (Cammalleri et al., 2023). The results also show a substantial decrease of NPP in the latter years after 2018, this change may not be attributed solely to the impacts of 2018 drought. There was a drought in-between late 2016 and early 2017 (García-Herrera et al., 2019). Multi-year droughts from 2018 onwards have been found in the literatures; for instance, Rakovec et al. (2022) reported that the entire span from 2018 to 2020 was a drought period, provided that the drought fluctuated temporarily and spatially. The European Drought Observatory (EDO) also reported several drought events in 2019 and 2020 in its annual drought report (P et al., 2021). Furthermore, 2022 was also reported as a drought year, one of the worst in centuries, mainly due to heat waves and water stress conditions (Commission et al., 2022). Another characteristic of the drought's impact on the ecosystem function is that the impacts of the drought may appear later. This lag period of drought impact, also known as drought legacy, can cause the cumulative impacts of drought in addition to the immediate impacts felt during the drought (Müller & Bahn, 2022). Therefore, we may argue that the reduction of NPP after 2018 is a cumulative consequence of 2018 and other subsequent droughts, including immediate and legacy impacts. The findings of other studies may support this argument. For instance, Schnabel et al. (2022) reported that tree growth was not reduced significantly in 2018, likely due to the available soil moisture that partly compensated for the meteorological water stress. However, a significant decrease in vegetation growth was observed in 2019, which can be attributed to the legacy impacts of the 2018 drought and the succeeding impacts of the latter drought (Schnabel et al., 2022). Similarly, the reduction in NPP in 2018 detected by MOD17 might have been influenced by the 2016 drought in addition to the immediate impact of the 2018 drought.

After 2018, a prevalence of negative NPP and significantly lower NPP have been observed in the results for the years 2019, 2020, and 2021. This occurrence can be attributed to decrease in productivity due to drought and drought-induced tree mortality (Senf et al., 2020). Arend et al. (2022) found that the European Beech (*fagus sylvatica*), the dominant deciduous tree in BFNP, suffered from defoliation due to the drought. This impact extended to the following years also, as the embolized xylem does not regain function in the season following a drought (Arend et al., 2022). Furthermore, the immature leaf senescence and crown dieback that increasingly led to the mortality of European Beech trees were also observed in the subsequent years of drought in northern Switzerland (Frei et al., 2022). Moreover, The surviving trees also showed more crown dieback tendencies than the natural occurrence in the following years of the drought (Frei et al., 2022). Additionally, the drought-affected trees (i.e., premature leaf senescence) were susceptible to infestation (i.e., bark beetle, bleeding cankers) by more than double compared to other trees in the subsequent years (Frei et al., 2022; Nardi et al., 2023). Besides the deciduous trees (i.e., European Beech), the coniferous or evergreen trees were also affected by the 2018-2020 drought-induced disturbances. Research showed that the impacts on coniferous trees were more than those of the deciduous trees

(Thonfeld et al., 2022). The study reported that the Spruce trees (*Picea abies*), which considers as a dominant evergreen species in BFNP, largely suffered from canopy cover loss due to the 2018-2020 drought and drought-induced insect infestations and forced clear-cut in Germany (Thonfeld et al., 2022). Another study by Obladen et al. (2021) also reported dieback in Beech and Spruce trees, especially high mortality in Spruce trees induced by the 2018-2019 drought in Bavaria, Germany. Conversely, in addition to drought-related productivity and tree loss, other reasons, such as windthrow and regular harvesting, also took place (Thonfeld et al., 2022), possibly contributing to the NPP reduction. In short, the substantial decrease and negative values in the NPP estimation of this study may be attributed to the combined impacts of drought in 2018 and the subsequent droughts that caused reduced productivity, insect infestation, tree mortality, and additional forced clear-cut. Another reason for the thorough detection of negative NDVI may be the spatial resolution. The coarse-resolution image aggregates the reflectance from all the vegetation within the pixel, which may attenuate or neutralize the poor reflectance from the stressed or dead vegetation by the strong reflectance from the healthy vegetation. On the other hand, Sentinel-2 has a 10 m spatial resolution, and the heterogeneity of the signal persists; thus, the NPP reduction might have been discriminated rightly.

The correlation between estimated NPP and climate data reflects the drought very well. The higher r-values of NPP with lagged soil moisture deficit than real-time soil moisture deficit indicates that the impacts of soil moisture deficit on NPP take some time to appear. These findings are consistent with the legacy impact of drought (Müller & Bahn, 2022). However, the negative r-values of real-time soil moisture deficit suggest an immediate impact. On the other hand, the positive r-values of the real-time VPD suggest that the negative impact of the VPD increase was not felt immediately. One possible reason is that the available soil water may compensate for the atmospheric water stress for a short time, which helps the plants keep their stomata open (Xu et al., 2023). However, the higher negative r-values for lagged correlation of VPD indicate the delayed influence of water stress on NPP, which is also consistent with the drought legacy impact.

Another interesting finding of this study is the higher lag period in the correlation between NPP and monthly SPEI values. This result implies that the maximum impact of drought on vegetation productivity occurs 6 and 8 monthly-timestep later for MOD17 and GLO-PEM, respectively. However, due to the gap month in this study's Sentinel-2 time series data, lag-6 and lag-8 would be converted to one or more years. For instance, lag 8 for GLO-PEM represents the effects of SPEI in May 2016 on the NPP in August 2017, similarly August 2017 correlates to August 2018, August 2018 to July 2019, July 2019 to August 2020, and August 2020 to July 2022 (due to data gap in 2021). This finding justifies the legacy impact of drought and the substantial reduction of NPP after 2018 up to 2021. The previous studies also found one to two or more years of lagged impacts of drought on tree mortality (Bigler et al., 2007). Moreover, the monthly SPEI with the 03-month time scale has been found more effective in establishing the relationship between drought and NPP than the 01-month time scale.

Overall, the r-values for all the climate variables are mostly around 0.45. It suggests that one single environmental factor only partially controls NPP as there are many other forcing factors that might be involved, including plant physiology, nutrients, atmospheric carbon dioxide, nitrogen, etc. This scenario points out one of the limitations of these LUE-based models: they do not consider many essential variables.

## 5. CONCLUSION

This study intended to assess the performance of two LUE-based models in estimating NPP using high spatial resolution Sentinel-2 imageries and to investigate the 2018 drought impacts on NPP in BFNP. Two models, namely MOD17 and GLO-PEM, have been selected that require PAR, FAPAR, maximum LUE values, and environmental scalars. MOD17 requires daily minimum temperature scalars and VPD scalars, whereas GLO-PEM requires daily mean temperature, VPD, and soil moisture deficit scalars. FAPAR was estimated using the NDVI values retrieved from the Sentinel-2 imageries. PAR and environmental scalars have been estimated based on the required climate data collected from the ERA5 reanalysis data of ECMWF. Other necessary data, including land covers, forest inventory data, and MODIS-NPP products, have also been collected for model implementation and verification. In addition, monthly SPEI values have been collected for drought impact analysis. Several geospatial data computing platforms and environments, including GEE, SNAP, ArcGIS Pro, MATLAB, and Python, have been used in different stages of data analysis. The model outputs were used to perform several statistical analyses.

The results show that the MOD17 model overestimated the NPP compared to the forest inventory NPP. NPP estimated using the GLO-PEM model showed a better accuracy versus the forest inventory NPP data. The comparison of estimated NPP with MODIS-NPP shows that both models perform almost similarly; however, the prediction accuracy of the NPP retrieved from GLO-PEM were slightly lower than MOD17. Significant reductions in NPP value have been observed during the post-drought (i.e., 2019-2022) compared to the pre-drought (i.e., 2016-2018) period. The slope values of the linear trend in all the sample points show a downward trend of NPP. Estimated NPP from MOD17 and GLO-PEM models positively correlate with minimum and mean temperatures. On the other hand, retrieved NPP shows negative relation with real-time and lagged soil moisture deficit and lagged VPD, whereas, however, a positive relation was observed between retrieved NPP and real-time VPD. In addition, negative relation has been found between predicted NPP and lagged SPEI values. The negative correlations of NPP with lagged VPD, lagged soil moisture deficit, and lagged SPEI indicate drought's negative impact on NPP.

Despite the limitations in the verification of the estimated NPP due to the unavailability of the forest inventory dataset and temporal distortion in the MODIS products, important findings may be drawn to support the first hypothesis. Both models generate promising outputs as the estimated NPP has positive relations with the forest inventory NPP and MODIS-NPP. Although the forest inventory data has a shorter period, a better fit of GLO-PEM shows this model's compatibility in NPP estimation. The study produced substantial information to support the second hypothesis as well. The significant reduction of NPP after 2018 is a consequence of the cumulative impacts of 2018 and subsequent droughts and associated disturbances (i.e., tree mortality, insect infestation, and forced logging). Moreover, the reduction of NPP (in MOD17) in 2018 than 2016 and 2017 may be attributed to the immediate impact of the 2018 drought and the legacy impact of the 2016 drought. The lagged correlation of VPD, soil moisture deficit, and SPEI values with NPP also supports the drought-caused impacts.

The study has some limitations that influenced the current results on the one hand and open opportunities for future studies on the other hand. The cloud cover and atmospheric distortions prevented obtaining a frequent time series of Sentinel-2 images which caused difficulty in temporal change detection and correlation with the climate data. A fusion between Sentinel-2 and Landsat could have increased the data frequency. Estimating  $R_a$  with a fraction of GPP is another study limitation. The MOD17 lacks methods to estimate  $R_a$  at daily timesteps. The GLO-PEM's  $R_a$  estimation method also was not applicable to Sentinel-2 data due to the difference in spectral resolution between AVHRR and Sentinel-2. Therefore,

further studies are required to adjust the model adopting appropriate methods to estimate  $R_a$  at daily timestep using these models with Sentinel-2 data. Moreover, the models used NDVI for FAPAR estimation, which may have caused errors due to the inherent limitations of this vegetation index. A comparative study can be undertaken to evaluate FAPAR from NDVI and LAI to see if it improves the model's performance. Another limitation was the unavailability of field-measured data. In future, calibrating the maximum LUE parameters against the field-measured data may generate a more accurate estimation of NPP. It will improve the validation and verification also. In short, LUE-based models with Sentinel-2 has the prospect of estimating NPP with high spatial resolution. The high spatial resolution discriminates the NPP change more precisely. The models are able to detect drought and associated impacts on NPP.

## REFERENCES

- Aalbers, E. E., van Meijgaard, E., Lenderink, G., de Vries, H., & van den Hurk, B. J. J. M. (2023). The 2018 west-central European drought projected in a warmer climate: how much drier can it get? *Natural Hazards and Earth System Sciences*, 23(5), 1921–1946. <https://doi.org/10.5194/nhess-23-1921-2023>
- Ahmed, K. R., Paul-Limoges, E., Rascher, U., & Damm, A. (2021). A first assessment of the 2018 European drought impact on ecosystem evapotranspiration. *Remote Sensing*, 13(1), 1–17. <https://doi.org/10.3390/rs13010016>
- Ardö, J. (2015). Comparison between remote sensing and a dynamic vegetation model for estimating terrestrial primary production of Africa. *Carbon Balance and Management*, 10(1). <https://doi.org/10.1186/s13021-015-0018-5>
- Arend, M., Link, R. M., Zahnd, C., Hoch, G., Schuldt, B., & Kahmen, A. (2022). Lack of hydraulic recovery as a cause of post-drought foliage reduction and canopy decline in European beech. *New Phytologist*, 234(4), 1195–1205. <https://doi.org/10.1111/nph.18065>
- Asrar, G., Fuchs, M., Kanemasu, E. T., & Hatfield, J. L. (1984). Estimating Absorbed Photosynthetic Radiation and Leaf Area Index from Spectral Reflectance in Wheat <sup>1</sup>. *Agronomy Journal*, 76(2), 300–306. <https://doi.org/10.2134/agronj1984.00021962007600020029x>
- Bigler, C., Gavin, D. G., Gunning, C., & Veblen, T. T. (2007). Drought induces lagged tree mortality in a subalpine forest in the Rocky Mountains. *Oikos*, 116(12), 1983–1994. <https://doi.org/10.1111/j.2007.0030-1299.16034.x>
- Bruhn, D., Newman, F., Hancock, M., Povlsen, P., Slot, M., Sitch, S., Drake, J., Weedon, G. P., Clark, D. B., Pagter, M., Ellis, R. J., Tjoelker, M. G., Andersen, K. M., Correa, Z. R., McGuire, P. C., & Mercado, L. M. (2022). Nocturnal plant respiration is under strong non-temperature control. *Nature Communications*, 13(1), 5650. <https://doi.org/10.1038/s41467-022-33370-1>
- Burchard-Levine, V., Nieto, H., Riaño, D., Migliavacca, M., El-Madany, T. S., Guzinski, R., Carrara, A., & Martín, M. P. (2021). The effect of pixel heterogeneity for remote sensing based retrievals of evapotranspiration in a semi-arid tree-grass ecosystem. *Remote Sensing of Environment*, 260, 112440. <https://doi.org/10.1016/j.rse.2021.112440>
- Cammalleri, C., Acosta Navarro, J. C., Bavera, D., Diaz, V., Di Ciollo, C., Maetens, W., Magni, D., Masante, D., Spinoni, J., & Toreti, A. (2023). An event-oriented database of meteorological droughts in Europe based on spatio-temporal clustering. *Scientific Reports*, 13(1), 3145. <https://doi.org/10.1038/s41598-023-30153-6>
- Cao, M., Prince, S. D., Small, J., & Goetz, S. J. (2004a). Remotely sensed interannual variations and trends in terrestrial net primary productivity 1981-2000. *Ecosystems*, 7(3), 233–242. <https://doi.org/10.1007/s10021-003-0189-x>
- Cao, M., Prince, S. D., Small, J., & Goetz, S. J. (2004b). Remotely sensed interannual variations and trends in terrestrial net primary productivity 1981-2000. *Ecosystems*, 7(3), 233–242. <https://doi.org/10.1007/s10021-003-0189-x>
- Cassel, D. K., & Nielsen, D. R. (2018). *Field Capacity and Available Water Capacity* (pp. 901–926). <https://doi.org/10.2136/sssabookser5.1.2ed.c36>
- Chirici, G., Chiesi, M., Fibbi, L., Giannetti, F., Corona, P., & Maselli, F. (2022). High spatial resolution modelling of net forest carbon fluxes based on ground and remote sensing data. *Agricultural and Forest Meteorology*, 316. <https://doi.org/10.1016/j.agrformet.2022.108866>

- Choat, B., Jansen, S., Brodribb, T. J., Cochard, H., Delzon, S., Bhaskar, R., Bucci, S. J., Feild, T. S., Gleason, S. M., Hacke, U. G., Jacobsen, A. L., Lens, F., Maherali, H., Martínez-Vilalta, J., Mayr, S., Mencuccini, M., Mitchell, P. J., Nardini, A., Pittermann, J., ... Zanne, A. E. (2012). Global convergence in the vulnerability of forests to drought. *Nature*, *491*(7426), 752–755. <https://doi.org/10.1038/nature11688>
- Ciais, Ph., Reichstein, M., Viovy, N., Granier, A., Ogé, J., Allard, V., Aubinet, M., Buchmann, N., Bernhofer, Chr., Carrara, A., Chevallier, F., de Noblet, N., Friend, A. D., Friedlingstein, P., Grünwald, T., Heinesch, B., Keronen, P., Knohl, A., Krinner, G., ... Valentini, R. (2005). Europe-wide reduction in primary productivity caused by the heat and drought in 2003. *Nature*, *437*(7058), 529–533. <https://doi.org/10.1038/nature03972>
- Clevers, J. G. P. W. (2014). *Beyond NDVI: Extraction of Biophysical Variables From Remote Sensing Imagery* (pp. 363–381). [https://doi.org/10.1007/978-94-007-7969-3\\_22](https://doi.org/10.1007/978-94-007-7969-3_22)
- Commission, E., Centre, J. R., Toreti, A., Bavera, D., Acosta Navarro, J., Jager, A., Di Ciollo, C., Maetens, W., Magni, D., Masante, D., Mazzeschi, M., Spinoni, J., Niemeier, S., Cammalleri, C., & Hrast Essenfelder, A. (2022). *Drought in Europe : August 2022 : GDO analytical report*. Publications Office of the European Union. <https://doi.org/doi/10.2760/264241>
- Cramer, W., Kicklighter, D. W., Bondeau, A., Iii, B. M., Churkina, G., Nemry, B., Ruimy, A., Schloss, A. L., & Intercomparison, ThE. P. OF. ThE. P. (1999). Comparing global models of terrestrial net primary productivity (NPP): overview and key results. *Global Change Biology*, *5*(S1), 1–15. <https://doi.org/10.1046/j.1365-2486.1999.00009.x>
- de Souza, B. C., Carvalho, E. C. D., Oliveira, R. S., de Araujo, F. S., de Lima, A. L. A., & Rodal, M. J. N. (2020). Drought response strategies of deciduous and evergreen woody species in a seasonally dry neotropical forest. *Oecologia*, *194*(1–2), 221–236. <https://doi.org/10.1007/s00442-020-04760-3>
- di Francescantonio, D., Villagra, M., Goldstein, G., & Campanello, P. I. (2020). Drought and frost resistance vary between evergreen and deciduous Atlantic Forest canopy trees. *Functional Plant Biology*, *47*(9), 779. <https://doi.org/10.1071/FP19282>
- Du, D., Zheng, C., Jia, L., Chen, Q., Jiang, M., Hu, G., & Lu, J. (2022). Estimation of Global Cropland Gross Primary Production from Satellite Observations by Integrating Water Availability Variable in Light-Use-Efficiency Model. *Remote Sensing*, *14*(7). <https://doi.org/10.3390/rs14071722>
- European Commission. (2021). *EU Forest Strategy for 2030*.
- Frei, E. R., Gossner, M. M., Vitasse, Y., Queloz, V., Dubach, V., Gessler, A., Ginzler, C., Hagedorn, F., Meusburger, K., Moor, M., Samblás Vives, E., Rigling, A., Uitentuis, I., von Arx, G., & Wohlgemuth, T. (2022). European beech dieback after premature leaf senescence during the 2018 drought in northern Switzerland. *Plant Biology*, *24*(7), 1132–1145. <https://doi.org/10.1111/plb.13467>
- Garbulsky, M. F., Peñuelas, J., Papale, D., Ardö, J., Goulden, M. L., Kiely, G., Richardson, A. D., Rotenberg, E., Veenendaal, E. M., & Filella, I. (2010). Patterns and controls of the variability of radiation use efficiency and primary productivity across terrestrial ecosystems. *Global Ecology and Biogeography*, *19*(2), 253–267. <https://doi.org/10.1111/j.1466-8238.2009.00504.x>
- García-Herrera, R., Garrido-Perez, J. M., Barriopedro, D., Ordóñez, C., Vicente-Serrano, S. M., Nieto, R., Gimeno, L., Sorí, R., & Yiou, P. (2019). The European 2016/17 Drought. *Journal of Climate*, *32*(11), 3169–3187. <https://doi.org/10.1175/JCLI-D-18-0331.1>
- GOBRON, N., PINTY, B., AUSSEDT, O., TABERNER, M., FABER, O., MELIN, F., LAVERGNE, T., ROBUSTELLI, M., & SNOEIJ, P. (2008). Uncertainty estimates for the FAPAR operational products derived from MERIS — Impact of top-of-atmosphere radiance uncertainties and validation with field data. *Remote Sensing of Environment*, *112*(4), 1871–1883. <https://doi.org/10.1016/j.rse.2007.09.011>

- Goetz, S. J., Prince, S. D., Goward, S. N., Thawley, M. M., & Small, J. (1999). Satellite remote sensing of primary production: an improved production efficiency modeling approach. In *Ecological Modelling* (Vol. 122). [www.elsevier.com/locate/ecolmodel](http://www.elsevier.com/locate/ecolmodel)
- Goward, S. N., Tucker, C. J., & Dye, D. G. (1985). North American vegetation patterns observed with the NOAA-7 advanced very high resolution radiometer. *Vegetatio*, *64*(1), 3–14. <https://doi.org/10.1007/BF00033449>
- He, B., Cui, X., Wang, H., & Chen, A. (2014). Drought: The most important physical stress of terrestrial ecosystems. *Acta Ecologica Sinica*, *34*(4), 179–183. <https://doi.org/10.1016/j.chnaes.2014.05.004>
- He, L., Chen, J. M., Pan, Y., Birdsey, R., & Kattge, J. (2012). Relationships between net primary productivity and forest stand age in U.S. forests. *Global Biogeochemical Cycles*, *26*(3). <https://doi.org/10.1029/2010GB003942>
- Jähne, B. (1993). *Digital Image Processing*. Springer Berlin Heidelberg. <https://doi.org/10.1007/978-3-662-21817-4>
- Jin, C., Xiao, X., Merbold, L., Arneith, A., Veenendaal, E., & Kutsch, W. L. (2013). Phenology and gross primary production of two dominant savanna woodland ecosystems in Southern Africa. *Remote Sensing of Environment*, *135*, 189–201. <https://doi.org/10.1016/j.rse.2013.03.033>
- Junttila, S., Ardö, J., Cai, Z., Jin, H., Kljun, N., Klemetsson, L., Krasnova, A., Lange, H., Lindroth, A., Mölder, M., Noe, S. M., Tagesson, T., Vestin, P., Weslien, P., & Eklundh, L. (2023). Estimating local-scale forest GPP in Northern Europe using Sentinel-2: Model comparisons with LUE, APAR, the plant phenology index, and a light response function. *Science of Remote Sensing*, *7*, 100075. <https://doi.org/10.1016/j.srs.2022.100075>
- Kayiranga, A., Chen, B., Wang, F., Nthangeni, W., Dilawar, A., Hategekimana, Y., Zhang, H., & Guo, L. (2022). Spatiotemporal Variation in Gross Primary Productivity and Their Responses to Climate in the Great Lakes Region of Sub-Saharan Africa during 2001–2020. *Sustainability*, *14*(5), 2610. <https://doi.org/10.3390/su14052610>
- Krzystek, P., Serebryanyk, A., Schnörr, C., Červenka, J., & Heurich, M. (2020). Large-Scale Mapping of Tree Species and Dead Trees in Šumava National Park and Bavarian Forest National Park Using Lidar and Multispectral Imagery. *Remote Sensing*, *12*(4), 661. <https://doi.org/10.3390/rs12040661>
- Kucharik, C. J., Foley, J. A., Delire, C., Fisher, V. A., Coe, M. T., Lenters, J., Young-Molling, C., Ramankutty, N., Norman, J. M., & Gower, S. T. (2000). Testing the performance of a dynamic global ecosystem model: Water balance, carbon balance and vegetation structure. *Global Biogeochemical Cycles*, *14*(3), 795–825.
- Lai, C., Li, J., Wang, Z., Wu, X., Zeng, Z., Chen, X., Lian, Y., Yu, H., Wang, P., & Bai, X. (2018). Drought-induced reduction in net primary productivity across mainland China from 1982 to 2015. *Remote Sensing*, *10*(9). <https://doi.org/10.3390/rs10091433>
- Lieth, H. (1975). *Historical Survey of Primary Productivity Research* (pp. 7–16). [https://doi.org/10.1007/978-3-642-80913-2\\_2](https://doi.org/10.1007/978-3-642-80913-2_2)
- Lin, X., Chen, B., Chen, J., Zhang, H., Sun, S., Xu, G., Guo, L., Ge, M., Qu, J., Li, L., & Kong, Y. (2017). Seasonal fluctuations of photosynthetic parameters for light use efficiency models and the impacts on gross primary production estimation. *Agricultural and Forest Meteorology*, *236*, 22–35. <https://doi.org/10.1016/j.agrformet.2016.12.019>
- Liu, J. (1997). A process-based boreal ecosystem productivity simulator using remote sensing inputs. *Remote Sensing of Environment*, *62*(2), 158–175. [https://doi.org/10.1016/S0034-4257\(97\)00089-8](https://doi.org/10.1016/S0034-4257(97)00089-8)
- Liu, L., Gao, X., Cao, B., Ba, Y., Chen, J., Cheng, X., Zhou, Y., Huang, H., & Zhang, J. (2022). Comparing Different Light Use Efficiency Models to Estimate the Gross Primary Productivity of a Cork Oak Plantation in Northern China. *Remote Sensing*, *14*(22), 5905. <https://doi.org/10.3390/rs14225905>

- Liu, Q., Zhao, L., Sun, R., Yu, T., Cheng, S., Wang, M., Zhu, A., & Li, Q. (2022). Estimation and Spatiotemporal Variation Analysis of Net Primary Productivity in the Upper Luanhe River Basin in China from 2001 to 2017 Combining with a Downscaling Method. *IEEE Journal of Selected Topics in Applied Earth Observations and Remote Sensing*, *15*, 353–363. <https://doi.org/10.1109/JSTARS.2021.3132723>
- Machwitz, M., Gessner, U., Conrad, C., Falk, U., Richters, J., & Dech, S. (2015). Modelling the Gross Primary Productivity of West Africa with the Regional Biomass Model RBM+, using optimized 250 m MODIS FPAR and fractional vegetation cover information. *International Journal of Applied Earth Observation and Geoinformation*, *43*, 177–194. <https://doi.org/10.1016/j.jag.2015.04.007>
- Madani, N., Kimball, J. S., Affleck, D. L. R., Kattge, J., Graham, J., van Bodegom, P. M., Reich, P. B., & Running, S. W. (2014). Improving ecosystem productivity modeling through spatially explicit estimation of optimal light use efficiency. *Journal of Geophysical Research: Biogeosciences*, *119*(9), 1755–1769. <https://doi.org/10.1002/2014JG002709>
- Madani, N., Kimball, J. S., & Running, S. W. (2017). Improving Global Gross Primary Productivity Estimates by Computing Optimum Light Use Efficiencies Using Flux Tower Data. *Journal of Geophysical Research: Biogeosciences*, *122*(11), 2939–2951. <https://doi.org/10.1002/2017JG004142>
- Main-Knorn, M., Pflug, B., Louis, J., Debaecker, V., Müller-Wilm, U., & Gascon, F. (2017). Sen2Cor for Sentinel-2. In L. Bruzzone, F. Bovolo, & J. A. Benediktsson (Eds.), *Image and Signal Processing for Remote Sensing XXIII* (p. 3). SPIE. <https://doi.org/10.1117/12.2278218>
- Martínez, B., Sanchez-Ruiz, S., Gilabert, M. A., Moreno, A., Campos-Taberner, M., García-Haro, F. J., Trigo, I. F., Aurela, M., Brümmer, C., Carrara, A., De Ligne, A., Gianelle, D., Grünwald, T., Limousin, J. M., Lohila, A., Mammarella, I., Sottocornola, M., Steinbrecher, R., & Tagesson, T. (2018). Retrieval of daily gross primary production over Europe and Africa from an ensemble of SEVIRI/MSG products. *International Journal of Applied Earth Observation and Geoinformation*, *65*, 124–136. <https://doi.org/10.1016/j.jag.2017.10.011>
- Miettinen, J., Carlier, S., Häme, L., Mäkelä, A., Minunno, F., Penttilä, J., Pisl, J., Rasinmäki, J., Rauste, Y., Seitsonen, L., Tian, X., & Häme, T. (2021). Demonstration of large area forest volume and primary production estimation approach based on Sentinel-2 imagery and process based ecosystem modelling. *International Journal of Remote Sensing*, *42*(24), 9492–9514. <https://doi.org/10.1080/01431161.2021.1998715>
- Mngadi, M., Odindi, J., Mutanga, O., & Sibanda, M. (2022). Estimating aboveground net primary productivity of reforested trees in an urban landscape using biophysical variables and remotely sensed data. *Science of the Total Environment*, *802*. <https://doi.org/10.1016/j.scitotenv.2021.149958>
- Monteith, J. L. (1972). Solar Radiation and Productivity in Tropical Ecosystems. *The Journal of Applied Ecology*, *9*(3), 747. <https://doi.org/10.2307/2401901>
- Monteith, J. L. (1977). Climate and the efficiency of crop production in Britain. *Philosophical Transactions of the Royal Society of London. B, Biological Sciences*, *281*(980), 277–294. <https://doi.org/10.1098/rstb.1977.0140>
- Müller, L. M., & Bahn, M. (2022). Drought legacies and ecosystem responses to subsequent drought. *Global Change Biology*, *28*(17), 5086–5103. <https://doi.org/10.1111/gcb.16270>
- Myneni, R. B., Ramakrishna, R., Nemani, R., & Running, S. W. (1997). Estimation of global leaf area index and absorbed par using radiative transfer models. *IEEE Transactions on Geoscience and Remote Sensing*, *35*(6), 1380–1393. <https://doi.org/10.1109/36.649788>
- Myneni, R. B., & Williams, D. L. (1994). On the relationship between FAPAR and NDVI. *Remote Sensing of Environment*, *49*(3), 200–211. [https://doi.org/10.1016/0034-4257\(94\)90016-7](https://doi.org/10.1016/0034-4257(94)90016-7)

- Nanzad, L., Zhang, J., Tuvdendorj, B., Yang, S., Rinzin, S., Prodhon, F. A., & Pangali Sharma, T. P. (2021). Assessment of drought impact on net primary productivity in the terrestrial ecosystems of mongolia from 2003 to 2018. *Remote Sensing*, *13*(13). <https://doi.org/10.3390/rs13132522>
- Nardi, D., Jactel, H., Pagot, E., Samalens, J., & Marini, L. (2023). Drought and stand susceptibility to attacks by the European spruce bark beetle: A remote sensing approach. *Agricultural and Forest Entomology*, *25*(1), 119–129. <https://doi.org/10.1111/afe.12536>
- Nemani, R. R., Keeling, C. D., Hashimoto, H., Jolly, W. M., Piper, S. C., Tucker, C. J., Myneni, R. B., & Running, S. W. (2003). Climate-Driven Increases in Global Terrestrial Net Primary Production from 1982 to 1999. *Science*, *300*(5625), 1560–1563. <https://doi.org/10.1126/science.1082750>
- Nouri, H., Nagler, P., Chavoshi Borujeni, S., Barreto Munez, A., Alaghmand, S., Noori, B., Galindo, A., & Didan, K. (2020). Effect of spatial resolution of satellite images on estimating the greenness and evapotranspiration of urban green spaces. *Hydrological Processes*, *34*(15), 3183–3199. <https://doi.org/10.1002/hyp.13790>
- Obladen, N., Dechering, P., Skiadaresis, G., Tegel, W., Keßler, J., Höllner, S., Kaps, S., Hertel, M., Dulamsuren, C., Seifert, T., Hirsch, M., & Seim, A. (2021). Tree mortality of European beech and Norway spruce induced by 2018-2019 hot droughts in central Germany. *Agricultural and Forest Meteorology*, *307*, 108482. <https://doi.org/10.1016/j.agrformet.2021.108482>
- Oomen, R. J., Ewert, F., & Snyman, H. A. (2016). Modelling rangeland productivity in response to degradation in a semi-arid climate. *Ecological Modelling*, *322*, 54–70. <https://doi.org/10.1016/j.ecolmodel.2015.11.001>
- P, M. F. B., D, M., C, A.-M., C, C., A, D. J., D, M., M, M., N, M., G, N., J, S., & J, V. (2021). *Droughts in Europe and Worldwide 2019-2020*. KJ-NA-30719-EN-N (online). <https://doi.org/10.2760/415204> (online)
- Palma, A., Chu, C. Y., Petracchini, F., Yeh, M. L., Wu, C. T., & Lai, Y. C. (2021). A modeling application for ghg fluxes estimates in betel nuts plantations in taiwan. *Processes*, *9*(5). <https://doi.org/10.3390/pr9050895>
- Pan, G., Sun, G.-J., & Li, F.-M. (2009). Using QuickBird imagery and a production efficiency model to improve crop yield estimation in the semi-arid hilly Loess Plateau, China. *Environmental Modelling & Software*, *24*(4), 510–516. <https://doi.org/10.1016/j.envsoft.2008.09.014>
- Potter, C. S., Randerson, J. T., Field, C. B., Matson, P. A., Vitousek, P. M., Mooney, H. A., & Klooster, S. A. (1993). Terrestrial ecosystem production: A process model based on global satellite and surface data. *Global Biogeochemical Cycles*, *7*(4), 811–841. <https://doi.org/10.1029/93GB02725>
- Prince, S. D., & Goward, S. N. (1995a). Global Primary Production: A Remote Sensing Approach. *Journal of Biogeography*, *22*(4/5), 815. <https://doi.org/10.2307/2845983>
- Prince, S. D., & Goward, S. N. (1995b). Global Primary Production: A Remote Sensing Approach. *Journal of Biogeography*, *22*(4/5), 815. <https://doi.org/10.2307/2845983>
- Rakovec, O., Samaniego, L., Hari, V., Markonis, Y., Moravec, V., Thober, S., Hanel, M., & Kumar, R. (2022). The 2018–2020 Multi-Year Drought Sets a New Benchmark in Europe. *Earth's Future*, *10*(3). <https://doi.org/10.1029/2021EF002394>
- Reichstein, M., Running, S., Tenhunen, J., & Carboeuroflux-Modis Comparison Team. (2003). Evaluation of MODIS-driven estimates of vegetation productivity at European FLUXNET sites. *EGS - AGU - EUG Joint Assembly*, 5608.
- Rhee, J., & Im, J. (2017). Meteorological drought forecasting for ungauged areas based on machine learning: Using long-range climate forecast and remote sensing data. *Agricultural and Forest Meteorology*, *237–238*, 105–122. <https://doi.org/10.1016/j.agrformet.2017.02.011>

- Roy, J., Saugier, B., & Mooney, H. A. (2001). *Terrestrial Global Productivity*. Academic Press.  
<https://doi.org/10.1016/B978-0-12-505290-0.X5000-5>
- Running, S. W., & Hunt, E. R. (1993). Generalization of a Forest Ecosystem Process Model for Other Biomes, BIOME-BGC, and an Application for Global-Scale Models. In *Scaling Physiological Processes* (pp. 141–158). Elsevier. <https://doi.org/10.1016/B978-0-12-233440-5.50014-2>
- RUNNING, S. W., JUSTICE, C. O., SALOMONSON, V., HALL, D., BARKER, J., KAUFMANN, Y. J., STRAHLER, A. H., HUETE, A. R., MULLER, J.-P., VANDERBILT, V., WAN, Z. M., TEILLET, P., & CARNEGGIE, D. (1994). Terrestrial remote sensing science and algorithms planned for EOS/MODIS. *International Journal of Remote Sensing*, 15(17), 3587–3620.  
<https://doi.org/10.1080/01431169408954346>
- Running, S. W., Nemani, R. R., Peterson, D. L., Band, L. E., Potts, D. F., Pierce, L. L., & Spanner, M. A. (1989). Mapping Regional Forest Evapotranspiration and Photosynthesis by Coupling Satellite Data with Ecosystem Simulation. *Ecology*, 70(4), 1090–1101. <https://doi.org/10.2307/1941378>
- Running, S. W., Thornton, P. E., Nemani, R., & Glassy, J. M. (2000). Global Terrestrial Gross and Net Primary Productivity from the Earth Observing System. In *Methods in Ecosystem Science* (pp. 44–57). Springer New York. [https://doi.org/10.1007/978-1-4612-1224-9\\_4](https://doi.org/10.1007/978-1-4612-1224-9_4)
- Running, S. W., & Zhao, M. (2019). *User's Guide Daily GPP and Annual NPP (MOD17A2H/A3H) and Year-end Gap-Filled (MOD17A2HGF/A3HGF) Products NASA Earth Observing System MODIS Land Algorithm (For Collection 6)*.
- Sala Osvaldo E. and Austin, A. T. (2000). Methods of Estimating Aboveground Net Primary Productivity. In R. B. and M. H. A. and H. R. W. Sala Osvaldo E. and Jackson (Ed.), *Methods in Ecosystem Science* (pp. 31–43). Springer New York. [https://doi.org/10.1007/978-1-4612-1224-9\\_3](https://doi.org/10.1007/978-1-4612-1224-9_3)
- Sasai, T., Ichii, K., Yamaguchi, Y., & Nemani, R. (2005). Simulating terrestrial carbon fluxes using the new biosphere model “biosphere model integrating eco-physiological and mechanistic approaches using satellite data” (BEAMS). *Journal of Geophysical Research: Biogeosciences*, 110(G2), n/a-n/a.  
<https://doi.org/10.1029/2005jg000045>
- Sasai, T., Okamoto, K., Hiyama, T., & Yamaguchi, Y. (2007). Comparing terrestrial carbon fluxes from the scale of a flux tower to the global scale. *Ecological Modelling*, 208(2–4), 135–144.  
<https://doi.org/10.1016/j.ecolmodel.2007.05.014>
- Schnabel, F., Purrucker, S., Schmitt, L., Engelmann, R. A., Kahl, A., Richter, R., Seele-Dilbat, C., Skiadaresis, G., & Wirth, C. (2022). Cumulative growth and stress responses to the 2018–2019 drought in a European floodplain forest. *Global Change Biology*, 28(5), 1870–1883.  
<https://doi.org/10.1111/gcb.16028>
- Seaquist, J. W., Olsson, L., & Ardö, J. (2003). A remote sensing-based primary production model for grassland biomes. *Ecological Modelling*, 169(1), 131–155. [https://doi.org/10.1016/S0304-3800\(03\)00267-9](https://doi.org/10.1016/S0304-3800(03)00267-9)
- Senf, C., Buras, A., Zang, C. S., Rammig, A., & Seidl, R. (2020). Excess forest mortality is consistently linked to drought across Europe. *Nature Communications*, 11(1), 6200.  
<https://doi.org/10.1038/s41467-020-19924-1>
- Shah, M., Thakkar, A., & Shastri, H. (2023). A Comparative Study of Spatial Interpolation Methods for CMIP6 Monthly Historical and Future Hydro-climatic Datasets for Indian Region. *2023 International Conference on Machine Intelligence for GeoAnalytics and Remote Sensing (MIGARS)*, 1–4.  
<https://doi.org/10.1109/MIGARS57353.2023.10064528>
- Shim, C., Hong, J., Hong, J., Kim, Y., Kang, M., Malla Thakuri, B., Kim, Y., & Chun, J. (2014). Evaluation of MODIS GPP over a complex ecosystem in East Asia: A case study at Gwangneung flux tower in Korea. *Advances in Space Research*, 54(11), 2296–2308. <https://doi.org/10.1016/j.asr.2014.08.031>

- Sims, D. A., Rahman, A. F., Cordova, V. D., El-Masri, B. Z., Baldocchi, D. D., Flanagan, L. B., Goldstein, A. H., Hollinger, D. Y., Misson, L., Monson, R. K., Oechel, W. C., Schmid, H. P., Wofsy, S. C., & Xu, L. (2006). On the use of MODIS EVI to assess gross primary productivity of North American ecosystems. *Journal of Geophysical Research: Biogeosciences*, *111*(G4).  
<https://doi.org/10.1029/2006JG000162>
- Sitch, S., Smith, B., Prentice, I. C., Arneth, A., Bondeau, A., Cramer, W., Kaplan, J. O., Levis, S., Lucht, W., Sykes, M. T., Thonicke, K., & Venevsky, S. (2003). Evaluation of ecosystem dynamics, plant geography and terrestrial carbon cycling in the LPJ dynamic global vegetation model. *Global Change Biology*, *9*(2), 161–185. <https://doi.org/10.1046/j.1365-2486.2003.00569.x>
- Sjöström, M., Ardö, J., Eklundh, L., El-Tahir, B. A., El-Khidir, H. A. M., Hellström, M., Pilesjö, P., & Seaquist, J. (2009). Evaluation of satellite based indices for gross primary production estimates in a sparse savanna in the Sudan. *Biogeosciences*, *6*(1), 129–138. <https://doi.org/10.5194/bg-6-129-2009>
- Sjöström, M., Zhao, M., Archibald, S., Arneth, A., Cappelaere, B., Falk, U., de Grandcourt, A., Hanan, N., Kergoat, L., Kutsch, W., Merbold, L., Mougin, E., Nickless, A., Nouvellon, Y., Scholes, R. J., Veenendaal, E. M., & Ardö, J. (2013). Evaluation of MODIS gross primary productivity for Africa using eddy covariance data. *Remote Sensing of Environment*, *131*, 275–286.  
<https://doi.org/10.1016/j.rse.2012.12.023>
- Smith, M.-L., Ollinger, S. v., Martin, M. E., Aber, J. D., Hallett, R. A., & Goodale, C. L. (2002). Direct Estimation of Aboveground Forest Productivity through Hyperspectral Remote Sensing of Canopy Nitrogen. *Ecological Applications*, *12*(5), 1286. <https://doi.org/10.2307/3099972>
- Song, C., Dannenberg, M. P., & Hwang, T. (2013). Optical remote sensing of terrestrial ecosystem primary productivity. *Progress in Physical Geography*, *37*(6), 834–854.  
<https://doi.org/10.1177/0309133313507944>
- Tagesson, T., Fensholt, R., Cropley, F., Guiro, I., Horion, S., Ehammer, A., & Ardö, J. (2015). Dynamics in carbon exchange fluxes for a grazed semi-arid savanna ecosystem in West Africa. *Agriculture, Ecosystems & Environment*, *205*, 15–24. <https://doi.org/10.1016/j.agee.2015.02.017>
- Thonfeld, F., Gessner, U., Holzwarth, S., Kriese, J., da Ponte, E., Huth, J., & Kuenzer, C. (2022). A First Assessment of Canopy Cover Loss in Germany's Forests after the 2018–2020 Drought Years. *Remote Sensing*, *14*(3), 562. <https://doi.org/10.3390/rs14030562>
- Tomlinson, K. W., Poorter, L., Sterck, F. J., Borghetti, F., Ward, D., de Bie, S., & van Langevelde, F. (2013). Leaf adaptations of evergreen and deciduous trees of semi-arid and humid savannas on three continents. *Journal of Ecology*, *101*(2), 430–440. <https://doi.org/10.1111/1365-2745.12056>
- Tucker, C. J., & Sellers, P. J. (1986). Satellite remote sensing of primary production. *International Journal of Remote Sensing*, *7*(11), 1395–1416. <https://doi.org/10.1080/01431168608948944>
- Turner, D. P., Ritts, W. D., Cohen, W. B., Gower, S. T., Running, S. W., Zhao, M., Costa, M. H., Kirschbaum, A. A., Ham, J. M., Saleska, S. R., & Ahl, D. E. (2006a). Evaluation of MODIS NPP and GPP products across multiple biomes. *Remote Sensing of Environment*, *102*(3–4), 282–292.  
<https://doi.org/10.1016/j.rse.2006.02.017>
- Turner, D. P., Ritts, W. D., Cohen, W. B., Gower, S. T., Running, S. W., Zhao, M., Costa, M. H., Kirschbaum, A. A., Ham, J. M., Saleska, S. R., & Ahl, D. E. (2006b). Evaluation of MODIS NPP and GPP products across multiple biomes. *Remote Sensing of Environment*, *102*(3–4), 282–292.  
<https://doi.org/10.1016/j.rse.2006.02.017>
- TURNER, D. P., URBANSKI, S., BREMER, D., WOFYSY, S. C., MEYERS, T., GOWER, S. T., & GREGORY, M. (2003). A cross-biome comparison of daily light use efficiency for gross primary production. *Global Change Biology*, *9*(3), 383–395. <https://doi.org/10.1046/j.1365-2486.2003.00573.x>
- United Nations. (1992, June). Agenda 21. *United Nations Conference on Environment & Development*.

- United Nations. (2018). *The 2030 Agenda and the Sustainable Development Goals: An opportunity for Latin America and the Caribbean (LC/G.2681-P/Rev.3)*.
- van der Knaap, W. O., van Leeuwen, J. F. N., Fahse, L., Szidat, S., Studer, T., Baumann, J., Heurich, M., & Tinner, W. (2020). Vegetation and disturbance history of the Bavarian Forest National Park, Germany. *Vegetation History and Archaeobotany*, 29(2), 277–295. <https://doi.org/10.1007/s00334-019-00742-5>
- Veroustraete, F., Patyn, J., & Myneni, R. B. (1994). Forcing of a simple ecosystem model with fAPAR and climatic data to estimate regional scale photosynthetic assimilation. In F. Veroustraete, R. Ceulemans, & et al. (Eds.), *Vegetation, Modelling and Climate Change Effects* (pp. 151–177). SPB Academic Publishing.
- Vicente-Serrano, S. M., Beguería, S., & López-Moreno, J. I. (2010). A Multiscalar Drought Index Sensitive to Global Warming: The Standardized Precipitation Evapotranspiration Index. *Journal of Climate*, 23(7), 1696–1718. <https://doi.org/10.1175/2009JCLI2909.1>
- Wang, D., Qin, W., Jia, G., Shan, Z., & Hao, M. (2022). Assessing the effects of climate variability and vegetation conversion on variations of net primary productivity in the mountainous area of North China. *Forest Ecology and Management*, 506. <https://doi.org/10.1016/j.foreco.2021.119957>
- Waring, R. H., Landsberg, J. J., & Williams, M. (1998). Net primary production of forests: a constant fraction of gross primary production? *Tree Physiology*, 18(2), 129–134. <https://doi.org/10.1093/treephys/18.2.129>
- Wu, J., & Bauer, M. E. (2012). Estimating Net Primary Production of Turfgrass in an Urban-Suburban Landscape with QuickBird Imagery. *Remote Sensing*, 4(4), 849–866. <https://doi.org/10.3390/rs4040849>
- Xiao, X., Li, X., Jiang, T., Tan, M., Hu, M., Liu, Y., & Zeng, W. (2019). Response of net primary production to land use and climate changes in the middle-reaches of the Heihe River Basin. *Ecology and Evolution*, 9(8), 4651–4666. <https://doi.org/10.1002/ece3.5068>
- Xu, Z., Tian, Y., Liu, Z., & Xia, X. (2023). Comprehensive Effects of Atmosphere and Soil Drying on Stomatal Behavior of Different Plant Types. *Water*, 15(9), 1675. <https://doi.org/10.3390/w15091675>
- Yan, Y., Liu, X., Ou, J., Li, X., & Wen, Y. (2018). Assimilating multi-source remotely sensed data into a light use efficiency model for net primary productivity estimation. *International Journal of Applied Earth Observation and Geoinformation*, 72, 11–25. <https://doi.org/10.1016/j.jag.2018.05.013>
- Yang, F., Ren, H., Li, X., Hu, M., & Yang, Y. (2014). Assessment of MODIS, MERIS, GEOV1 FPAR Products over Northern China with Ground Measured Data and by Analyzing Residential Effect in Mixed Pixel. *Remote Sensing*, 6(6), 5428–5451. <https://doi.org/10.3390/rs6065428>
- Yuan, W., Liu, S., Zhou, G., Zhou, G., Tieszen, L. L., Baldocchi, D., Bernhofer, C., Gholz, H., Goldstein, A. H., Goulden, M. L., Hollinger, D. Y., Hu, Y., Law, B. E., Stoy, P. C., Vesala, T., & Wofsy, S. C. (2007a). Deriving a light use efficiency model from eddy covariance flux data for predicting daily gross primary production across biomes. *Agricultural and Forest Meteorology*, 143(3–4), 189–207. <https://doi.org/10.1016/j.agrformet.2006.12.001>
- Yuan, W., Liu, S., Zhou, G., Zhou, G., Tieszen, L. L., Baldocchi, D., Bernhofer, C., Gholz, H., Goldstein, A. H., Goulden, M. L., Hollinger, D. Y., Hu, Y., Law, B. E., Stoy, P. C., Vesala, T., & Wofsy, S. C. (2007b). Deriving a light use efficiency model from eddy covariance flux data for predicting daily gross primary production across biomes. *Agricultural and Forest Meteorology*, 143(3–4), 189–207. <https://doi.org/10.1016/j.agrformet.2006.12.001>

- Zeng, N., Qian, H., Roedenbeck, C., & Heimann, M. (2005). Impact of 1998-2002 midlatitude drought and warming on terrestrial ecosystem and the global carbon cycle. *Geophysical Research Letters*, *32*(22), n/a-n/a. <https://doi.org/10.1029/2005GL024607>
- Zhang, F., Zhou, G., & Nilsson, C. (2015). Remote estimation of the fraction of absorbed photosynthetically active radiation for a maize canopy in Northeast China. *Journal of Plant Ecology*, *8*(4), 429–435. <https://doi.org/10.1093/jpe/rtu027>
- Zhao, M., Heinsch, F. A., Nemani, R. R., & Running, S. W. (2005). Improvements of the MODIS terrestrial gross and net primary production global data set. *Remote Sensing of Environment*, *95*(2), 164–176. <https://doi.org/10.1016/j.rse.2004.12.011>
- Zhao, M., & Running, S. W. (2010). Drought-Induced Reduction in Global Terrestrial Net Primary Production from 2000 Through 2009. *Science*, *329*(5994), 940–943. <https://doi.org/10.1126/science.1192666>
- Zheng, Y., & Takeuchi, W. (2022). Estimating mangrove forest gross primary production by quantifying environmental stressors in the coastal area. *Scientific Reports*, *12*(1). <https://doi.org/10.1038/s41598-022-06231-6>
- Zhu, H., Lin, A., Wang, L., Xia, Y., & Zou, L. (2016). Evaluation of MODIS Gross Primary Production across Multiple Biomes in China Using Eddy Covariance Flux Data. *Remote Sensing*, *8*(5), 395. <https://doi.org/10.3390/rs8050395>

# ANNEX I

An overview of the maximum LUE values for different vegetation types collected from the literatures. The unit of LUE is  $\text{gCMJ}^{-1}$  except the blue coloured values are in  $\text{gCmolPPED}^{-1}$  unit.

| No. | Vegetation Type   | Max. LUE | Range (SD) | MAT (°C)  | MAP (mm) | Reference                |
|-----|---|----------|------------|-----------|----------|--------------------------|
| 1   | Grassland   | 2        | 1.8-3      |           |          | (Oomen et al., 2016)     |
| 2   | Cropland  | 2.7      | 1.996-3.55 |           |          | (Du et al., 2022)        |
| 3   | Tropical Savanna  | 0.8      | 0.5-2.9    | 25.7      | 1150     | (Lin et al., 2017)       |
| 4   | Tropical Broadleaf Deciduous  | 1.044    | 0.75-1.4   | 25        | 945      | (Lin et al., 2017)       |
| 5   | Herbaceous  | 1.5      |            |           |          | (Machwitz et al., 2015)  |
| 6   | Woody vegetation  | 1.1      |            |           |          | (Machwitz et al., 2015)  |
| 7   | Bare soil   | 0.1      |            |           |          | (Machwitz et al., 2015)  |
| 8   | Savanna [C3+C4]   | 0.9      |            | 22.6      | 464      | (Jin et al., 2013)       |
| 9   | Savanna   | 1.66     | 0.33-3.50  | 22-26.1   | 458-1200 | (Sjöström et al., 2009)  |
| 10  | Grassland   | 2.01     | 1.58-2.92  | 29.5-30.2 | 374-510  | (Sjöström et al., 2009)  |
| 11  | Deciduous broadleaf   | 1.8      | 0.55-3.5   |           |          | (Martínez et al., 2018)  |
| 12  | Evergreen needleleaf  | 1.5      | 0.55-3.5   |           |          | (Martínez et al., 2018)  |
| 13  | Grassland, Savanna, Cropland, Evergreen broadleaf                                       | 1.2      | 0.55-3.5   |           |          | (Martínez et al., 2018)  |
| 14  | C3 Plants   |          | 0.5-4.0    |           |          | (Prince & Goward, 1995a) |
| 15  | C4 Plants   | 2.76     |            |           |          | (Prince & Goward, 1995a) |
| 16  | Deciduous broadleaf   | 0.542    |            | 25        | 1200     | (Kayiranga et al., 2022) |
| 17  | Grass and crops   | 0.542    |            | 25        | 1200     | (Kayiranga et al., 2022) |
| 18  | Evergreen needleleaf  | 0.985    |            | 25        | 1200     | (Kayiranga et al., 2022) |
| 19  | Evergreen broadleaf   | 0.485    |            | 25        | 1200     | (Kayiranga et al., 2022) |
| 20  | Deciduous needleleaf  | 0.692    |            | 25        | 1200     | (Kayiranga et al., 2022) |
| 21  | Cropland  | 1.94     | --- (0.55) |           |          | (Madani et al., 2017)    |
| 22  | Grassland   | 1.19     | --- (0.45) |           |          | (Madani et al., 2017)    |
| 23  | Savanna   | 0.93     | --- (0.38) |           |          | (Madani et al., 2017)    |
| 24  | Woody savanna   | 0.93     | --- (0.37) |           |          | (Madani et al., 2017)    |
| 25  | Open shrubland  | 0.74     | --- (0.21) |           |          | (Madani et al., 2017)    |
| 26  | Closed shrubland  | 0.2      | --- (0.38) |           |          | (Madani et al., 2017)    |
| 27  | Mixed forest  | 1.43     | --- (0.37) |           |          | (Madani et al., 2017)    |
| 28  | Deciduous broadleaf   | 1.68     | --- (0.35) |           |          | (Madani et al., 2017)    |
| 29  | Evergreen broadleaf   | 1.4      | --- (0.2)  |           |          | (Madani et al., 2017)    |
| 30  | Evergreen needleleaf  | 0.98     | --- (0.32) |           |          | (Madani et al., 2017)    |
| 31  | Savanna   | 2.27     | 0.33-3.5   | 28.25     | 524      | (Tagesson et al., 2015)  |
| 32  | Grassland (C3+C4)   | 5        |            |           |          | (Sequist et al., 2003)   |
| 33  | Different biomes (deciduous broadleaf, evergreen needleleaf, grassland, mixed, savanna) | 2.14     |            |           |          | (Yuan et al., 2007b)     |

| No. | Vegetation Type             | Max. LUE | Range (SD) | MAT (°C)  | MAP (mm) | Reference                |
|-----|-----------------------------|----------|------------|-----------|----------|--------------------------|
| 34  | Savanna (mostly C4 + C3)    | 0.489    |            | 26        | 320      | (Sjöström et al., 2009)  |
| 35  | Cropland                    | 2.201    | --- (0.66) |           |          | (Madani et al., 2014)    |
| 36  | Grassland                   | 1.294    | --- (0.32) |           |          | (Madani et al., 2014)    |
| 38  | Woody savanna               | 0.983    | --- (0.20) |           |          | (Madani et al., 2014)    |
| 39  | Open shrubland              | 0.631    | --- (0.37) |           |          | (Madani et al., 2014)    |
| 40  | Closed shrubland            | 0.508    | --- (0.01) |           |          | (Madani et al., 2014)    |
| 41  | Mixed forest                | 1.171    | --- (0.23) |           |          | (Madani et al., 2014)    |
| 42  | Deciduous broadleaf         | 1.453    | --- (0.14) |           |          | (Madani et al., 2014)    |
| 43  | Evergreen broadleaf         | 0.98     | --- (0.21) |           |          | (Madani et al., 2014)    |
| 44  | Evergreen needleleaf        | 0.835    | --- (0.24) |           |          | (Madani et al., 2014)    |
| 45  | Cropland                    | 2.8      |            | 10.9      | 973      | (Garbulsky et al., 2010) |
| 46  | Shrubland                   | 1.35     |            | 17.7      | 377      | (Garbulsky et al., 2010) |
| 47  | Grassland                   | 2.2      | 1.0-3.1    | 5.2-24.9  | 335-1990 | (Garbulsky et al., 2010) |
| 48  | Savanna                     | 1.5      | 1.2-1.55   | 15.3-26.8 | 404-449  | (Garbulsky et al., 2010) |
| 49  | Cropland                    | 3.8      |            | 10.9      | 973      | (Garbulsky et al., 2010) |
| 50  | Shrubland                   | 2        |            | 17.7      | 377      | (Garbulsky et al., 2010) |
| 51  | Grassland                   | 3.7      | 1.9-4.5    | 5.2-24.9  | 335-1990 | (Garbulsky et al., 2010) |
| 52  | Savanna                     | 2.4      | 1.7-2.5    | 15.3-26.8 | 404-449  | (Garbulsky et al., 2010) |
| 53  | Cropland                    | 2.4      | --- (0.6)  |           |          | (TURNER et al., 2003)    |
| 54  | Grassland                   | 1.9      | --- (0.5)  |           |          | (TURNER et al., 2003)    |
| 55  | Mixed forest                | 1.9      | --- (1.0)  |           |          | (TURNER et al., 2003)    |
| 56  | Boreal conifer              | 1.2      | --- (0.6)  |           |          | (TURNER et al., 2003)    |
| 57  | Broad-leaved Deciduous      | 1.165    |            |           |          | (Running & Zhao, 2019)   |
| 58  | Needle-leaved Coniferous    | 0.962    |            |           |          | (Running & Zhao, 2019)   |
| 59  | Mixed Forest                | 1.051    |            |           |          | (Running & Zhao, 2019)   |
| 60  | Grass                       | 0.860    |            |           |          | (Running & Zhao, 2019)   |
| 61  | Transitional woodland shrub | 1.281    |            |           |          | (Running & Zhao, 2019)   |
| 62  | Pasture                     | 0.860    |            |           |          | (Running & Zhao, 2019)   |

Note: SD = standard deviation, MAT = mean annual temperature, MAP = mean annual precipitation. --- means range information is not available.

## ANNEX II

Biome-Property-Look-Up-Table (BPLUT) for MOD17 NPP algorithm contains the biome-specific constant values of different parameters (Running & Zhao, 2019). The parameters are mainly used to estimate GPP and plant respiration. Although the model used the parameter values as constant, it is possible to optimize any of them to get better result. This study intends to optimize maximum LUE value.

| UMD_VEG_LC                                       | ENF      | EBF      | DNF      | DBF      | MF       | CShrub   | OShrub   | WSavanna | Savanna  | Grass    | Crop     |
|--|----------|----------|----------|----------|----------|----------|----------|----------|----------|----------|----------|
| LUE <sub>max</sub><br>(KgC/m <sup>2</sup> /d/MJ) | 0.000962 | 0.001268 | 0.001086 | 0.001165 | 0.001051 | 0.001281 | 0.000841 | 0.001239 | 0.001206 | 0.000860 | 0.001044 |
| Tmin_min (C)                                     | -8.00    | -8.00    | -8.00    | -6.00    | -7.00    | -8.00    | -8.00    | -8.00    | -8.00    | -8.00    | -8.00    |
| Tmin_max (C)                                     | 8.31     | 9.09     | 10.44    | 9.94     | 9.50     | 8.61     | 8.80     | 11.39    | 11.39    | 12.02    | 12.02    |
| VPD_min (Pa)                                     | 650.0    | 800.0    | 650.0    | 650.0    | 650.0    | 650.0    | 650.0    | 650.0    | 650.0    | 650.0    | 650.0    |
| VPD_max (Pa)                                     | 4600.0   | 3100.0   | 2300.0   | 1650.0   | 2400.0   | 4700.0   | 4800.0   | 3200.0   | 3100.0   | 5300.0   | 4300.0   |
| SLA (LAI/KgC)                                    | 14.1     | 25.9     | 15.5     | 21.8     | 21.5     | 9.0      | 11.5     | 27.4     | 27.1     | 37.5     | 30.4     |
| Q10*   | 2.0      | 2.0      | 2.0      | 2.0      | 2.0      | 2.0      | 2.0      | 2.0      | 2.0      | 2.0      | 2.0      |
| Froot_leaf_ratio                                 | 1.2      | 1.1      | 1.7      | 1.1      | 1.1      | 1.0      | 1.3      | 1.8      | 1.8      | 2.6      | 2.0      |
| Livewood_leaf_ratio                              | 0.182    | 0.162    | 0.165    | 0.203    | 0.203    | 0.079    | 0.040    | 0.091    | 0.051    | 0.000    | 0.000    |
| Leaf_mr_base                                     | 0.00604  | 0.00604  | 0.00815  | 0.00778  | 0.00778  | 0.00869  | 0.00519  | 0.00869  | 0.00869  | 0.0098   | 0.0098   |
| Froot_mr_base                                    | 0.00519  | 0.00519  | 0.00519  | 0.00519  | 0.00519  | 0.00519  | 0.00519  | 0.00519  | 0.00519  | 0.00819  | 0.00819  |
| Livewood_mr_base                                 | 0.00397  | 0.00397  | 0.00397  | 0.00371  | 0.00371  | 0.00436  | 0.00218  | 0.00312  | 0.00100  | 0.00000  | 0.00000  |

Note: Evergreen Needleleaf Forest (ENF), Evergreen Broadleaf Forest (EBF), Deciduous Needleleaf Forest (DNF), Deciduous Broadleaf Forest (DBF), Mixed forests (MF), Closed Shrublands (CShrub), Open Shrublands (OShrub), Woody Savannas (WSavanna), Savannas (Savanna), Grassland (Grass), Croplands (Crop), and Specific Leaf Area (SLA)

## ANNEX III

The list of Sentinel-2 acquisition dates and the nearest available dates for MODIS GPP data.

| S-2 acquisition date | Nearest MODIS GPP date | S-2 acquisition date | Nearest MODIS GPP date |
|----------------------|------------------------|----------------------|------------------------|
| 2016-05-09           | 2016-05-08             | 2019-06-28           | 2019-06-26             |
| 2016-07-08           | 2016-07-11             | 2019-07-23           | 2019-07-20             |
| 2016-08-27           | 2016-08-28             | 2019-08-27           | 2019-08-29             |
| 2016-10-16           | 2016-10-15             | 2019-10-31           | 2019-11-01             |
| 2017-03-25           | 2017-03-22             | 2019-12-30           | 2020-01-01             |
| 2017-04-24           | 2017-04-23             | 2020-03-24           | 2020-03-21             |
| 2017-06-13           | 2017-06-10             | 2020-05-18           | 2020-05-16             |
| 2017-07-13           | 2017-07-12             | 2020-06-02           | 2020-06-01             |
| 2017-08-17           | 2017-08-13             | 2020-07-22           | 2020-07-19             |
| 2017-09-26           | 2017-09-22             | 2020-08-21           | 2020-08-20             |
| 2017-10-16           | 2017-10-16             | 2020-09-20           | 2020-09-21             |
| 2018-03-25           | 2018-03-22             | 2021-02-25           | 2021-02-26             |
| 2018-04-19           | 2018-04-15             | 2021-04-28           | 2021-05-01             |
| 2018-05-29           | 2018-06-02             | 2021-06-17           | 2021-06-18             |
| 2018-06-08           | 2018-06-10             | 2021-09-25           | 2021-09-22             |
| 2018-07-03           | 2018-07-04             | 2022-03-09           | 2022-03-06             |
| 2018-08-27           | 2018-08-29             | 2022-03-24           | 2022-03-22             |
| 2018-09-16           | 2018-09-14             | 2022-06-27           | 2022-06-26             |
| 2018-10-16           | 2018-10-16             | 2022-07-17           | 2022-07-20             |
| 2018-11-15           | 2018-11-17             | 2022-08-16           | 2022-08-13             |
| 2019-03-30           | 2019-03-30             | 2022-10-10           | 2022-10-08             |
| 2019-04-24           | 2019-04-23             | 2022-11-14           | 2022-11-17             |
| 2019-05-19           | 2019-05-17             |                      |                        |

## ANNEX IV

The p-values of the intercomparison between MOD17 and GLO-PEM models are in the table below. The p-values have been estimated based on r-values. The numbers are given in scientific notation as they are very small. All the p-values are significant at a 0.01 significance level.

| Dates      | P-value     | Dates      | P-value     | Dates      | P-value     |
|------------|-------------|------------|-------------|------------|-------------|
| 2016-05-09 | 2.6112E-64  | 2018-07-03 | 4.12263E-34 | 2020-06-02 | 4.4424E-127 |
| 2016-07-08 | 1.5688E-11  | 2018-08-27 | 6.93197E-31 | 2020-07-22 | 8.92662E-13 |
| 2016-08-27 | 3.82515E-09 | 2018-09-16 | 8.92885E-46 | 2020-08-21 | 3.27335E-95 |
| 2016-10-16 | 4.3767E-124 | 2018-10-16 | 7.6314E-57  | 2020-09-20 | 6.9649E-118 |
| 2017-03-25 | 2.34553E-64 | 2018-11-15 | 3.18972E-61 | 2021-02-25 | 7.43091E-96 |
| 2017-04-24 | 2.64987E-46 | 2019-03-30 | 6.73392E-49 | 2021-04-28 | 1.89657E-50 |
| 2017-06-13 | 2.93221E-68 | 2019-04-24 | 5.7073E-112 | 2021-06-17 | 1.60102E-36 |
| 2017-07-13 | 1.22944E-42 | 2019-05-19 | 2.4927E-113 | 2021-09-25 | 3.2013E-103 |
| 2017-08-17 | 3.83848E-95 | 2019-06-28 | 8.3937E-118 | 2022-03-09 | 6.46817E-81 |
| 2017-09-26 | 1.03977E-47 | 2019-07-23 | 2.4407E-69  | 2022-03-24 | 5.81068E-87 |
| 2017-10-16 | 7.52421E-60 | 2019-08-27 | 8.6022E-246 | 2022-06-27 | 1.90181E-33 |
| 2018-03-25 | 4.8022E-29  | 2019-10-31 | 1.66565E-44 | 2022-07-17 | 1.17928E-59 |
| 2018-04-19 | 1.58091E-68 | 2019-12-30 | 3.62511E-06 | 2022-08-16 | 4.24108E-58 |
| 2018-05-29 | 3.40312E-32 | 2020-03-24 | 1.55129E-18 | 2022-10-10 | 1.01847E-59 |
| 2018-06-08 | 1.4083E-179 | 2020-05-18 | 1.2728E-99  | 2022-11-14 | 6.12843E-66 |

The p-values of the t-test between the mean NPP during the pre-2018 (2016-2018) and post-2018 (2019-2022) periods. All the p-values are lower than the significance level of 0.01 at 99% confidence intervals. The table below shows the p-values in scientific notations.

| Sample point number | P-values of t-test |          | Sample point numbers | P-values of t-test |          |
|---------------------|--------------------|----------|----------------------|--------------------|----------|
|                     | MOD17              | GLO-PEM  |                      | MOD17              | GLO-PEM  |
| 1                   | 5.14E-06           | 1.15E-07 | 53                   | 0.000172           | 5.61E-05 |
| 2                   | 7.21E-11           | 2.44E-14 | 54                   | 1.56E-05           | 1.39E-06 |
| 3                   | 8.17E-10           | 6.98E-13 | 55                   | 0.000136           | 1.04E-05 |
| 4                   | 0.000204           | 2.57E-05 | 56                   | 2.29E-06           | 2.44E-08 |
| 5                   | 1.92E-06           | 1.76E-08 | 57                   | 2.4E-06            | 1.26E-07 |
| 6                   | 1.75E-06           | 1.58E-07 | 58                   | 6.9E-06            | 3.36E-07 |
| 7                   | 9.59E-08           | 8.01E-10 | 59                   | 1.3E-05            | 6.27E-07 |
| 8                   | 0.001209           | 0.000584 | 60                   | 7.46E-08           | 8.45E-11 |
| 9                   | 1.08E-08           | 3.37E-11 | 61                   | 4.09E-05           | 2.57E-06 |
| 10                  | 5.34E-05           | 1.57E-05 | 62                   | 6.85E-06           | 5.11E-08 |
| 11                  | 3.67E-05           | 2.38E-06 | 63                   | 0.00015            | 5.76E-06 |
| 12                  | 9.27E-06           | 1.57E-06 | 64                   | 0.000101           | 1.71E-06 |
| 13                  | 7.98E-09           | 6.64E-11 | 65                   | 2.68E-09           | 3.65E-12 |
| 14                  | 2.25E-06           | 2.04E-07 | 66                   | 4.26E-05           | 1.79E-05 |
| 15                  | 4.69E-08           | 4.17E-10 | 67                   | 2.44E-06           | 8.8E-08  |
| 16                  | 5.35E-06           | 4.58E-08 | 68                   | 0.000104           | 3.38E-06 |
| 17                  | 2.75E-05           | 5.9E-07  | 69                   | 2.66E-05           | 6.59E-07 |
| 18                  | 1.09E-06           | 1.38E-08 | 70                   | 3.4E-05            | 9.68E-07 |
| 19                  | 1.41E-07           | 5.99E-10 | 71                   | 2.07E-06           | 3.2E-08  |
| 20                  | 1.86E-06           | 3.38E-08 | 72                   | 6.28E-10           | 8.58E-13 |

| Sample point number | P-values of t-test |          | Sample point numbers | P-values of t-test |          |
|---------------------|--------------------|----------|----------------------|--------------------|----------|
|                     | MOD17              | GLO-PEM  |                      | MOD17              | GLO-PEM  |
| 21                  | 3.02E-06           | 1.43E-07 | 73                   | 1.05E-06           | 2.56E-08 |
| 22                  | 1.55E-07           | 2.73E-10 | 74                   | 2.99E-07           | 7.74E-09 |
| 23                  | 9.67E-09           | 5.06E-12 | 75                   | 2.83E-10           | 5.58E-13 |
| 24                  | 0.000532           | 0.000171 | 76                   | 5.57E-12           | 4.26E-15 |
| 25                  | 2.98E-05           | 1.28E-06 | 77                   | 9.5E-08            | 2.86E-10 |
| 26                  | 4.58E-07           | 2.33E-09 | 78                   | 1.65E-06           | 8.86E-09 |
| 27                  | 2.54E-05           | 1.96E-06 | 79                   | 3.18E-08           | 1.39E-10 |
| 28                  | 1.49E-10           | 8.52E-14 | 80                   | 5.63E-09           | 3.65E-12 |
| 29                  | 2.5E-05            | 1.95E-06 | 81                   | 5.93E-10           | 1.68E-12 |
| 30                  | 3.64E-06           | 2.63E-08 | 82                   | 5.24E-08           | 1.99E-11 |
| 31                  | 1.45E-07           | 1.53E-08 | 83                   | 3.87E-05           | 2.04E-06 |
| 32                  | 6.1E-08            | 7.84E-11 | 84                   | 1.73E-07           | 8.91E-10 |
| 33                  | 8.46E-06           | 2.56E-07 | 85                   | 4.3E-09            | 2.51E-11 |
| 34                  | 6.45E-10           | 1.38E-12 | 86                   | 3.27E-10           | 4.86E-13 |
| 35                  | 1.19E-05           | 4.58E-07 | 87                   | 7.01E-09           | 9.19E-11 |
| 36                  | 1.99E-06           | 1.1E-07  | 88                   | 0.00045            | 6.75E-05 |
| 37                  | 0.000933           | 0.000342 | 89                   | 1.08E-08           | 8.19E-11 |
| 38                  | 9.98E-07           | 2.82E-09 | 90                   | 6.44E-07           | 2.52E-08 |
| 39                  | 0.000114           | 4.7E-05  | 91                   | 4.17E-09           | 2.19E-12 |
| 40                  | 7.18E-06           | 1.13E-07 | 92                   | 4.73E-06           | 1.26E-07 |
| 41                  | 2.51E-10           | 3.32E-13 | 93                   | 0.004694           | 0.001938 |
| 42                  | 1.07E-05           | 6.64E-07 | 94                   | 0.000638           | 0.000853 |
| 43                  | 3.82E-09           | 3.51E-11 | 95                   | 5.57E-06           | 1.04E-06 |
| 44                  | 1.09E-06           | 3.43E-09 | 96                   | 2.6E-07            | 3.1E-09  |
| 45                  | 0.000389           | 0.000221 | 97                   | 0.000219           | 5.07E-05 |
| 46                  | 4.64E-09           | 1.36E-12 | 98                   | 7.26E-08           | 6.61E-11 |
| 47                  | 1.56E-07           | 5.63E-10 | 99                   | 4.12E-10           | 6.72E-14 |
| 48                  | 0.000433           | 2.01E-05 | 100                  | 2.73E-05           | 6.66E-06 |
| 49                  | 3.96E-05           | 1.84E-05 | 101                  | 2.99E-05           | 3.16E-06 |
| 50                  | 3.57E-06           | 1.71E-08 | 102                  | 0.000162           | 2.45E-05 |
| 51                  | 4.46E-07           | 9.19E-09 | 103                  | 1.85E-05           | 2.17E-06 |
| 52                  | 0.00016            | 1.63E-05 |                      |                    |          |

P-values of the correlation values of MOD17 NPP with climate variables and SPEI values. The table also contains the percentage of significant and insignificant p-values for every climate variables at 0.05 significance level.

| Sample point no. | P-values of correlation of MOD17 NPP with climates variables and SPEI values |               |           |               |           |            |
|------------------|--|---------------|-----------|---------------|-----------|------------|
|                  | Min. Temp.   | Real-time SMD | Lag-1 SMD | Real-time VPD | Lag-3 VPD | Lag-6 SPEI |
| 1.               | 0.018732   | 0.022697      | 0.002021  | 0.011042      | 0.002609  | 0.000416   |
| 2.               | 0.121017   | 0.104301      | 0.012333  | 0.075611      | 0.019506  | 0.000225   |
| 3.               | 0.032347   | 0.041449      | 0.005166  | 0.047127      | 0.006756  | 0.000427   |
| 4.               | 0.001301   | 0.007127      | 0.001451  | 0.002844      | 0.001854  | 0.001006   |
| 5.               | 0.00022  | 0.003395      | 0.000262  | 0.001298      | 0.000862  | 0.005167   |
| 6.               | 0.017999   | 0.03285       | 0.015285  | 0.021573      | 0.011381  | 0.000826   |
| 7.               | 0.002896   | 0.019446      | 0.000841  | 0.003869      | 0.010361  | 0.001517   |

| Sample point no. | P-values of correlation of MOD17 NPP with climates variables and SPEI values |               |           |               |           |            |
|------------------|--|---------------|-----------|---------------|-----------|------------|
|                  | Min. Temp.   | Real-time SMD | Lag-1 SMD | Real-time VPD | Lag-3 VPD | Lag-6 SPEI |
| 8.               | 0.002407   | 0.042901      | 0.00423   | 0.0024        | 0.012789  | 0.001568   |
| 9.               | 0.019128   | 0.037708      | 0.002885  | 0.018229      | 0.004689  | 0.000445   |
| 10.              | 0.000339   | 0.004134      | 0.000262  | 0.00131       | 0.001164  | 0.00081    |
| 11.              | 0.003865   | 0.011873      | 0.001015  | 0.003982      | 0.00098   | 0.001499   |
| 12.              | 0.015197   | 0.028769      | 0.071294  | 0.062296      | 0.024353  | 0.001207   |
| 13.              | 0.122268   | 0.117845      | 0.019046  | 0.052177      | 0.051212  | 0.000805   |
| 14.              | 0.001704   | 0.010321      | 0.00091   | 0.005627      | 0.00241   | 0.000425   |
| 15.              | 0.055772   | 0.068968      | 0.015207  | 0.033535      | 0.031818  | 0.00019    |
| 16.              | 0.003023   | 0.006964      | 0.001926  | 0.00428       | 0.002832  | 0.00264    |
| 17.              | 0.003052   | 0.016324      | 0.001487  | 0.002541      | 0.001172  | 0.001825   |
| 18.              | 0.018118   | 0.022791      | 0.002886  | 0.012623      | 0.003731  | 0.000369   |
| 19.              | 0.024183   | 0.04748       | 0.011279  | 0.016364      | 0.019382  | 0.000303   |
| 20.              | 0.013749   | 0.018285      | 0.008142  | 0.017028      | 0.018427  | 0.0021     |
| 21.              | 0.008268   | 0.015779      | 0.008052  | 0.009468      | 0.003892  | 0.003356   |
| 22.              | 0.003567   | 0.021115      | 0.000474  | 0.005537      | 0.00119   | 0.002186   |
| 23.              | 0.017438   | 0.052306      | 0.001776  | 0.016085      | 0.005196  | 0.000936   |
| 24.              | 0.000356   | 0.004464      | 0.000324  | 0.000822      | 0.001488  | 0.000927   |
| 25.              | 0.00321  | 0.016837      | 0.000582  | 0.001764      | 0.003129  | 0.000213   |
| 26.              | 0.002275   | 0.02038       | 0.000557  | 0.00423       | 0.002258  | 0.001373   |
| 27.              | 0.004251   | 0.004668      | 0.00098   | 0.005863      | 0.001697  | 0.002573   |
| 28.              | 0.071202   | 0.062346      | 0.027278  | 0.061222      | 0.029661  | 0.003257   |
| 29.              | 0.000157   | 0.004311      | 0.000439  | 0.00042       | 0.000508  | 0.001082   |
| 30.              | 0.010034   | 0.031699      | 0.001023  | 0.00376       | 0.001743  | 0.00104    |
| 31.              | 0.05417  | 0.039793      | 0.015024  | 0.055762      | 0.012049  | 0.000975   |
| 32.              | 0.020158   | 0.053668      | 0.00999   | 0.011251      | 0.018272  | 0.000339   |
| 33.              | 0.001421   | 0.009698      | 0.001154  | 0.002467      | 0.002462  | 0.00204    |
| 34.              | 0.081091   | 0.075169      | 0.018532  | 0.056081      | 0.026524  | 0.000495   |
| 35.              | 0.004791   | 0.01647       | 0.001293  | 0.002861      | 0.004284  | 0.00053    |
| 36.              | 0.009365   | 0.010378      | 0.001362  | 0.007731      | 0.00529   | 0.000808   |
| 37.              | 0.001109   | 0.005073      | 0.036947  | 0.013634      | 0.00884   | 0.00407    |
| 38.              | 0.000459   | 0.014219      | 0.001184  | 0.001293      | 0.001656  | 0.00087    |
| 39.              | 0.000274   | 0.010171      | 0.002619  | 0.001109      | 0.018927  | 0.00813    |
| 40.              | 0.001042   | 0.01328       | 0.002171  | 0.004468      | 0.001422  | 0.00193    |
| 41.              | 0.132553   | 0.112628      | 0.028071  | 0.079935      | 0.119215  | 0.001228   |
| 42.              | 9.46E-05   | 0.001621      | 0.000525  | 0.000651      | 0.003213  | 0.006554   |
| 43.              | 0.031464   | 0.108949      | 0.010737  | 0.026871      | 0.033414  | 0.003303   |
| 44.              | 0.014018   | 0.033343      | 0.006392  | 0.008765      | 0.00576   | 0.000966   |
| 45.              | 0.003239   | 0.019706      | 0.001144  | 0.002508      | 0.016316  | 0.000501   |
| 46.              | 0.005495   | 0.020844      | 0.00197   | 0.008524      | 0.018632  | 0.000661   |
| 47.              | 0.023181   | 0.048844      | 0.009934  | 0.015854      | 0.018772  | 0.000651   |
| 48.              | 0.000775   | 0.011396      | 0.000263  | 0.000959      | 0.001165  | 0.000796   |
| 49.              | 0.000367   | 0.001695      | 0.000348  | 0.00193       | 0.003619  | 0.000208   |
| 50.              | 4.1E-05  | 0.002204      | 0.00022   | 0.000462      | 0.001349  | 0.001366   |

| Sample point no. | P-values of correlation of MOD17 NPP with climates variables and SPEI values |               |           |               |           |            |
|------------------|--|---------------|-----------|---------------|-----------|------------|
|                  | Min. Temp.   | Real-time SMD | Lag-1 SMD | Real-time VPD | Lag-3 VPD | Lag-6 SPEI |
| 51.              | 0.014826   | 0.017699      | 0.01253   | 0.022801      | 0.003757  | 0.001917   |
| 52.              | 0.002744   | 0.013832      | 0.001021  | 0.002212      | 0.000702  | 0.001588   |
| 53.              | 0.00182  | 0.006402      | 0.008515  | 0.012216      | 0.004516  | 0.005339   |
| 54.              | 0.00257  | 0.002933      | 0.001178  | 0.003877      | 0.008345  | 6.87E-05   |
| 55.              | 0.000667   | 0.005907      | 0.000562  | 0.001728      | 0.00189   | 0.014948   |
| 56.              | 0.004617   | 0.048406      | 0.003353  | 0.00472       | 0.039281  | 0.01165    |
| 57.              | 0.004967   | 0.028197      | 0.001015  | 0.009754      | 0.000561  | 0.017849   |
| 58.              | 0.010495   | 0.014481      | 0.002482  | 0.010151      | 0.003838  | 0.000395   |
| 59.              | 0.009092   | 0.022042      | 0.004752  | 0.009635      | 0.001815  | 0.002351   |
| 60.              | 0.001736   | 0.010657      | 0.00066   | 0.002876      | 0.007695  | 0.001551   |
| 61.              | 0.000493   | 0.003026      | 0.000483  | 0.001081      | 0.002113  | 0.001182   |
| 62.              | 0.006698   | 0.025352      | 0.002429  | 0.003185      | 0.002425  | 0.000414   |
| 63.              | 0.000821   | 0.013094      | 0.001484  | 0.002097      | 0.001596  | 0.002585   |
| 64.              | 0.00083  | 0.010885      | 0.00069   | 0.000674      | 0.001277  | 0.002751   |
| 65.              | 0.013139   | 0.027451      | 0.002969  | 0.009815      | 0.021714  | 0.000604   |
| 66.              | 9.46E-05   | 0.000976      | 0.000435  | 0.001683      | 0.005066  | 0.001666   |
| 67.              | 0.010199   | 0.028808      | 0.00409   | 0.00553       | 0.006501  | 0.000292   |
| 68.              | 0.001244   | 0.013335      | 0.001724  | 0.001605      | 0.002049  | 0.009295   |
| 69.              | 0.004879   | 0.035319      | 0.004469  | 0.004545      | 0.004666  | 0.007441   |
| 70.              | 0.001822   | 0.014737      | 0.001595  | 0.002076      | 0.001873  | 0.005534   |
| 71.              | 0.002067   | 0.00725       | 0.000798  | 0.003146      | 0.006358  | 0.000857   |
| 72.              | 0.053708   | 0.066021      | 0.006988  | 0.051132      | 0.080712  | 0.000311   |
| 73.              | 0.003367   | 0.01193       | 0.001243  | 0.009551      | 0.002354  | 0.000686   |
| 74.              | 0.002111   | 0.003736      | 0.0012    | 0.007929      | 0.016328  | 0.002187   |
| 75.              | 0.099379   | 0.139602      | 0.021079  | 0.071615      | 0.02302   | 0.001767   |
| 76.              | 0.1354   | 0.150443      | 0.025588  | 0.164984      | 0.016601  | 0.004761   |
| 77.              | 0.036241   | 0.039754      | 0.004632  | 0.015771      | 0.015078  | 0.000451   |
| 78.              | 0.022896   | 0.032059      | 0.006904  | 0.026386      | 0.004211  | 0.001115   |
| 79.              | 0.057935   | 0.047888      | 0.008502  | 0.028361      | 0.03688   | 0.000117   |
| 80.              | 0.030176   | 0.043877      | 0.006398  | 0.018772      | 0.021423  | 0.000451   |
| 81.              | 0.09295  | 0.089216      | 0.019964  | 0.054909      | 0.065437  | 0.002436   |
| 82.              | 0.005558   | 0.026874      | 0.001452  | 0.007025      | 0.010229  | 0.000944   |
| 83.              | 1.12E-05   | 0.001342      | 0.000298  | 0.000141      | 0.001384  | 0.005786   |
| 84.              | 0.03499  | 0.063495      | 0.014436  | 0.026823      | 0.008708  | 0.001133   |
| 85.              | 0.128679   | 0.127002      | 0.019545  | 0.048278      | 0.044141  | 0.000865   |
| 86.              | 0.024182   | 0.057915      | 0.006854  | 0.032994      | 0.012343  | 0.001597   |
| 87.              | 0.148488   | 0.098821      | 0.01867   | 0.068919      | 0.008379  | 0.000557   |
| 88.              | 0.000734   | 0.018902      | 0.001459  | 0.000451      | 0.014732  | 0.00168    |
| 89.              | 0.125076   | 0.175672      | 0.033755  | 0.051898      | 0.0442    | 0.000987   |
| 90.              | 0.004126   | 0.016256      | 0.002667  | 0.005022      | 0.005035  | 0.001057   |
| 91.              | 0.009329   | 0.023363      | 0.002466  | 0.008421      | 0.019573  | 0.000867   |
| 92.              | 0.00061  | 0.002129      | 0.000441  | 0.002337      | 0.001531  | 0.000661   |
| 93.              | 0.000144   | 0.001642      | 0.013469  | 0.003551      | 0.003623  | 0.007087   |

| Sample point no. | P-values of correlation of MOD17 NPP with climates variables and SPEI values |               |           |               |           |            |
|------------------|--|---------------|-----------|---------------|-----------|------------|
|                  | Min. Temp.   | Real-time SMD | Lag-1 SMD | Real-time VPD | Lag-3 VPD | Lag-6 SPEI |
| 94.              | 0.146918   | 0.17759       | 0.031604  | 0.120402      | 0.070594  | 0.001639   |
| 95.              | 0.003498   | 0.008949      | 0.001119  | 0.008131      | 0.005733  | 0.001123   |
| 96.              | 0.011491   | 0.067544      | 0.004233  | 0.010355      | 0.029225  | 0.011841   |
| 97.              | 0.001409   | 0.006877      | 0.000488  | 0.001229      | 0.00188   | 0.000291   |
| 98.              | 0.004378   | 0.030218      | 0.001799  | 0.009204      | 0.026648  | 0.001316   |
| 99.              | 0.046609   | 0.132888      | 0.032516  | 0.047958      | 0.066682  | 0.005596   |
| Significant (%)  | 83.8   | 78.8          | 99.0      | 85.9          | 93.9      | 100        |

Note: SMD = Soil moisture deficit

P-values of r-values of GLO-PEM NPP with climate variables and SPEI values. The table also contains the percentage of significant and insignificant p-values for every climate variables at 0.05 significance level.

| Sample point no. | P-values of correlations of GLO-PEM with climate variables and SPEI values |               |             |               |             |             |
|------------------|--|---------------|-------------|---------------|-------------|-------------|
|                  | Mean. Temp.  | Real-time SMD | Lag-1 SMD   | Real-time VPD | Lag-3 VPD   | Lag-8 SPEI  |
| 1.               | 0.021735   | 0.016103726   | 0.000711047 | 0.075665627   | 0.004991903 | 4.49737E-05 |
| 2.               | 0.221168   | 0.107194658   | 0.008975243 | 0.460220322   | 0.051025602 | 0.000114108 |
| 3.               | 0.086874   | 0.037584093   | 0.003284579 | 0.311758749   | 0.01566838  | 0.000805022 |
| 4.               | 0.004  | 0.00085798    | 0.000488982 | 0.021738976   | 0.004535298 | 5.43378E-05 |
| 5.               | 0.004774   | 0.001688611   | 0.000111203 | 0.019352376   | 0.004079574 | 0.00028796  |
| 6.               | 0.058009   | 0.008559224   | 0.00732294  | 0.113533433   | 0.02642088  | 0.000501865 |
| 7.               | 0.031789   | 0.015920593   | 0.000249277 | 0.051537371   | 0.02433754  | 0.000252354 |
| 8.               | 0.002541   | 0.004991124   | 0.000444843 | 0.012576703   | 0.023555269 | 0.044684962 |
| 9.               | 0.078467   | 0.046468779   | 0.002167068 | 0.216426146   | 0.01542804  | 4.26399E-05 |
| 10.              | 0.000775   | 0.000422808   | 6.09004E-05 | 0.008662893   | 0.002218699 | 0.001219309 |
| 11.              | 0.004853   | 0.002670072   | 0.000280223 | 0.02592833    | 0.001888891 | 8.17672E-05 |
| 12.              | 0.091755   | 0.009251928   | 0.045521664 | 0.253998024   | 0.041638052 | 0.000299861 |
| 13.              | 0.290214   | 0.12968144    | 0.011500584 | 0.329309434   | 0.12170388  | 4.61847E-05 |
| 14.              | 0.004064   | 0.001831558   | 0.000261333 | 0.030953307   | 0.003678966 | 0.000690627 |
| 15.              | 0.146414   | 0.062628097   | 0.006987614 | 0.211933757   | 0.085065081 | 0.000113847 |
| 16.              | 0.019139   | 0.00430998    | 0.001093073 | 0.063279446   | 0.010642211 | 9.76005E-05 |
| 17.              | 0.007778   | 0.0050972     | 0.000574099 | 0.033213582   | 0.003555475 | 0.000136141 |
| 18.              | 0.031964   | 0.015797263   | 0.001365857 | 0.094555103   | 0.009272432 | 6.0969E-05  |
| 19.              | 0.07603  | 0.028899261   | 0.006688658 | 0.142341921   | 0.059775838 | 0.00019141  |
| 20.              | 0.074074   | 0.012454105   | 0.004526129 | 0.129234879   | 0.052833845 | 5.40497E-05 |
| 21.              | 0.018  | 0.001881085   | 0.003652593 | 0.065973478   | 0.009377499 | 0.000533914 |
| 22.              | 0.017777   | 0.025790372   | 0.000412814 | 0.107924678   | 0.005124165 | 0.000239258 |
| 23.              | 0.056441   | 0.070291312   | 0.001483005 | 0.241511435   | 0.020097302 | 0.000508964 |
| 24.              | 0.000927   | 0.000641386   | 6.43055E-05 | 0.006430229   | 0.003284826 | 0.000583927 |
| 25.              | 0.014264   | 0.007686898   | 0.000129179 | 0.02377889    | 0.008092569 | 0.000145295 |
| 26.              | 0.007794   | 0.011824371   | 0.000334159 | 0.066532265   | 0.008086098 | 0.000660844 |
| 27.              | 0.005727   | 0.000609192   | 0.000303805 | 0.05156399    | 0.003656708 | 0.000343662 |
| 28.              | 0.238591   | 0.063952141   | 0.020523584 | 0.375266698   | 0.074970514 | 0.002120454 |
| 29.              | 0.000227   | 0.000441926   | 4.29119E-05 | 0.005092927   | 0.000553357 | 0.000888862 |
| 30.              | 0.030476   | 0.032483356   | 0.000760002 | 0.093765965   | 0.005970707 | 2.14137E-05 |

| Sample point no. | P-values of correlations of GLO-PEM with climate variables and SPEI values |               |             |               |             |             |
|------------------|--|---------------|-------------|---------------|-------------|-------------|
|                  | Mean. Temp.  | Real-time SMD | Lag-1 SMD   | Real-time VPD | Lag-3 VPD   | Lag-8 SPEI  |
| 31.              | 0.146584   | 0.013299652   | 0.007386418 | 0.252450408   | 0.031624925 | 6.3099E-05  |
| 32.              | 0.101533   | 0.066336291   | 0.009063291 | 0.166685357   | 0.072771237 | 0.000428431 |
| 33.              | 0.006741   | 0.003398398   | 0.000541559 | 0.028900064   | 0.010811254 | 0.00030412  |
| 34.              | 0.268247   | 0.0876183     | 0.013411146 | 0.379239224   | 0.073800457 | 0.000179892 |
| 35.              | 0.014664   | 0.005240987   | 0.000291823 | 0.029176914   | 0.010627158 | 0.000253683 |
| 36.              | 0.038099   | 0.00262113    | 0.000409702 | 0.061487599   | 0.012013446 | 8.13836E-05 |
| 37.              | 0.009233   | 0.000142524   | 0.017973523 | 0.118645755   | 0.025760206 | 0.06775229  |
| 38.              | 0.008882   | 0.005641583   | 0.000444575 | 0.052169345   | 0.005400974 | 0.001824414 |
| 39.              | 0.001826   | 0.000894369   | 0.000775847 | 0.021062934   | 0.047707519 | 0.012893479 |
| 40.              | 0.011418   | 0.00353418    | 0.000679613 | 0.107795899   | 0.004144341 | 0.002612179 |
| 41.              | 0.324839   | 0.118062123   | 0.013386213 | 0.393948213   | 0.191860268 | 0.000215987 |
| 42.              | 0.001164   | 0.00017345    | 0.000188473 | 0.010852461   | 0.008230275 | 0.002476122 |
| 43.              | 0.104905   | 0.091817467   | 0.00533369  | 0.204013177   | 0.069636393 | 0.000269585 |
| 44.              | 0.035926   | 0.022856288   | 0.00502492  | 0.120095669   | 0.022659013 | 0.000250818 |
| 45.              | 0.002606   | 0.002390537   | 0.000224784 | 0.023594835   | 0.045672183 | 0.016936653 |
| 46.              | 0.068496   | 0.03272467    | 0.001498126 | 0.126844685   | 0.060285959 | 0.00035966  |
| 47.              | 0.099499   | 0.05003956    | 0.006084048 | 0.159578662   | 0.062877512 | 9.86762E-05 |
| 48.              | 0.002317   | 0.003497088   | 0.000136219 | 0.02171985    | 0.006172322 | 8.86983E-05 |
| 49.              | 0.000948   | 7.38507E-05   | 7.13538E-05 | 0.00873606    | 0.005980292 | 0.001890679 |
| 50.              | 0.001185   | 0.000896328   | 7.13637E-05 | 0.010246242   | 0.005021237 | 0.003642478 |
| 51.              | 0.03669  | 0.003787754   | 0.006952268 | 0.138069716   | 0.010726654 | 0.001677361 |
| 52.              | 0.003755   | 0.002618785   | 0.000327706 | 0.020831628   | 0.002057854 | 0.000140247 |
| 53.              | 0.005983   | 0.000576211   | 0.004086542 | 0.079783641   | 0.009427893 | 0.003650648 |
| 54.              | 0.007781   | 0.000359802   | 0.000404937 | 0.032947681   | 0.020567903 | 0.000793639 |
| 55.              | 0.001763   | 0.001245219   | 0.000267967 | 0.024302799   | 0.004403599 | 0.001349634 |
| 56.              | 0.017298   | 0.026678591   | 0.001204032 | 0.066126243   | 0.069393532 | 0.001040159 |
| 57.              | 0.009197   | 0.006307197   | 0.000394559 | 0.066782205   | 0.00091732  | 0.000431461 |
| 58.              | 0.024192   | 0.002285022   | 0.000533248 | 0.122849598   | 0.009150104 | 7.88138E-05 |
| 59.              | 0.010594   | 0.002729645   | 0.001672233 | 0.06088532    | 0.004371357 | 0.000521543 |
| 60.              | 0.021079   | 0.011209062   | 0.000344597 | 0.050376712   | 0.022423121 | 0.000689703 |
| 61.              | 0.002258   | 0.000958773   | 0.000135863 | 0.010747051   | 0.004120659 | 0.000120343 |
| 62.              | 0.01144  | 0.014112064   | 0.000704065 | 0.045431812   | 0.00448808  | 0.000155222 |
| 63.              | 0.002005   | 0.004255187   | 0.000522927 | 0.014043257   | 0.004805454 | 0.000352954 |
| 64.              | 0.002445   | 0.005534728   | 0.000503457 | 0.020200486   | 0.007046304 | 0.000245367 |
| 65.              | 0.060405   | 0.026343516   | 0.001139018 | 0.11125592    | 0.044007382 | 0.000320157 |
| 66.              | 0.000973   | 6.48997E-05   | 9.98987E-05 | 0.008730903   | 0.006656892 | 0.004045882 |
| 67.              | 0.02501  | 0.012254369   | 0.000824343 | 0.062287947   | 0.009692126 | 1.25327E-05 |
| 68.              | 0.003328   | 0.004522812   | 0.001207117 | 0.026826624   | 0.0087272   | 0.000165678 |
| 69.              | 0.008373   | 0.012347456   | 0.002493861 | 0.050114255   | 0.015314672 | 0.000265631 |
| 70.              | 0.003303   | 0.004259738   | 0.000862027 | 0.026117215   | 0.007526868 | 0.000341057 |
| 71.              | 0.009685   | 0.003911003   | 0.000136802 | 0.025605173   | 0.006644659 | 0.000229246 |
| 72.              | 0.214419   | 0.092127736   | 0.005216999 | 0.369849343   | 0.202516142 | 0.000169648 |
| 73.              | 0.002071   | 0.003448278   | 0.000131003 | 0.035029085   | 0.00249454  | 0.001472253 |
| 74.              | 0.013149   | 0.001580526   | 0.000526782 | 0.056632843   | 0.024942862 | 0.00178617  |
| 75.              | 0.230652   | 0.151522044   | 0.016543311 | 0.438315628   | 0.061653965 | 0.000124508 |
| 76.              | 0.299881   | 0.134141695   | 0.024939583 | 0.663708056   | 0.067174499 | 0.000539096 |
| 77.              | 0.138736   | 0.051953631   | 0.003424415 | 0.183036582   | 0.040701071 | 3.19436E-05 |
| 78.              | 0.044461   | 0.020781591   | 0.004135469 | 0.165453774   | 0.011566807 | 4.22103E-05 |

| Sample point no. | P-values of correlations of GLO-PEM with climate variables and SPEI values |               |             |               |             |             |
|------------------|--|---------------|-------------|---------------|-------------|-------------|
|                  | Mean. Temp.  | Real-time SMD | Lag-1 SMD   | Real-time VPD | Lag-3 VPD   | Lag-8 SPEI  |
| 79.              | 0.266775   | 0.080080205   | 0.00610768  | 0.295059488   | 0.08637162  | 1.68584E-05 |
| 80.              | 0.193656   | 0.073037999   | 0.006603956 | 0.250981829   | 0.081457473 | 0.000106505 |
| 81.              | 0.235771   | 0.068679248   | 0.01098327  | 0.2895923     | 0.137483908 | 0.000103594 |
| 82.              | 0.022775   | 0.045937689   | 0.000804318 | 0.124994835   | 0.023083749 | 0.001699305 |
| 83.              | 0.000701   | 0.000110776   | 6.35834E-05 | 0.009516608   | 0.004273508 | 0.002217405 |
| 84.              | 0.08978  | 0.042049511   | 0.009454028 | 0.175085932   | 0.031591569 | 8.94757E-05 |
| 85.              | 0.308467   | 0.148670173   | 0.01286066  | 0.325199209   | 0.104392296 | 3.05663E-05 |
| 86.              | 0.078089   | 0.036820621   | 0.004223036 | 0.236560535   | 0.031865873 | 0.000581539 |
| 87.              | 0.209425   | 0.073699135   | 0.010716432 | 0.408040552   | 0.022256128 | 0.000280457 |
| 88.              | 0.003417   | 0.003349977   | 0.000254014 | 0.01693963    | 0.04017391  | 4.11357E-05 |
| 89.              | 0.306992   | 0.168935373   | 0.02138368  | 0.315952542   | 0.101725267 | 3.43684E-05 |
| 90.              | 0.018867   | 0.004765192   | 0.00065751  | 0.044243024   | 0.007742983 | 0.000206379 |
| 91.              | 0.069905   | 0.025791004   | 0.001473371 | 0.111144074   | 0.051178593 | 0.000237616 |
| 92.              | 0.004075   | 0.00056587    | 0.000126871 | 0.017013333   | 0.003132139 | 0.000715628 |
| 93.              | 0.001245   | 2.64363E-05   | 0.007453032 | 0.05529308    | 0.018531075 | 0.04590334  |
| 94.              | 0.116798   | 0.045247959   | 0.003917127 | 0.223173835   | 0.119027631 | 0.115841886 |
| 95.              | 0.007575   | 0.002586808   | 0.000314968 | 0.06412027    | 0.013047571 | 0.000223481 |
| 96.              | 0.048694   | 0.054513171   | 0.001435699 | 0.089569292   | 0.057740968 | 0.00076181  |
| 97.              | 0.001088   | 0.000570724   | 0.000106835 | 0.012369276   | 0.005217414 | 0.003141561 |
| 98.              | 0.061065   | 0.042956385   | 0.001972844 | 0.154681301   | 0.093088371 | 0.000143175 |
| 99.              | 0.202937   | 0.124493048   | 0.026056425 | 0.319829053   | 0.14362573  | 0.001000986 |
| Significant (%)  | 64.6   | 77.8          | 100         | 35.4          | 73.7        | 98.0        |

Note: SMD = Soil moisture deficit